Chemical signatures of planet formation in field and open cluster stars

Fan Liu

A thesis submitted for the degree of

Doctor of Philosophy

of the Australian National University

Research School of Astronomy & Astrophysics

30th June 2016

Disclaimer

I hereby declare that this thesis is an account of my research undertaken between August 2012 and January 2016 at the Research School of Astronomy & Astrophysics, College of Science, the Australian National University. The material presented in this thesis is original, and has not been submitted in whole or part for a degree in any university. The thesis is compiled from three papers that are published by peer reviewed journals. I have made significant contributions to each paper. Where appropriate, the work of others are acknowledged within the forward of each chapter.

Chapter 2 is originally published as F. Liu, M. Asplund, I. Ramírez, D. Yong, J. Meléndez, 2014, *A high-precision chemical abundance analysis of the HAT-P-1 stellar binary: constraints on planet formation*, MNRAS, 442, L51.

Chapter 3 is originally published as F. Liu, D. Yong, M. Asplund, I. Ramírez, J. Meléndez, B. Gustafsson, L. M. Howes, I. U. Roederer, D. L. Lambert, T. Bensby, 2016, *The detailed chemical composition of the terrestrial planet host Kepler-10*, MNRAS, 456, 2636.

Chapter 4 is originally published as F. Liu, D. Yong, M. Asplund, I. Ramírez, J. Meléndez, 2016, *The Hyades open cluster is chemically inhomogeneous*, MNRAS, 457, 3934.

Fan Liu

30th June 2016

Acknowledgments

I am truly grateful to my supervisors, Prof. Martin Asplund and Dr. David Yong for their patient and suggestive supervisions. They always give me kind and detailed guidance throughout my whole PhD time at Mt Stromlo. Martin and David have provided me with countless suggestions and opportunities regarding my research projects. They also kindly support me to attend domestic and international conferences related to my research field, to present my research and build up collaborations with other astronomers. I thank them sincerely for their care, help and encouragements, for giving me the best start to my future academic career. I also thank Ivan Ramírez and Jorge Meléndez for their continued guidance. Ivan for his kind help when I was visiting him to set up my pipeline for high-precision spectroscopic data reduction and analysis, for all the opportunities that come with the collaborations, and for my wonderful experience at University of Texas, Austin. Jorge for his patient help for my first-time oversea observation, using 10.4 m Keck telescope at Hawaii, USA, for all the suggestions, discussions, and collaborations on my PhD research projects.

I want to thank my dear friends, Wladimir, Akimasa, Anish, George, Jane, Suryashree, Louise, Ly, Anshu, Haiyang and all the other students and staff at Mt Stromlo for making my PhD life enjoyable and memorable for the past three and half years. I am truly grateful to my working place, Mt Stromlo Observatory, Research School of Astronomy & Astrophysics. It is the most wonderful environment for scientific research and personal life. I acknowledge the support of the Alex Rogers Travel Scholarship, for funding my travel to attend academic conferences.

Finally, I want to thank my parents for their sincere love and constant support.

Abstract

In this thesis, I have conducted a strictly line-by-line differential abundance analysis using high resolution, high signal-to-noise ratio spectra of field stars (e.g., stellar binaries, terrestrial planet hosts etc.) and open cluster stars (e.g., the Hyades stars) in order to identify the chemical signatures of planet formation. My research can help to answer a few fundamental questions: does planet formation affect the chemical composition of the host stars and does stellar birth environment affect the formation of planet? This thesis also has ramifications for Galactic archeology since I measured accurate abundances in a benchmark open cluster and identified, for the first time, real star-to-star abundance variations in any open cluster. These results present a new challenge to the current view of Galactic archaeology.

The three main results from this thesis are:

First, we present a high-precision, differential abundance analysis of the HAT-P-1 stellar binary. The secondary star in this double system is known to host a transiting giant planet while no planets have yet been detected around the primary star. The derived elemental abundances of the primary and secondary stars are identical within the errors. The striking similarity in the chemical compositions of the two stellar components in HAT-P-1 indicates that the formation of giant planets does not necessarily imply differences in the chemical abundances of the host stars. The elemental abundances of each star in HAT-P-1 relative to the Sun show an identical, positive correlation with the condensation temperature, thus we speculate based on the scenario put forward by Meléndez et al. (2009) that HAT-P-1 experienced less efficient formation of terrestrial planets than the Sun. This would be in line with the expectation that the presence of close-in giant planets prevents the formation or survival of terrestrial planets.

Secondly, in order to further examine the possibility of planet formation imprinting chemical signatures in the host star, we conduct a detailed differential abundance analysis of the

terrestrial planet host Kepler-10 and 14 of its stellar twins. Stellar parameters and elemental abundances of Kepler-10 and its stellar twins were obtained with very high precision. When compared to the majority of thick disc twins, Kepler-10 shows a depletion in the refractory elements relative to the volatile elements, which could be due to the formation of terrestrial planets in the Kepler-10 system. The average abundance pattern corresponds to roughly 13 Earth masses, while the two known planets in Kepler-10 system have a combined mass of 20 Earth. Although our results demonstrate that several factors (e.g., planet signature, stellar age, stellar birth location and Galactic chemical evolution) could lead to or affect abundance trends with condensation temperature, we find that the trends give further support for the planetary signature hypothesis. Based on a similar comparison with thin disc stars, we conclude that having a careful selected comparison sample of otherwise similar stars is critical for reliable conclusions regarding the impact of planet formation to be drawn.

Thirdly, we present a high-precision differential abundance analysis of 16 solar-type stars in the Hyades open cluster based on high resolution, high signal-to-noise ratio spectra. We derived stellar parameters and differential abundances for 19 elements with total uncertainties as low as 0.01 - 0.02 dex. Our main results include: (1) there is no clear chemical signature of planet formation detected among the sample stars, i.e., no correlations in elemental abundances versus condensation temperature; (2) the observed abundance dispersions are a factor of ≈2 larger than the average measurement errors for most elements; (3) there are positive correlations, of high statistical significance, between the abundances of at least 90% of pairs of elements. We demonstrate that none of these findings can be explained by errors in the inferred stellar parameters. Our results reveal that the Hyades is chemically inhomogeneous at the 0.02 dex level. Possible explanations for the abundance variations include (1) inhomogeneous chemical evolution in the proto-cluster environment, (2) supernova ejection in the proto-cluster cloud, and (3) pollution of metal-poor gas before complete mixing of the proto-cluster cloud. Our results provide significant constraints on the chemical compositions of open cluster stars and for Galactic archeology, especially the concept of chemical tagging.

CONTENTS

LIST OF FIGURES

LIST OF TABLES

CHAPTER 1

INTRODUCTION

1.1. Background

The discovery of extra-solar planets is one of the significant breakthroughs in modern astronomy of the past two decades. Since the first discovery of a giant planet orbiting 51 Peg by Mayor & Queloz (1995), 2041 exoplanets[1] around other stars have been confirmed to date. The detection and characterization of exoplanets has evolved into a mature but rapidly developing field in astronomy. The vast majority of these planets have been detected with the radial velocity (RV) or transit techniques. Most of RV detected planets are giant planets orbiting relatively close to the host star (e.g., Udry & Santos 2007 for a review). Great progress has been made in discovering ever smaller planets, in particular through the Kepler satellite (e.g., Batalha et al. 2013; Coughlin et al. 2015) and European Southern Observatory's (ESO) HARPS spectrograph (e.g., Udry et al. 2007; Mayor et al. 2011). Figure 1.1 shows the detections of exoplanets, emphasizing the improvement of precision in terms of planetary mass. No true Earth analog has yet been found although the terrestrial planet

[1] exoplanet.eu, 2016-01-05

regime is now starting to be within reach.

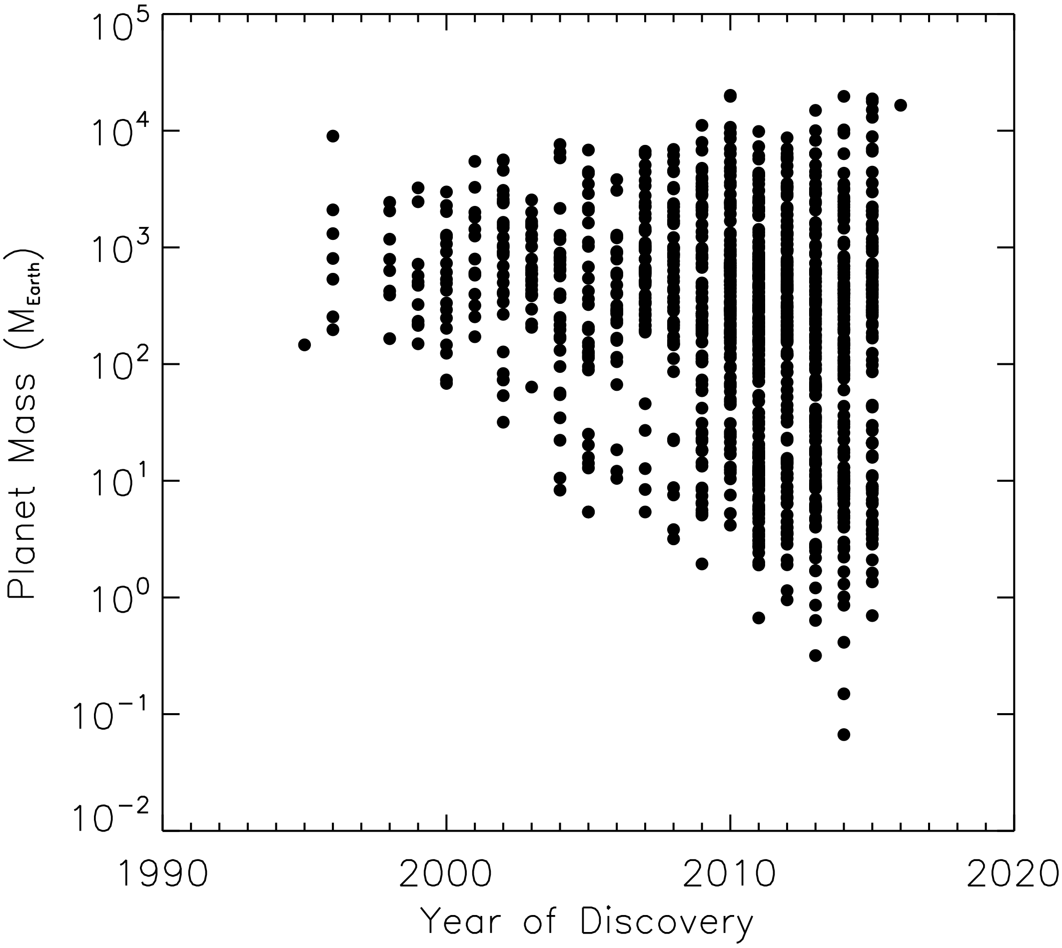

Figure 1.1 Masses of known exoplanets as a function of the year of discovery.

Meanwhile, understanding the formation of planets, in particular terrestrial planets, is another great challenge in modern astronomy. Although the discoveries of exoplanets are occurring at an ever increasing rate, the mechanisms involved in the planet formation continue to be debated. The giant planets could have formed in the circum-stellar disc, followed by rapid gas accretion on to their cores (Pollack et al. 1996) or by gravitational instability of the gas (Boss 1997). Such planets could then have migrated toward the host star by disc-planet interactions (Lin et al. 1996; Ida & Lin 2004), leaving only their rocky cores or forming ocean planets in the very inner region of the system since the high temperature can evaporate a large fraction of gas and melt most of the ice (Baraffe et al. 2005). Chiang &

Laughlin (2013) argued that the formation of close-in super Earths could be different from that of giant planets and favour in-situ formation with no large-scale migration, which can generate short-period planets with a lot of rocks, metal and very little water. Although it is widely accepted that planet formation starts from the coagulation of dust particles to larger objects in a circum-stellar disc of gas and dust, the details of such processes remain unclear and the formation of giant and terrestrial planets is still poorly understood (Haghighipour 2011).

With the large amount of discoveries of exoplanets, lots of research was undertaken in attempting to uncover the differences in chemical composition between planet host stars and stars without (known) planets. It is now well established that the likelihood of hosting giant planets increases rapidly with higher metallicity (Gonzalez 1997; Santos et al. 2004; Fischer & Valenti 2005) although smaller planets may show less [Fe/H]-dependence (Buchhave et al. 2012). This feature is thought to keep fossil traces of the processes of formation and evolution of the planetary systems, which is helpful to constrain the planet-formation models. Yet identifying any other abundance differences has however been much less forthcoming (e.g., Ecuvillon et al. 2006; Adibekyan et al. 2012). The few claimed anomalies, such as Li enhancement of the planet hosts (Israelian et al. 2009), either have low statistical significance or have been challenged and/or found to be incorrect, e.g., stemming from selection biases (Baumann et al. 2010). Recent discoveries have demonstrated that one particular planet host - the Sun - systematically departs from otherwise identical stars in its detailed chemical composition (e.g., Meléndez et al. 2009; Ramírez et al. 2009, 2010). This could be attributed to the formation of planets in the Solar system, perhaps even the terrestrial planets. Such discoveries enable us to probe the processes involved in forming planets and may also open up the enthralling possibility to identify stars harbouring planets solely from their chemical composition.

1.2. A possible chemical signature of terrestrial planet formation

Meléndez et al. (2009) demonstrated that the chemical abundances in the Sun, which exhibits a deficiency of refractory elements relative to volatile elements, are anomalous when compared to most (about 85%) nearby solar twins (i.e. stars with effective temperature T_{eff}, surface gravity $\log g$ and overall metallicity [Fe/H] indistinguishable from the Sun). Only $\sim$ 15% of solar twins carry similar abundance patterns as the Sun although the frequency seems to increase with [Fe/H] (Ramírez et al. 2009). They tentatively concluded that such a particular abundance pattern, namely, depletion of refractory elements, could be the signature imprinted by the terrestrial planet formation process. Such subtle abundance differences can only be revealed based on the extremely high-quality spectra with resolving power of R = 65,000 and signal-to-noise ratio (S/N) $\sim$ 450, using a newly developed strictly line-by-line differential abundance analysis of the Sun and a sample of carefully selected solar twins. This technique enables unprecedentedly high-precision ($\approx$ 0.01 dex, 2%) to be obtained in the relative chemical abundances as most systematic errors from e.g., stellar parameters, selection of lines, adoption of gf-values, atmospheric models, non-local thermal equilibrium (NLTE) effects largely cancel out and thus can be greatly reduced. As shown in Figure 1.2, the abundance differences between the Sun and the solar twins strongly correlate with the dust condensation temperature (T_{cond}) with a negative slope, i.e., abundance differences decrease with increasing T_{cond}. The values of T_{cond} of each element were taken from Lodders (2003), corresponding to equilibrium chemistry and dust formation in a solar composition mixture. Refractory elements that easily form dust (high T_{cond}, such as Al, Sc, Ti) are under-abundant in the Sun relative to the solar twins while volatile elements (low T_{cond}, such as C, N, O) are more abundant when using Fe as a reference element. The difference between volatile and refractory elements amounts to about 0.08 dex ($\approx$ 20%). This subtle signature ($\sim$ 0.08 dex) could only be seen when the abundance measurements were sufficiently precise (<< 0.05 dex). The peculiar surface composition of the Sun could be attributed to the formation of the terrestrial planets in the Solar system because of the accretion of chemically fractionated material into the solar convection zone during the planet formation epoch, i.e., the "missing" refractories from the solar photosphere were locked up in planets.

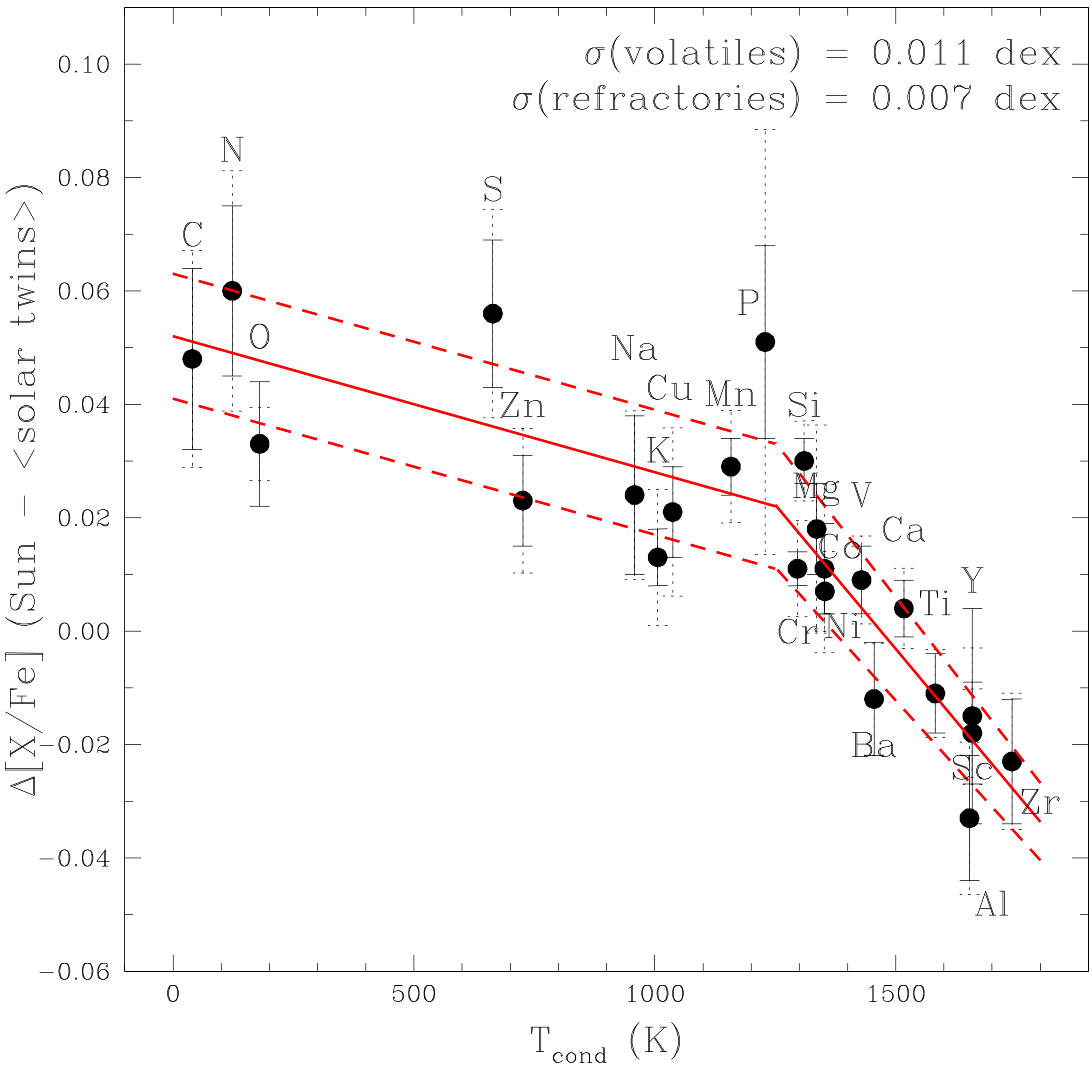

Figure 1.2 The differences in elemental abundances (Δ[X/Fe] between the Sun and the average of a sample of solar twins as a function of condensation temperature T_{cond}. (Meléndez et al. 2009)

This discovery has been subsequently confirmed by Ramírez et al. (2009, 2010) using more solar twins as well as when using stellar twins (i.e. stars slightly different from the Sun but all very similar to each other). Ramírez et al. (2009) found a clear trend of abundance as a function of T_{cond} for 900 < T_{cond} < 1800 K, while abundances of lower T_{cond} elements appear to be roughly constant. The study of Ramírez et al. (2010) combined the results of elemental abundances derived for solar-type stars from several independent studies and analysed the abundances - T_{cond} trends. They found a negative slope (when compared to the Sun) of abundances versus condensation temperature at T_{cond} > 900 K, which indicates that a large fraction of refractory elements have been removed from the solar-forming cloud to make up dust grains, suggesting planet formation. The restricted sample leads to the results of better accuracy and thus makes it possible to see abundances - T_{cond} trend which were absent in original studies.

The strong correlation with dust condensation temperature implies an intimate connection with planet formation because dust condensation is a necessary first step in the process of forming planets in the Solar system. A plausible scenario is that during the planet forming epoch the refractory elements were preferentially locked up in planetesimals and subsequently planets compared to the volatile elements, with the remaining dust-cleaned gas being accreted on to the Sun (Meléndez et al. 2009; Chambers 2010). For whatever reason planet formation proceeded more efficiently around the Sun than in the majority of otherwise similar stars. There are tantalizing suggestions that the chemical fingerprint is related to the formation of terrestrial planets: the estimated mass of the removed refractory elements to produce the abundance differences in the present-day solar convection zone amount to $\approx 4\,M_{\oplus}$ and such differences would roughly disappear if the total mass of refractory elements in the terrestrial planets were added to the solar convective zone. The fact that the total mass of refractories in the terrestrial planets of the Solar system today is of the same order of magnitude as the mean observed difference between refractories and volatiles in the Sun relative to solar twins supports the hypothesis proposed by Meléndez et al. (2009). The break in the abundance vs. T_{cond} trend at ~ 900 - 1200 K implies condensation close to proto-Sun (< 1 AU) and thus more consistent with formation of terrestrial planets rather than giant planets. Meléndez et al. (2012) stated that other possible nucleosynthetic explanations (e.g., Galactic chemical evolution, migration of stars, pollution of nearby supernovae) are unlikely to produce the peculiar chemical abundance pattern in the Sun.

This scenario, however, has been challenged by González Hernández et al. (2010) and Adibekyan et al. (2014) among others. González Hernández et al. (2010) claimed that their abundance results do not show a clear trend for stars with or without planets. Adibekyan et al. (2014) argued that the observed trend between chemical abundances and condensation temperature (T_{cond}) could possibly be due to the differences in stellar ages rather than the presence of planets. Nissen (2015) conducted a high-precision differential abundance analysis of a sample of solar twins in the solar neighbourhood using very high signal-to-noise ratio (S/N > 600) spectra. His results showed abundance-age correlations for most elements, which indicates that chemical evolution in the Galactic disc might play an important role in the explanation of the T_{cond} trend and must be considered when interpreting the results. Spina et al. (2016) confirmed that the abundance ratios ([X/Fe]) of most species correlate with age, which can be used to track the Galactic chemical evolution (GCE) effect on the chemical patterns. In contrast, after subtracting the GCE effect, they were still able to disentangle the T_{cond} trends which might be purely affected by the planet formation process. They concluded that roughly < 40% of the observed trends with condensation temperature is on age effect, leaving > 60% unexplained unless planet formation is involved.

Another explanation for the peculiar solar composition is that the pre-solar nebula was radiatively cleansed from some of its dust by luminous hot stars in the solar neighbourhood before the formation of the Sun and its planets. This possibility is supported by the finding that the solar-age and rich open cluster M67 seems to have a chemical composition closer to the solar composition than most solar twins (Önehag et al. 2011, 2014). A similar scenario was discussed by Gaidos (2015), who suggests that abundance-T_{cond} correlations could be explained by dust-gas segregation in circum-stellar discs.

In addition, Meléndez et al. (2009) also found that stars which host very close-in giant planets are more likely to share the abundance patterns of those solar twins or solar analogs without (known) planets, i.e., they tend to differ from the Sun. Schuler et al. (2011b) presented a differential abundance analysis, with internal uncertainties of about 0.05 dex, of 10 solar-type stars known to host giant planets. They found that four of these stars have positive slopes for $T_{\rm cond} > 900$ K when compared with the Sun and all of them host very close-in giant planets (less than 0.05 AU). The remaining six stars share the flat or negative slopes which are consistent with suggestions of the planet formation signature. This study indicates that the presence of hot Jupiters might prevent the formation of terrestrial planets. This idea is supported by Latham et al. (2011) based on the Kepler data. They demonstrated that systems with multiple transiting planets are less likely to include a transiting giant planet, suggested that close-in giant planets tend to disrupt the orbits of small planets in flat systems, maybe even prevent the formation of such systems in the first place. One could also speculate that in these systems, the smaller planets have already been accreted on to the host star during the migration process of Jupiter-like planets, thus removing the initial imprinted abundance signature.

Assuming that the chemical signature of terrestrial planet formation is the correct interpretation, then we can detect exoplanets, especially terrestrial planet candidates by identifying the chemical pattern ($\rm T_{cond}$ trends) of the host stars. Detailed chemical abundance analysis of the host stars can also provide important constraints on planet formation models. However, the interpretation of the $\rm T_{cond}$ trends are currently under debate due to the restricted and relative small samples in the previous studies. Therefore it is crucial to conduct the high-precision differential abundance analysis of different type of stars e.g., stellar binaries, small or terrestrial planet hosts, open cluster stars etc. to increase the diversity and size of the samples, in order to confirm and quantify chemical signatures of planet formation.

1.3. Chemical signatures of planet formation in field stars

The components of stellar binaries are usually assumed to share the same origins and identical chemical compositions. Several studies, however, find that the stars in binary systems do not necessarily have identical metallicities and chemical composition as naively expected (Gratton et al. 2001; Laws & Gonzalez 2001; Desidera et al. 2004, 2006; Ramírez et al. 2011, 2015; Liu et al. 2014; Tucci Maia et al. 2014; Teske et al. 2015). The exact sources of such abundance differences remain unclear but one likely explanation is that any chemical abundance differences in a binary system could be due to planet formation. Following the method and hypothesis proposed by Meléndez et al. (2009), the binaries consisting of two very similar stars but in which one component is hosting known planets are thus ideal targets for high-precision differential abundance analysis since almost all the systematic errors will cancel and we do not need to worry about selection effects such as age and membership of Galactic stellar population.

Abundance differences in a binary system 16 Cyg A+B was initially reported by Ramírez et al. (2011). They found that 16 Cyg A is more metal-rich than 16 Cyg B by ≈ 0.04 dex. They tentatively attributed this to planet formation in 16 Cyg B, with the fact that 16 Cyg B hosts a giant planet of 1.68 Jupiter masses (minimum mass, Cochran et al. 1997) while no planet has been detected around 16 Cyg A. Schuler et al. (2011a) claimed that no abundance differences are detected in 16 Cyg A+B though. Tucci Maia et al. (2014) achieved extremely high-precision in differential abundance analysis of 16 Cyg A+B (≤ 0.01 dex) and revealed a trend between abundance differences and condensation temperature (T_{cond}) in this binary system, which supports and strengthens the planet signature hypothesis. Teske et al. (2015) reported abundance differences in a binary system XO-2, in which both components host planets: XO-2 N hosts a planet of > 0.6 Jupiter masses (Burke et al. 2007), XO-2 S hosts two planets of > 0.26 Jupiter masses and > 1.4 Jupiter masses (Desidera et al. 2014). Ramírez et al.

(2015) found that the chemical differences are correlated with the condensation temperature (T_{cond}), which favours the hypothesis of planet formation. The explanations for these results have yet been confirmed but given the possible connection between chemical composition of host stars and planet formation, it is crucial to have additional binary systems hosting planets to be examined with high-precision differential abundance analysis. We note that the detailed abundance analysis of stellar binaries hosting planets can provide significant clues on how the planets formed in the binary systems and how the formation of giant or terrestrial planets can affect the chemical composition of the stellar binaries. In this thesis, I presented a high-precision differential abundance analysis of a planet hosting binary system HAT-P-1 (Liu et al. 2014), in which a close-in giant planet orbits around the secondary star (Bakos et al. 2007); no planet around the primary star has been detected.

The chemical composition of terrestrial planet host stars are of particular interests. Following the hypothesis proposed by Meléndez et al. (2009), the stars hosting terrestrial planets should also depleted in refractory elements relative to volatile elements when compared to the majority of otherwise similar stars, which can be examined by addressing high-precision chemical abundance analyses of terrestrial planet hosts relative to their stellar twins without such planets. In this thesis, I presented a strictly line-by-line differential abundance analysis of a terrestrial planet host: Kepler-10 and a sample of its stellar twins (Liu et al. 2016b) to examine the terrestrial planet formation hypothesis. Two small planets (Kepler-10b and Kepler-10c) around Kepler-10 were detected by (Batalha et al. 2011). Kepler-10b is an Earth-like planet, while Kepler-10c is Neptune-like and both planets are likely rocky based on their densities (Dumusque et al. 2014). Although Kepler-10c is more likely to have a volatile envelope (Rogers 2015), given the fact that Kepler-10 hosts at least one rocky planet make it ideal target to detect the possible chemical signatures of terrestrial planet formation. We would expect to find a similar chemical pattern that a deficiency of refractory elements relative to volatile elements in the photosphere of Kepler-10 when compared to other stars sharing similar stellar parameters but without known planets, assuming the hypothesis proposed by Meléndez et al. (2009) is correct. Similar analyses of more terrestrial planet hosts are necessary and can help to further understand the impact of terrestrial planet formation.

1.4. Chemical signatures of planet formation in open cluster stars

One aim of this thesis is to detect the possible chemical signature of planet formation in open cluster stars. Most field stars and their planets form in open clusters (e.g., Lada & Lada 2003 and references therein). Much effort has been devoted to search for planets in open clusters using radial velocity (RV) methods (e.g., Paulson et al. 2004b; Pasquini et al. 2012), as well as variety of transit searches in other open clusters (Mochejska et al. 2006; Pepper et al. 2008; Hartman et al. 2009). However, in contrast to planets detected around field stars, only a few planets have been found orbiting stars in open clusters: to date only 11 (Lovis & Mayor 2007; Sato et al. 2007; Quinn et al. 2012, 2014; Meibom et al. 2013; Brucalassi et al. 2014; Mann et al. 2015), most of which are giant planets. Eisner et al. (2008) stated that most solar-type stars in the open clusters do not possess discs massive enough to form gas giant planets, and that for the few stars capable of forming planets, the remaining disc masses may be insufficient to support inward migration (Debes & Jackson 2010). However, it turns out that at least for the transit searches, failure to detect a planet can be explained by the small sample size of the surveys. van Saders & Gaudi (2011) combined the null results from the transit surveys for open cluster stars and implied that upper limits on the open cluster planet fraction are not inconsistent with the frequency of short-period giant planets around field stars from both RV and transit surveys. In addition, nearby open clusters are all younger than ~ 1 Gyr and thus it is intrinsically more difficult to find small planets there due to stellar variability. Quinn et al. (2014) detected one hot Jupiter around a Hyades open cluster star and they suggested a hot Jupiter frequency of $1.97^{+0.92}_{-1.07}\%$ in the Hyades open cluster, which is consistent with the hot Jupiter frequency in the field stars (1.2± 0.38%, Wright et al. 2012). Meibom et al. (2013) detected two planets smaller than Neptunes around two Sun-like stars in the old open cluster NGC 6811 and argued that the small planet frequency in the open cluster stars is the same as the frequency in the field stars. It remains unclear whether the environment of open cluster do support the formation and survival of terrestrial planets since these planets might experience different formation and evolutionary histories. Nevertheless, stars in open clusters share the same age, initial chemical composition and dynamical environment (Randich et al. 2005), and thus offer advantages over field stars for studying planet formation: while field stars have been selected to have the same [Fe/H] now, their initial abundances prior to planet formation may have differed. On the other hand, all cluster stars being coeval will also facilitate precise relative mass determinations, corrections for stellar diffusion and also the accurate differential abundance analysis.

Open clusters are particularly useful objects in the context of Galactic archaeology, i.e., the study of the formation and evolution of the Galaxy using chemical abundances in stars. As mentioned, all field stars are believed to have formed in clusters, and thus the Galactic disc is believed to be made up of disrupted clusters. Despite decades of studies, we still lack a thorough knowledge of the sequence of events involved in the formation of the Galactic disc (e.g., Edvardsson et al. 1993; Chiappini et al. 2001; Bensby et al. 2014; Kubryk et al. 2015; Masseron & Gilmore 2015). Stellar chemical abundances are expected to keep the fossil record of the conditions of the Galactic disc at the time of its formation. Therefore, careful measurements of stellar chemical abundances using high resolution spectroscopy can reveal the nature of star-forming aggregates, and the detailed chemical and dynamical evolution of the Galactic disc. In the current view of Galactic archeology, star-forming aggregates imprint unique chemical signatures, which can be used to identify and track individual stars back to a common birth site, a concept named chemical tagging (Freeman & Bland-Hawthorn 2002). Such associations would therefore provide key new insights into the early star formation processes. However, several conditions must be met in order for chemical tagging to be successful (Bland-Hawthorn et al. 2010a; Blanco-Cuaresma et al. 2015; De Silva et al. 2015). The pre-requisite is that the open clusters, which are likely the remnants of star-forming aggregates in the Galactic disc, should be chemically homogeneous. The second pre-requisite is that there should be clear cluster-to-cluster abundance differences. Determining the level of chemical homogeneity in open clusters is thus of fundamental importance in the study of the evolution of star-forming clouds and that of the Galactic disc.

Previous studies (e.g., Friel & Boesgaard 1992; Paulson et al. 2003; De Silva et al. 2006, 2007; Ting et al. 2012; Friel et al. 2014) have argued that open clusters are chemically homogeneous, except for Li (Boesgaard & Tripicco 1986), Be (Smiljanic et al. 2010), C and N, as they are affected by stellar evolution, implying that the progenitor cloud was uniformly mixed before its stars formed. However, the observational measurement uncertainties are typically rather large (> 0.05 dex), preventing conclusions regarding chemical homogeneity at finer levels. Önehag et al. (2011) and Önehag et al. (2014) successfully achieved a very high precision level (~ 0.03 dex) by using strictly differential analysis on the open cluster M67 and found that this rich open cluster has a chemical composition very close to the solar composition. This provides significant clues regarding the solar birth place, although Pichardo et al. (2012) argued against this point based on dynamical modelling. Theoretical studies from Bland-Hawthorn et al. (2010b) indicate that a proto-cluster cloud should have sufficient time to homogenize before the first supernova explodes, for clusters with mass of $\sim 10^5 - 10^7$ $M_{\odot}$. Simulations by Feng & Krumholz (2014) showed that turbulent mixing could homogenize the elemental abundances of a proto-could and thus create an internal abundance dispersion at least five times more homogeneous than the proto-cluster cloud. Bovy (2016) investigated the abundance spread in open clusters and derive limits on the initial abundance spread of 0.01 - 0.03 dex for different elements. Both observations and theory agree that open clusters less massive than $\sim 10^7$ $M_{\odot}$ should be chemically homogeneous, except perhaps for the internal abundance trends observed in the light elements of all known globular clusters (e.g., Kraft 1994).

In this thesis, I revisited a close-by open cluster with intermediate age of ~ 625 - 750 Myr (Perryman et al. 1998; Brandt & Huang 2015): the Hyades, which has been studied before with spectroscopy (e.g., Paulson et al. 2003; De Silva et al. 2006; Carrera & Pancino 2011; Maderak et al. 2013; Dutra-Ferreira et al. 2016). I performed a strictly line-by-line differential abundance analysis on a sample of the Hyades stars, in order to: (1) distinguish minor abundance differences in the Hyades which can or can not be attributed to the planet formation, (2) determine the level of abundance dispersions in the Hyades if any, (3) investigate whether Hyades is indeed chemically homogeneous when a much better precision (~ 0.01 - 0.02 dex) can be achieved. I seek to understand that if planet formation will distort these chemical fingerprints beyond recognition or if it can be corrected through the observed variations with T_{cond} and derive detailed information about the abundance pattern with dust condensation and stellar mass (i.e. size of planet signature will depend on size of convection zone) in the open clusters. Furthermore this research can provide a crucial test of the concept of chemical tagging for Galactic archaeology.

1.5. Methodology

In order to reveal the subtle chemical signatures imprinted by planet formation, unprecedented precision in abundance analysis need to be achieved. Therefore high quality spectra ($R \geq 60{,}000$, $S/N > 300$) and strictly line-by-line differential analysis are both necessary.

We observed stellar binaries which host planets (e.g., HAT-P-1, XO-2, HD 80606/80607), terrestrial planet hosts (e.g., Kepler-10) and their stellar twins, large numbers of near-by stars in several open clusters (e.g., Hyades, Coma Berenices, Praesepe, Ruprecht 147, M67) using high resolution spectrographs at e.g., Keck, Very Large Telescope (VLT), Hobby-Eberly

Table 1.1 Observations of high quality spectra.

Sample	Number	Instrument	R	S/N	Status
HAT-P-1 binary	2	Keck/HIRES	67,000	> 300	Data published
XO-2 binary	2	Keck/HIRES	84,000	~ 350	Data published[a]
HD 80606/80607	2	Keck/HIRES	84,000	~ 350	Data collected
Kepler-10's twins	14	Magellan/MIKE[b]	83,000 (blue)	> 300	Data published
			65,000 (red)		
Hyades	16	McDonald 2.7 m[c]	60,000	> 350	Data published
Coma Berenices	19	HET/HRS[c]	60,000	~ 350	Data reduced
Praesepe	8	HET/HRS[c]	60,000	~ 350	Data reduced
Ruprecht 147	14	VLT/FLAMES	47,000	~ 300	Data collected
M67	3	Keck/HIRES	50,000	~ 300	Data reduced

[a] Data analysed and published by my collaborator (Ramírez et al. 2015).

[b] Magellan Inamori Kyocera Echelle spectrograph.

[c] Tull Coudé Spectrograph. [d] High Resolution Spectrograph.

Telescope (HET), Magellan, Canada-France-Hawaii Telescope(CFHT), McDonald 2.7m telescope and obtained spectra with very high S/N (> 300 per pixel) and wide wavelength coverage. In general, we can derive detailed abundances for ~ 20 - 25 elements including both volatile elements (e.g., C, N, O, Na, S, K, Zn) and refractory elements (e.g., Mg, Al, Si, Ca, Fe-peak, Sr, Y, Zr, Ba, La, Ce), which is crucial to accurately determine any correlation between elemental abundances and dust condensation temperature. Part of the data have been analysed and published as the main part of this thesis while the rest of them have been reduced and ready for further analysis. Table 1.1 lists the details of the accumulated observations of high quality spectra.

The technique of strictly line-by-line differential analysis for measuring relative chemical abundances in stars with very high-precision (0.01 dex, ~2%) has been further developed and applied to various cases over the past few years (Meléndez et al. 2009, 2012; Yong et al. 2013; Liu et al. 2014, 2016a,b; Ramírez et al. 2014b, 2015; Tucci Maia et al. 2014; Biazzo et al.

2015; Nissen 2015; Saffe et al. 2015; Spina et al. 2016). During my PhD, I have set up an automatic pipeline to perform the high-precision line-by-line differential analysis, which leads to fast and robust results. I describe the details of the analysis pipeline below. At first we need to establish stellar atmospheric parameters ($T_{\rm eff}$, log g, [Fe/H], and microturbulent velocity ξ_t) for the reference star(s). The pipeline performs a 1D, local thermodynamic equilibrium (LTE) abundance analysis using MOOG (Sneden 1973) with the ODFNEW grid of Kurucz model atmospheres (Castelli & Kurucz 2003). Stellar parameters are obtained by forcing excitation and ionization balance of Fe I and Fe II lines on a line-by-line basis relative to the Sun. The adopted parameters for the Sun are $T_{\rm eff}$ = 5777 K, log g = 4.44, [Fe/H] = 0.00, and ξ_t = 1.00 km s^{-1}. We note that the exact values of the reference star are not important in the differential abundance analysis. We then establish the stellar parameters of the comparison stars using an automatic grid searching method described by Liu et al. (2014, 2016a,b). The best combination of $T_{\rm eff}$, log g, [Fe/H] and ξ_t is obtained by minimizing the slopes in [Fe I/H] versus lower excitation potential (EP) and reduced equivalent width (EW) as well as the difference between [Fe I/H] and [Fe II/H], from a successively refined grid of stellar atmospheric models. The final solution is adopted when the grid step-size decreased to $\Delta T_{\rm eff} = 1$ K, $\Delta \log g = 0.01$ and $\Delta\xi_t = 0.01$ km s^{-1}. The adopted stellar parameters satisfy the excitation and ionization balance in a differential sense. Having established the stellar parameters relative to the selected reference star, we can derive differential chemical abundances for the volatile and refractory elements in which we are interested (e.g., C, O, Na, Mg, Al, Si, S, Ca, Sc, Ti, V, Cr, Mn, Fe, Co, Ni, Cu, Zn, Ba etc.) with a strictly line-by-line measurements. Hyperfine structure splitting is considered for Sc, V, Cr, Mn, Co, Cu, and Ba using the data from (Kurucz & Bell 1995). NLTE effects in the differential abundance analysis between similar stars such as our sample should be negligible (Meléndez et al. 2012; Monroe et al. 2013). However, we still applied differential NLTE corrections for the O I triplet using the NLTE calculations chosen from several studies (e.g., Ramírez et al.

2007; Fabbian et al. 2009; Amarsi et al. 2016). The total error in the differential abundance is estimated by adding in quadrature the standard error of the mean and the errors introduced by the uncertainties in stellar atmospheric parameters following the method of Epstein et al. (2010) which includes co-variance terms. For elements that only one spectral line is measured, we estimate the uncertainties by taking into consideration errors due to S/N, continuum setting and the stellar parameters. The quadratic sum of the three uncertainty sources give the total errors for these elements. Excellent precision in stellar parameters (e.g., $\sigma T_{\rm eff} \sim 10$ - 30 K) and differential abundances ($\sim$ 0.01 - 0.03 dex) can be achieved in our analysis due to the strictly line-by-line differential analysis technique, which greatly reduces the systematic errors from atomic line data and shortcomings in the 1D LTE modelling of the stellar atmospheres and spectral line formation (e.g., Asplund 2005; Asplund et al. 2009).

1.6. Outline of the thesis

This thesis seeks to address a few fundamental questions: how do planets form, does planet formation affect the chemical compositions of their host stars and whether we can detect and disentangle the chemical signature of planet formation?

Chapter 2 presents a high-precision differential abundance analysis of a stellar binary system HAT-P-1 which hosts a close-in giant planet, in order to investigate whether the giant planet formation can alter the chemical composition in the photospheres of the host stars.

Chapter 3 investigates the terrestrial planet host Kepler-10 and its stellar twins with detailed differential abundance analysis, in order to understand whether the formation of terrestrial planets affects the chemical composition of the host star.

Chapter 4 presents a differential abundance analysis of 16 stars in a bench mark open cluster: the Hyades with extremely high precision. The aim of this chapter is to understand whether it is possible to detect chemical signatures of planet formation in open cluster stars and provide a crucial test of the basic concept of Galactic archeology.

Finally Chapter 5 summarizes the conclusions drawn from my studies and briefly discusses ongoing and future work as stimulated by my thesis work.

CHAPTER 2

A HIGH PRECISION CHEMICAL ABUNDANCE ANALYSIS OF THE HAT-P-1 STELLAR BINARY

Context and contributions

The chapter is originally published as *'A high precision chemical abundance analysis of the HAT-P-1 stellar binary: constraints on planet formation'*, F. Liu, M. Asplund, I. Ramírez, D. Yong, J. Meléndez, 2014, MNRAS, 442, L51. Modifications of texts have been made in section 2.1 and 2.3. This chapter is included in the thesis as a representation of my contibution to the chemical signatures of planet formation in a stellar binary system hosting a planet. I have done all the observations, data reductions, and scientific analysis presented in this paper. The whole paper was written by myself with the suggestions provided by the co-authors.

2.1. Introduction

Binary stars, in which one star hosts a planet, offer a great opportunity to identify stellar chemical signatures of planet formation. Ramírez et al. (2011) demonstrated metallicity differences in the binary system 16 Cyg A+B to be 0.04 ± 0.01 dex (16 Cyg A is more metal-rich than 16 Cyg B) and related it to planet formation; 16 Cyg B is known to host a giant planet with a minimum mass of 1.68 Jupiter masses (Cochran et al. 1997). On the other hand, Schuler et al. (2011a) found no such abundance differences in 16 Cyg A+B. The reasons for these contrary results remain unknown but given the possible connection between planet formation and stellar host composition, there is an urgent need for additional binary systems hosting planets to be exposed to a high precision abundance analysis. Here we present such a study for the HAT-P-1 stellar binary, in which a close-in giant planet orbits around the secondary star (Bakos et al. 2007); no planet detection around the primary star has been reported.

2.2. Observations and data reduction

We obtained high resolution (R = $\lambda/\Delta\lambda$ = 67,000), high signal-to-noise ratio (S/N $\simeq$ 300 per pixel) spectra of the HAT-P-1 stellar binary with the High Resolution Echelle Spectrometer (HIRES, Vogt et al. 1994) on the 10 m Keck I telescope on August 15, 2013. A solar spectrum with higher S/N ($\simeq$ 450 per pixel) was also obtained through observations of the asteroid Iris. The wavelength coverage of these spectra is nearly complete from 380 to 800 nm. The Keck-MAKEE pipeline was used for standard echelle spectra reduction which include bias subtraction, flat-fielding, scattered-light subtraction, spectral extraction and wavelength calibration. We normalized and co-added the spectra with IRAF[1].

[1]IRAF is distributed by the National Optical Astronomy Observatory, which is operated by Association of Universities for Research in Astronomy, Inc., under cooperative agreement with National Science Foundation.

2.3. Stellar parameters and chemical abundance analysis

We started the analysis by measuring the equivalent width (EW) for a number of lines. Our adopted line-list come mainly from solar abundance analysis of Asplund et al. (2009) but complemented with additional largely unblended lines from Reddy et al. (2003), Bensby et al. (2005), Ramírez et al. (2007) and Neves et al. (2009); in a differential analysis such as ours the accuracy of the transition probabilities does not greatly influence the results. We measured the EW of each spectral line interactively using the *splot* task in IRAF and discarded lines with EW larger than 12 pm. The final atomic-line data used for our abundance analysis can be found online (Liu et al. 2014).

We performed a 1D, local thermodynamic equilibrium (LTE) abundance analysis with MOOG 2010 Version (Sneden 1973) using the ODFNEW grid of Kurucz model atmospheres (Castelli & Kurucz 2003); in our differential analysis the choice of model atmospheres is inconsequential. The stellar parameters were derived using excitation and ionization balance of Fe I and Fe II lines based on a line-by-line differential analysis relative to the Sun. Detailed description of our analysis technique can be found in chapter 1.5. We note that no sigma clipping was implemented in this work. The final adopted stellar parameters are listed in Table 2.1, which satisfy the excitation and ionization balance in a differential sense (Fig. 2.1).

The uncertainties in the stellar parameters were calculated based on the procedure laid out by Epstein et al. (2010) (see also Bensby et al. (2014)), which accounts for the co-variances between changes in the stellar parameters and the differential abundances. Table 2.1 lists the inferred errors, which highlights the excellent precision achieved: $\sigma T_{\mathrm{eff}} = 17$ and 8 K, respectively. These extremely low values for the errors correspond to the internal uncertainties of the differential method. Comparisons between sets of parameters derived in different studies show that the external uncertainties are usually higher (Bensby et al.

Table 2.1 Stellar atmospheric parameters for HAT-P-1.

Parameter	Primary	Secondary	S - P
$T_{\rm eff}$ (K)	6251 ± 17	6049 ± 8	−202 ± 11
$\log g$ (cgs)	4.36 ± 0.03	4.43 ± 0.02	+0.07 ± 0.03
[Fe/H] (dex)	0.146 ± 0.014	0.155 ± 0.007	+0.009 ± 0.009
$\varepsilon_{\rm t}$ (km/s)	1.45 ± 0.03	1.22 ± 0.02	−0.23 ± 0.02

2014). Our analysis demonstrates that the primary star is 200 K hotter than the secondary star while the metallicities of the primary and secondary stars are indistinguishable within the uncertainties: [Fe/H]=0.146 ± 0.014 dex (σ = 0.033 dex) and 0.155 ± 0.007 dex (σ = 0.023 dex), respectively. Here the uncertainties were derived using the Epstein approach while the values of σ represent the standard deviations of [Fe/H].

Having established the stellar parameters for the binary components, we derived chemical abundances for 23 elements: C, O, Na, Mg, Al, Si, S, Ca, Sc, Ti, V, Cr, Mn, Co, Ni, Cu, Zn, Sr, Y, Zr, Ba, La and Ce. Three elemental abundances (Sr, Zr and Ba) were derived through spectrum synthesis[2]. Hyperfine structure splitting was considered for Sc, V, Cr, Mn, Cu and Ba (Kurucz & Bell 1995). Departures from LTE were considered for oxygen according to Ramírez et al. (2007). We also compared the NLTE corrections with those from Fabbian et al. (2009) and note that the difference between two studies is 0.09 dex for the primary star and 0.06 dex for the secondary star, while the difference is 0.03 dex when comparing the primary and secondary star differentially.

The strictly line-by-line differential analysis greatly reduces the errors from atomic data and shortcomings in the 1D LTE modelling of the stellar atmospheres and spectral line formation. The abundances were determined using both the Sun and the primary star as reference stars; the inferred chemical compositions and associated 1σ uncertainties are listed in Table 2.2.

[2]The synthetic spectra were convolved with a Gaussian representing the combined effect of the atmospheric turbulence, stellar rotation, and the instrumental profile. The values of the broadening parameters for HAT-P-1 primary and secondary stars were 9.0, 6.0 km/s, respectively.

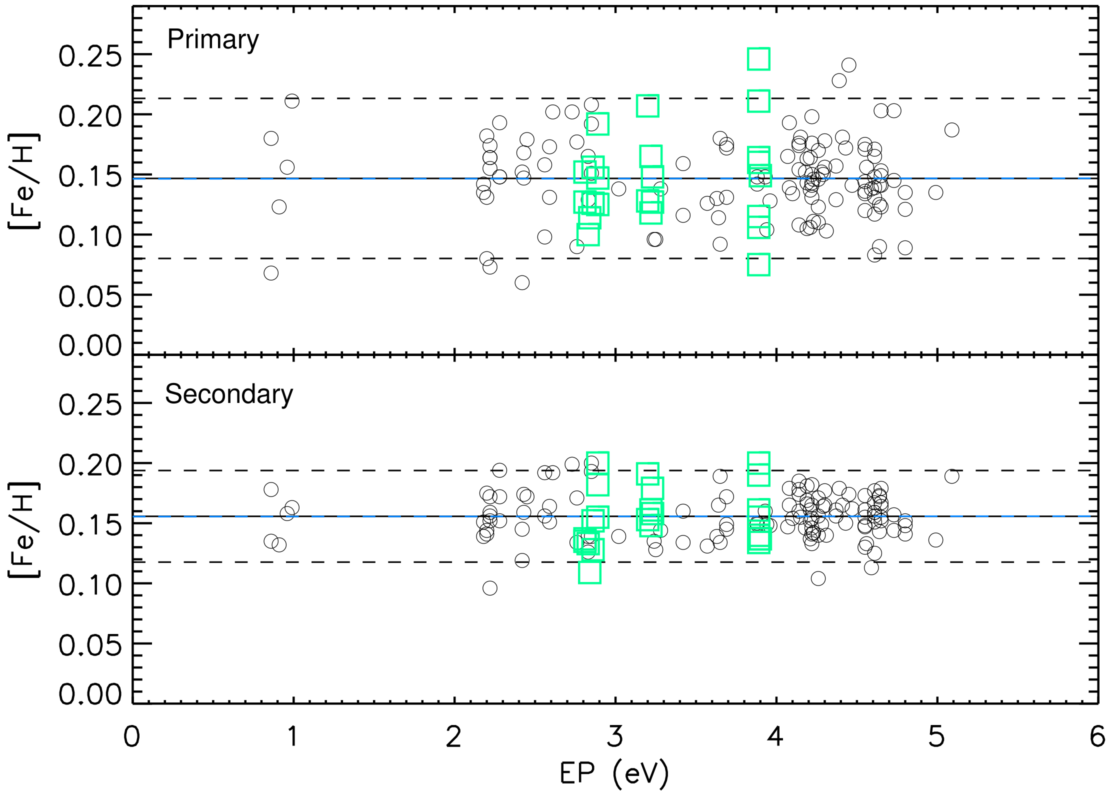

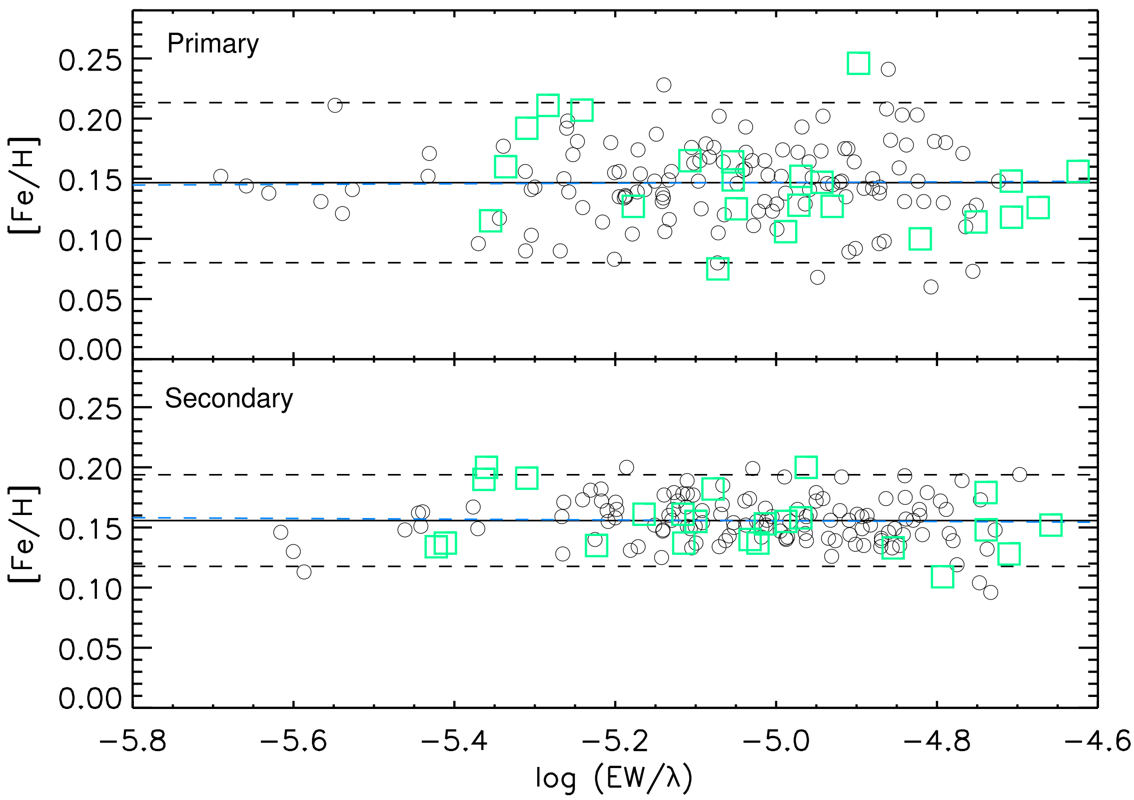

Figure 2.1 Top panels: [Fe/H] of the HAT-P-1 stellar binary derived on a line-by-line basis with respect to the Sun as a function of lower EP; open circles and green squares represent Fe I and Fe II lines, respectively. Solid lines show the locations of mean [Fe/H], while dashed lines represent twice the standard deviation, $\pm 2\sigma$. Bottom panels: same as in the top panels but as a function of reduced EW.

Table 2.2 Differential elemental abundances for HAT-P-1.

Element	Primary[a]	Secondary[a]	Δ[X/Fe][b]
[C I/Fe]	−0.158 ± 0.036	−0.156 ± 0.030	0.002 ± 0.015
[O I/Fe]	−0.063 ± 0.024	−0.067 ± 0.034	−0.004 ± 0.020
[Na I/Fe]	−0.067 ± 0.021	−0.065 ± 0.008	0.002 ± 0.016
[Mg I/Fe]	−0.060 ± 0.020	−0.050 ± 0.008	0.011 ± 0.014
[Al I/Fe]	−0.025 ± 0.018	−0.019 ± 0.011	0.006 ± 0.020
[Si I/Fe]	−0.004 ± 0.012	−0.002 ± 0.007	0.001 ± 0.008
[S I/Fe]	−0.090 ± 0.021	−0.097 ± 0.015	−0.007 ± 0.011
[Ca I/Fe]	0.009 ± 0.011	0.009 ± 0.008	0.000 ± 0.009
[Sc II/Fe]	0.052 ± 0.017	0.042 ± 0.014	−0.010 ± 0.012
[Ti I/Fe]	0.006 ± 0.012	0.006 ± 0.008	0.000 ± 0.009
[Ti II/Fe]	0.031 ± 0.015	0.023 ± 0.010	−0.008 ± 0.012
[V I/Fe]	0.017 ± 0.019	0.014 ± 0.012	−0.003 ± 0.014
[Cr I/Fe]	−0.032 ± 0.011	−0.018 ± 0.008	0.014 ± 0.009
[Cr II/Fe]	−0.032 ± 0.018	−0.022 ± 0.015	0.010 ± 0.013
[Mn I/Fe]	−0.055 ± 0.018	−0.044 ± 0.018	0.011 ± 0.012
[Co I/Fe]	−0.031 ± 0.015	−0.023 ± 0.011	0.008 ± 0.014
[Ni I/Fe]	−0.017 ± 0.011	−0.008 ± 0.006	0.009 ± 0.008
[Cu I/Fe]	−0.094 ± 0.012	−0.102 ± 0.015	−0.008 ± 0.010
[Zn I/Fe]	−0.112 ± 0.027	−0.106 ± 0.021	0.007 ± 0.009
[Sr I/Fe]	0.043 ± 0.019	0.031 ± 0.015	−0.012 ± 0.014
[Sr II/Fe]	−0.016 ± 0.019	−0.018 ± 0.015	−0.002 ± 0.014
[Y II/Fe]	0.019 ± 0.042	0.023 ± 0.029	0.004 ± 0.017
[Zr II/Fe]	0.021 ± 0.013	0.036 ± 0.012	0.015 ± 0.012
[Ba II/Fe]	0.072 ± 0.029	0.056 ± 0.013	−0.016 ± 0.018
[La II/Fe]	0.058 ± 0.017	0.065 ± 0.009	0.008 ± 0.014
[Ce II/Fe]	0.030 ± 0.027	0.028 ± 0.023	−0.002 ± 0.015

[a] Relative to the Sun.

[b] Secondary star relative to primary star.

The errors in the differential abundances correspond to the standard error of the mean added in quadrature to the errors introduced by the uncertainties in our atmospheric parameters following the method of Epstein et al. (2010). All elemental abundances (with the primary as reference star) have uncertainties ≤ 0.020 dex, which further underscores the advantages with a strictly differential analysis. The mean abundance difference of all elements between the secondary and primary is $+0.001 \pm 0.006$ dex ($\sigma = 0.008$ dex, secondary - primary), with no elemental abundance differing by more than 0.016 dex (18 out of 24 elements differ by ≤ 0.010 dex). Indeed, of the 26 species in Table 2.2, only three have differences outside the 1σ errors, which may suggest that we have in fact been overly conservative in the uncertainty estimations. For all purposes, the primary and secondary star in HAT-P-1 are chemically indistinguishable.

2.4. Discussion

The focus of this discussion is to examine the possible connection between planet formation and stellar host composition in the HAT-P-1 binary. Given that the secondary star in the HAT-P-1 stellar binary is known to harbor a giant planet, our high precision chemical abundances may place new constraints on the planet formation process, at least in this system.

As noted in the introduction, Meléndez et al. (2009) and follow-up studies (Ramírez et al. 2009, 2010) discovered that the Sun shows deficiency in refractory elements relative to volatiles when compare to the majority ($\sim 80-90\%$) of solar twins. The deficiencies correlate with the condensation temperature (T_c) of the elements such that the abundances of refractory elements ($T_c \geq 900$ K) decrease (Sun - solar twins) with increasing T_c. They argue that the special abundance pattern of the Sun is due to dust condensation and terrestrial planet formation in the proto-solar disc that for some reason proceeded more

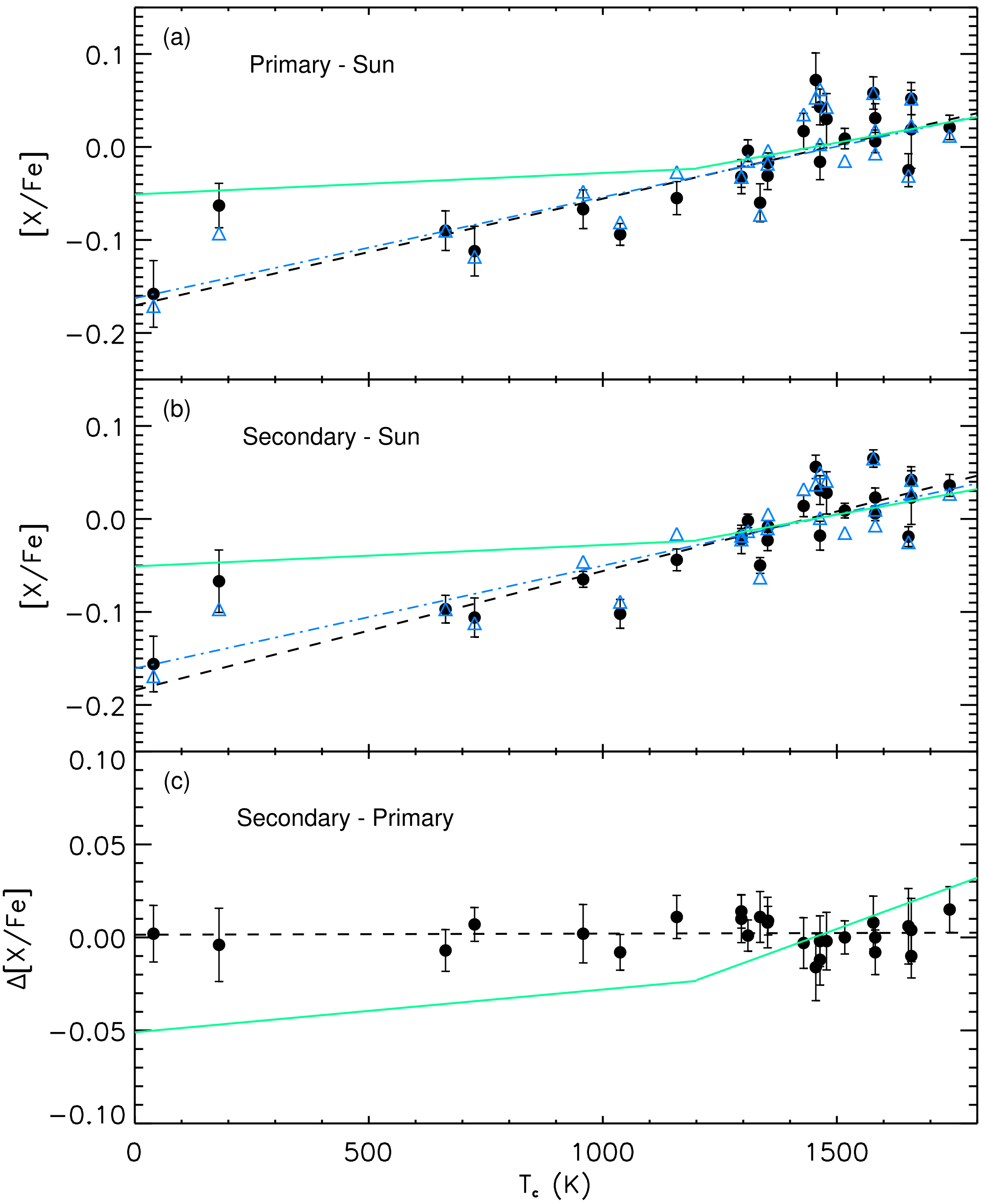

Figure 2.2 Differential elemental abundances of HAT-P-1 stellar binary relative to our solar abundances and to each other as a function of dust condensation temperature; filled circles and blue triangles represent [X/Fe] without and with GCE corrections, respectively. Black dashed lines and blue dot-dashed lines show the fitting slopes of our results without and with GCE corrections, respectively. Green solid lines show the mean trend of solar twin stars according to Meléndez et al. (2009).

efficiently than for the majority of solar twins. They then argue that terrestrial planets over giant planets as the cause for the peculiar abundance signature due to the presence of a break at $T_c \approx 1200\,\mathrm{K}$ (much higher than the expected temperatures in the proto-planetary disc where the Solar system giant planets formed), the required amount of refractory material necessary to imprint the signature ($4\,\mathrm{M}_\oplus$) and the higher frequency of stars sharing the solar abundance pattern that do *not* have a close-in giant planet.

We note however that Önehag et al. (2014) propose that the abundance differences found by Meléndez et al. (2009) are not the result of planet formation but are imprinted by dust-gas separation in the interstellar medium prior to star formation based on their finding that all of their 14 stars in the open cluster M67 resemble more the Sun than the solar twins of Meléndez et al. (2009). They conclude that the Sun formed in an unusually dense stellar environment like M67. The existence of a high temperature break in T_c and the apparent correlation with absence of close-in giant planets are not easily understood in that scenario however.

Our high quality data allow us to make robust conclusions about the [X/Fe] – T_c slopes of the HAT-P-1 stellar binary. Fig. 2.2 shows the differential abundances of HAT-P-1 primary and secondary star relative to the Sun and relative to each other versus T_c (Lodders 2003)[3]. All the elemental abundances were used to derive the slopes. The slopes of linear fitting for both stars compared to the Sun are positive and identical within errors: $(1.15 \pm 0.10) \times 10^{-4}$ dex K^{-1} and $(1.28 \pm 0.08) \times 10^{-4}$ dex K^{-1} for primary and secondary star, respectively. These slopes are very similar to the trends of refractories of the average of solar twins relative to the Sun (Meléndez et al. 2009; Ramírez et al. 2009), which with their interpretation would imply that both binary components formed less terrestrial planets than the Sun. This is consistent with the expectation that the presence of close-in giant planets prevents the

[3][O/Fe] of both stars relative to the Sun would fall to the fitting trends while Δ[O/Fe] (relative to each other) would be 0.03 dex larger if NLTE corrections are adopted from Fabbian et al. (2009).

formation or survival of terrestrial planets (Ida & Lin 2004). The positive slopes can also arise from Galactic chemical evolution (GCE). Therefore we applied the GCE corrections on our [X/Fe] values based on the studies of González Hernández et al. (2013). We adopted the González Hernández et al. (2013)'s data and fitting trends to derive the values of [X/Fe] at [Fe/H] ~ 0.15 dex to correct our results. The final results with GCE corrections only show tiny differences of the general trends (see Fig. 2.2a,b) which indicate that these positive slopes can not be erased even after GCE corrections.

When comparing the two HAT-P-1 components relative to each other, the slope of [X/Fe] – T_c is non-existent (Fig. 2.2c): $(0.60 \pm 6.36) \times 10^{-6}$ dex K^{-1}. As stated before, the mean elemental abundance difference between the secondary and primary star is +0.001 ± 0.006 dex (σ = 0.008 dex, secondary - primary). Clearly, the two stars have indistinguishable chemical compositions, which is interesting given the detection of a close-in giant planet with mass ~ 0.53 $M_{Jupiter}$ around the secondary star. We conclude that the formation process of giant planets does not necessarily affect the chemical pattern of the host star, which supports the conclusions of Meléndez et al. (2009) and Ramírez et al. (2009). This is contrary to the difference of 0.04 ± 0.01 dex seen in 16 Cyg A+B (Ramírez et al. 2011) but is consistent with the results from Schuler et al. (2011a).

Assuming for the moment that the 16 Cyg abundance differences are real, one possible explanation could be the higher mass (2.4 $M_{Jupiter}$) of the 16 Cyg planet (Plávalová & Solovaya 2013): it is still possible that such a more massive planet imprints a chemical signature in the host star. We note, however, the stellar masses in HAT-P-1 are slightly higher (1.16 and 1.12 $M_{\odot}$, Bakos et al. 2007) than in 16 Cyg (1.05 and 1.00 $M_{\odot}$, Ramírez et al. 2011), which makes the convection zone less massive and thus more prone to chemical imprints from planet formation. Albeit the smaller convection zone in HAT-P-1 would make it easier to imprint a planet signature, higher mass stars seem to have shorter disc lifetimes (Williams & Cieza 2011), making thus more difficult to imprint any planet signature in HAT-P-1 than in 16

Cyg. Which of these effects that dominate would depend on the exact size of the convection zone at the time of the accretion and the amount of material heavier than Helium locked up in the giant planet. For the time being, we conclude that the formation of giant planets do not necessarily have to introduce chemical signatures in their host stars.

Our detailed study of the HAT-P-1 double system underscores how high precision differential abundance measurements in binary stars with planets can provide important constraints on planet formation. Further efforts are needed to examine the physical characteristics and chemical abundances for additional stellar binaries with giant or terrestrial planets in order to understand the formation and evolution of planetary systems.

Acknowledgements

This work has been supported by the Australian Research Council (grants FL110100012 and DP120100991). J. M. thanks FAPESP (2012/24392-2). The authors thank the ANU Time Allocation Committee for awarding observation time to this project. The authors wish to recognize and acknowledge the very significant cultural role and reverence that the summit of Mauna Kea has always had within the indigenous Hawaiian community. We are most fortunate to have the opportunity to conduct observations from this mountain.

CHAPTER 3

THE DETAILED CHEMICAL COMPOSITION OF THE TERRESTRIAL PLANET HOST KEPLER-10

Context and contributions

The chapter is originally published as *'The detailed chemical composition of the terrestrial planet host Kepler-10'*, F. Liu, D. Yong, M. Asplund, I. Ramírez, J. Meléndez, B. Gustafsson, L. M. Howes, I. U. Roederer, D. L. Lambert, T. Bensby, 2016, MNRAS, 456, 2636. Modifications of texts have been made in section 3.1 and 3.3. This chapter is included in the thesis as a representation of my contibution to the chemical signatures of planet formation in a terrestrial planet host star. The observations were taken by the co-authors while I have done all the data reductions and scientific analysis presented

in this paper, except for the derivation of stellar ages for the sample stars which was done by my collaborator, I. Ramírez. The whole paper was written by myself with the suggestions provided by the co-authors.

3.1. Introduction

The scenario put forward by Meléndez et al. (2009) makes a testable prediction that the host star of a system with terrestrial planets should also exhibit a depletion in refractory elements relative to volatile elements when compared to otherwise identical stars (i.e., stellar parameters, ages, birth locations). Therefore, in order to test this scenario, we need to conduct high precision chemical abundance studies of stars hosting terrestrial planets relative to similar other stars without such planets. Kepler-10 hosts two planets, Kepler-10b and Kepler-10c (Batalha et al. 2011). Dumusque et al. (2014) reported that the mass of Kepler-10b is 3.33 ± 0.49 $M_{\oplus}$ with a density of 5.8 ± 0.8 g cm^{-3}, while the mass of Kepler-10c is 17.2 ± 1.9 $M_{\oplus}$ with a density of 7.1 ± 1.0 g cm^{-3}. Dumusque et al. (2014) characterized Kepler-10b and Kepler-10c as a hot Earth-like planet and a Neptune mass solid planet, respectively, although Rogers (2015) argued that Kepler-10c is likely to have a substantial volatile envelope and thus not rocky. The Kepler-10 system is thus a very suitable target to identify any chemical signatures of terrestrial planet formation. In particular, if the scenario presented by Meléndez et al. (2009) is correct, we should expect to find a deficiency of refractory elements relative to volatile elements in the photosphere of Kepler-10 when compared to other stars sharing similar stellar parameters but without known planets.

Here we present a strictly line-by-line differential abundance analysis of Kepler-10 and a sample of stellar twins to explore whether or not there is a chemical signature of terrestrial planet formation.

3.2. Observations and data reduction

We obtained high resolution and high SNR spectra with the Canada France Hawaii Telescope (CFHT), the Hobby-Eberly Telescope (HET) and the Magellan Clay Telescope.

We observed Kepler-10 with the Echelle SpectroPolarimetric Device for the Observation of Stars (ESPaDOnS) (Manset & Donati 2003) at the CFHT during June 2013. The spectral revolving power is 68,000 and the spectral range is 3800 – 8900 Å. In total eight spectra with exposures of 1700 s each were obtained. The individual frames were combined into a single spectrum with SNR ≈ 300 per pixel in most wavelength regions. A solar spectrum with even higher SNR (≈ 500 per pixel) was obtained by observing the asteroid Vesta. The spectra were reduced with the CFHT data reduction tool 'Libre-Espirit' while the continuum normalizations were addressed with IRAF[1].

We also observed Kepler-10 with the High Resolution Spectrograph (HRS; Tull 1998) on the HET at McDonald Observatory during 2011 May. A total integration time of 6.8 h was needed to achieve SNR > 350 per pixel. The spectrum has a spectral resolving power of 60,000 and covers 4100 to 7800 Å, with a gap of about 100 Å around 6000 Å. A solar spectrum with higher spectral resolution (R = 120,000) and higher SNR (≈ 500 per pixel) was obtained by observing the asteroid Iris. The HRS-HET data were reduced using IRAF's echelle package.

We selected 14 stars identified as Kepler-10 stellar twins, based on the similarity of their stellar parameters (T_{eff}, log g, [Fe/H]) to those of Kepler-10, using an updated version of the stellar parameter catalog of Ramírez & Meléndez (2005) and from the sample by Bensby et al. (2014). The comparison star sample was chosen randomly such that any individual star was not necessarily included in planet search programmes. Those "Kepler-10 twins" were

[1]IRAF is distributed by the National Optical Astronomy Observatory, which is operated by Association of Universities for Research in Astronomy, Inc., under cooperative agreement with National Science Foundation.

observed using the Magellan Inamori Kyocera Echelle (MIKE) spectrograph (Bernstein et al. 2003) during two runs: 2014 June and 2015 June. The spectrograph delivers wavelength coverage from about 3300 to 5000 Å (blue arm) and 4900 to 9400 Å (red arm) at a spectral resolving power of 83,000 and 65,000, respectively, the SNR exceeded 300 per pixel at 6000 Å. A solar spectrum using the asteroid Vesta was obtained each night in the first run. We reduced the spectra with standard procedures which include bias subtraction, flat-fielding, scattered-light subtraction, 1D spectral extraction, wavelength calibration, and continuum normalization, with IRAF.

Our thick disc twins were not observed with the northern telescopes, nor was it possible to observe Kepler-10 from the southern Magellan site. This limits our strictly differential study to the use of the solar-spectrum observations as a test calibration. We also carried out a number of tests which ensure that our results are not compromised by the use of different spectroscope/telescope combinations. The most important of these tests are described later in this paper.

3.3. Stellar atmospheric parameters

The line list employed in our analysis was adopted mainly from Asplund et al. (2009) and complemented with additional unblended lines from Bensby et al. (2005) and Neves et al. (2009); in a differential abundance analysis the accuracy of the *gf* values does not influence the results. Equivalent widths (EWs) were measured using the ARES code (Sousa et al. 2007) for most lines. The EWs for C, O, Mg, Al, S, Mn, Cu and Zn (i.e., elements with fewer lines) were measured manually with the *splot* task in IRAF. Weak (< 5 mÅ) and strong (> 110 mÅ) lines were excluded from the analysis. The atomic line data adopted for the abundance analysis can be found online (Liu et al. 2016b). We emphasize that in a differential analysis such as ours, the atomic data have essentially no influence on the results since Kepler-10 and its twins have very similar stellar parameters.

We performed a 1D, local thermodynamic equilibrium (LTE) abundance analysis using the 2013 version of MOOG (Sneden 1973; Sobeck et al. 2011) with the ODFNEW grid of Kurucz model atmospheres (Castelli & Kurucz 2003). Detailed description of our analysis technique can be found in chapter 1.5. We note that lines whose abundances departed from the average by $> 2.5\sigma$ were clipped.

Figure 3.1 shows an example of determining the stellar parameters of Kepler-10. The adopted stellar parameters satisfy the excitation and ionization balance in a differential sense. The best-fitting $\pm$ 1σ for the [Fe/H] versus EP roughly corresponds to an error in $T_{\rm eff}$ of 10 K, similarly for the reduced EW [log (EW/λ], which corresponds to an error of $\sim$ 0.02 - 0.03 km s^{-1} in $\xi_{\rm t}$. The abundance difference in Fe I and Fe II = 0.000 $\pm$ 0.006, which constrains $\log g$ to a precision of 0.02 - 0.03.

For the 14 stellar twins, differential stellar parameters were also obtained by the line-by-line differential analysis as described before, but relative to Kepler-10 rather than the Sun, i.e., Stellar twins (Magellan) − Kepler-10 (HET or CFHT). The adopted initial parameters for Kepler-10 were $T_{\rm eff}$ = 5700 K, $\log g$ = 4.35, [Fe/H] = −0.15, $\xi_{\rm t}$ = 1.00 km s^{-1}, taken from the Kepler-10 analysis relative to the Sun. We emphasize that the absolute values are not crucial for our differential abundance analysis. We did not consider α enhancements in the thick disc stars in the model atmospheres but this does not affect our results, in particular not in the differential study of Kepler-10 relative to its thick disc twins. We assume that the stellar spectrum is defined solely by the stellar parameters $T_{\rm eff}$, $\log g$, $\xi_{\rm t}$ and abundances, i.e., other individual stellar parameters, e.g. describing stellar activity is not considered in this study.

The final adopted atmospheric parameters of Kepler-10 and its stellar twins are listed in Table 3.1. The uncertainties in the stellar parameters were derived with the method described by Epstein et al. (2010) and Bensby et al. (2014), which accounts for the co-variances between changes in the stellar parameters and the differential abundances. Excellent precision was

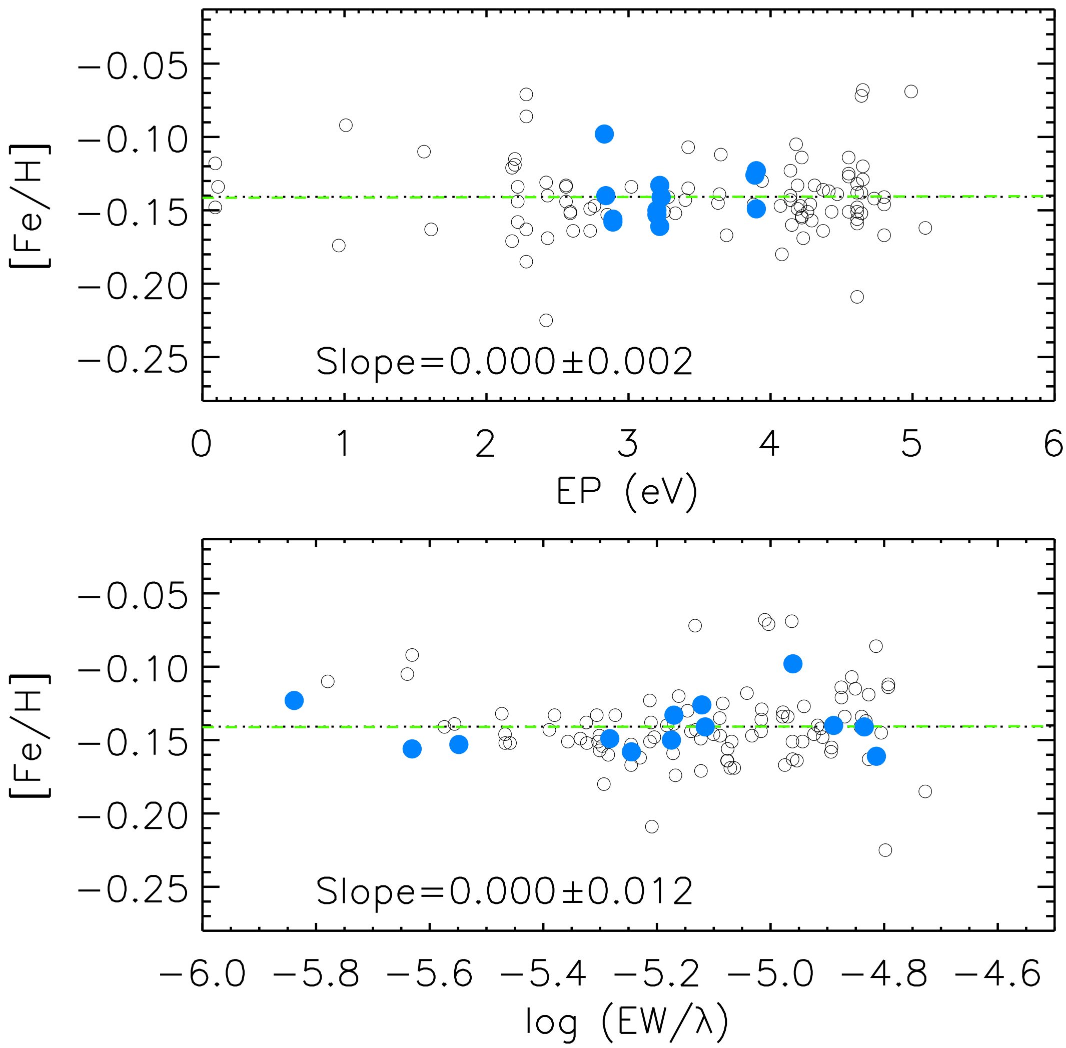

Figure 3.1 Top panel: [Fe/H] of Kepler-10 derived on a line-by-line basis with respect to the Sun as a function of lower EP; open circles and blue filled circles represent Fe I and Fe II lines, respectively. The black dotted line shows the location of mean [Fe/H], the green dashed line represents the best fit to the data. Bottom panel: same as in the top panel but as a function of reduced EW.

achieved due to the strictly differential method, which should greatly reduce the systematic errors from atomic line data and shortcomings in the 1D LTE modelling of the stellar atmospheres and spectral line formation (e.g., Asplund 2005).

Table 3.1 Stellar parameters of Kepler-10 and its stellar twins.

Object	$T_{\rm eff}$ (K)	$\log g$	ξ_t (km s^{-1})	[Fe/H]	Probability[a] Thin disc (%)	Probability[a] Thick disc (%)	Population	Age (Gyr)
Kepler-10[b]	5697±10	4.40±0.03	0.98±0.02	−0.141±0.009	3	96	thick	8.4±1.0
Kepler-10[c]	5695±13	4.38±0.04	0.96±0.03	−0.143±0.015	3	96	thick	9.0±1.1
HD 88084[d]	5780±13	4.40±0.03	1.05±0.03	−0.091±0.012	98	2	thin	5.8±1.4
HD 115382[d]	5776±12	4.38±0.03	1.05±0.03	−0.089±0.010	92	8	thin	6.7±1.4
HD 126525[d]	5687±19	4.50±0.03	1.00±0.04	−0.063±0.014	91	9	thin	2.6±1.5
HD 117939[d]	5729±13	4.45±0.03	1.00±0.03	−0.176±0.016	60	40	thin	4.7±1.5
HIP 113113[d]	5706±13	4.42±0.04	0.96±0.03	−0.071±0.012	58	42	thin	5.6±1.6
HD 117126[d]	5779±18	4.25±0.04	1.10±0.03	−0.032±0.015	55	44	thick	8.2±0.5
HD 115231[d]	5708±15	4.43±0.04	1.00±0.04	−0.095±0.015	38	61	thick	5.8±1.6
HD 106210[d]	5701±13	4.40±0.04	0.96±0.03	−0.131±0.014	18	80	thick	7.0±1.6
HIP 109821[d]	5772±14	4.32±0.03	1.06±0.03	−0.087±0.011	17	82	thick	7.7±0.8
HD 87320[d]	5666±12	4.40±0.03	0.93±0.03	−0.149±0.010	11	87	thick	7.5±1.4
HIP 96124[d]	5636±13	4.41±0.04	0.93±0.03	−0.197±0.012	9	90	thick	8.2±1.6
HIP 101857[d]	5798±14	4.34±0.03	1.06±0.03	+0.029±0.012	2	96	thin[e]	6.4±0.8
HIP 9381[d]	5734±14	4.39±0.04	1.02±0.03	−0.238±0.012	1	96	thick	8.0±1.7
HIP 99224[d]	5754±18	4.27±0.04	1.03±0.04	−0.004±0.014	0	96	thick	8.2±0.6

[a] Probabilities calculated based on kinematics (Ramírez et al. 2013). [b] Parameters derived with HET data.
[c] Parameters derived with CFHT data. [d] Parameters derived using Kepler-10 (HET) as the reference.
[e] HIP 101857 is assigned to the thin disc because of its abundance pattern rather than kinematics.

3.4. Results

3.4.1. Elemental abundances

Having established the stellar parameters for Kepler-10 and its stellar twins, we derived chemical abundances relative to the Sun for an additional 17 elements from atomic lines: C, O, Na, Mg, Al, Si, S, Ca, Sc, Ti, V, Cr, Mn, Co, Ni, Cu and Zn. We also obtained differential abundances of Kepler-10's stellar twins relative to Kepler-10. Hyperfine-structure splitting (HFS) was considered for Sc, V, Cr, Mn and Cu using data from Kurucz & Bell (1995). Departures from LTE were considered for the 777 nm oxygen triplet lines according to Ramírez et al. (2007) and the typical size of the correction is ≈ -0.01 dex. The errors in the differential abundances were calculated following the method of Epstein et al. (2010): the standard errors in the mean abundances, as derived from the different spectral lines, were added in quadrature to the errors introduced by the uncertainties in the atmospheric parameters. Most derived elemental abundances have uncertainties ≤ 0.02 dex, which further underscores the advantages of a strictly differential analysis. Indeed, when considering all elements, the average uncertainty is only 0.014 ± 0.002 ($\sigma = 0.006$) for Kepler-10 relative to the Sun.

We first compare the abundances of Kepler-10 as derived from HET and CFHT spectra (Figure 3.2). The values of T_c (specifically 50% condensation temperature for a solar-composition mixture) are given by Lodders (2003). The average abundance difference Δ[X/H] (HET − CFHT) is -0.004 ± 0.005 ($\sigma = 0.021$), consistent with zero. We perform a least-squares linear fit weighted by the errors in abundances while the uncertainties of the fitting are calculated considering the chi-square merit function and the relative derivatives[2]. We note that there is a slight negative trend between Δ[X/H] versus T_c with a slope of $(-0.19 \pm 0.09) \times 10^{-4}$ K^{-1}, which is mainly driven by the two volatile elements, C and O. We adopt the

[2]We applied the same manner to all the following linear fits.

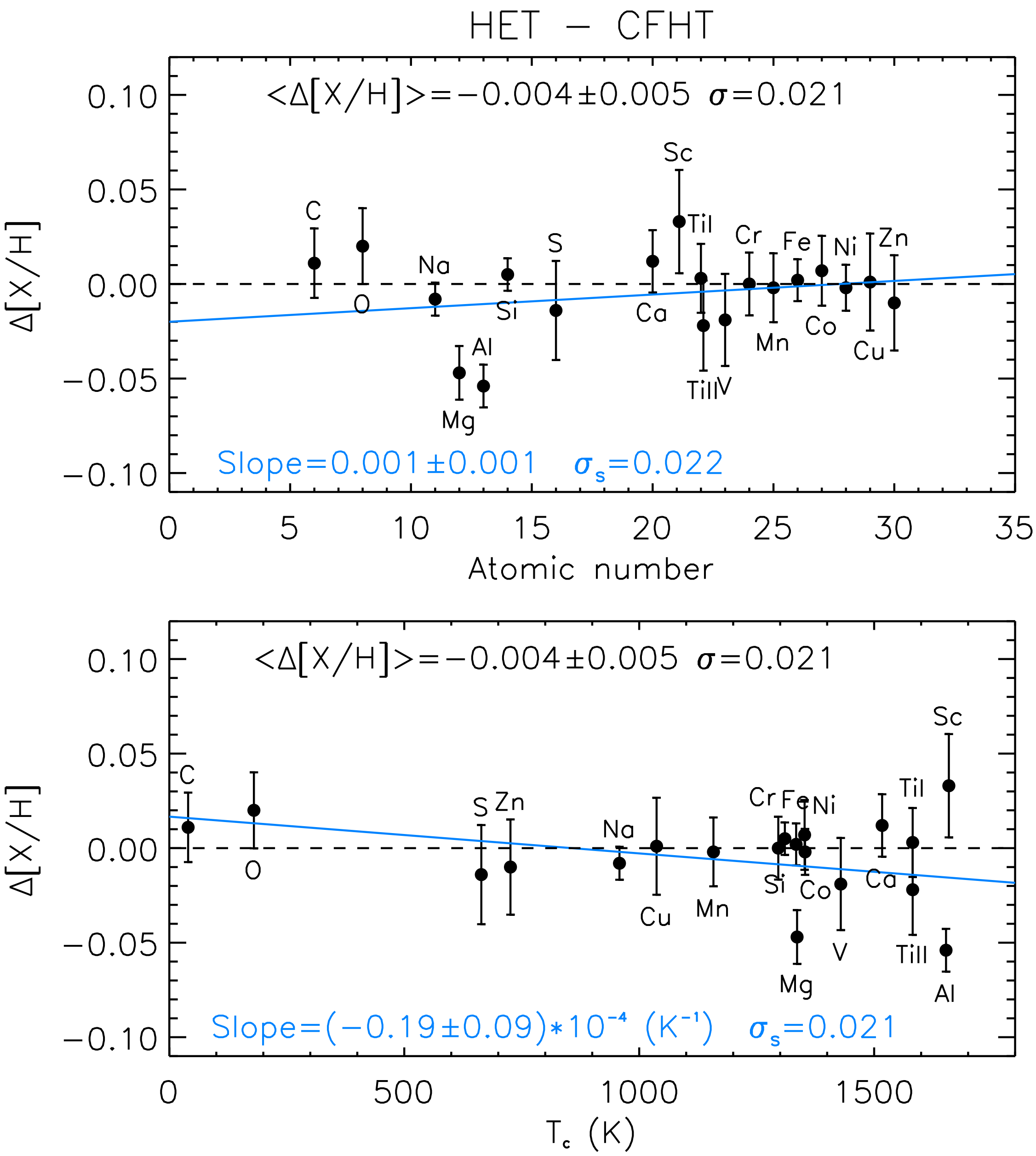

Figure 3.2 Top panel: abundance differences for Kepler-10 from two different telescopes, Δ[X/H] (HET − CFHT), versus atomic number; the blue solid line represents the linear fit to the data; σ_s is the dispersion about the linear fit. Bottom panel: abundance differences as a function of condensation temperature T_c.

results derived from the HET spectra. This choice does not affect our conclusions since the differences between HET and CFHT data are very small. We do explore the effects of using CFHT data below.

Another issue regarding systematic offsets that we need to consider carefully is whether the choice of the spectrograph affects the results. According to Bedell et al. (2014), systematic offsets may be introduced when comparing the results using spectra obtained from different instruments or when measurements are not performed consistently. While the Kepler-10 differential abundances were measured based on HET spectra, differential abundances for the Kepler-10 stellar twins were measured based on Magellan spectra. Therefore, it is crucial to check whether any systematic offsets exist. In Figure 3.3, we plot Δ[X/H] as a function of T_c derived from solar spectra obtained with different instruments [Sun (Magellan − HET)]. In that figure, we also include a comparison of the Sun (Magellan − CFHT) from Bedell et al. (2014). The average difference in our Δ[X/H] is 0.000 ± 0.004 (σ = 0.015) and the slope of the linear fit is $(-0.12 \pm 0.05) \times 10^{-4}$ K^{-1}. The systematic offsets in our work are much smaller than that in Bedell et al. (2014). One possible reason for this difference is that in Bedell et al. (2014), the normalization of spectra and the measurement of EWs involved not only different instruments, but also different investigators. In this work, the entire analysis was done consistently by one person using the same approach, minimizing the possible systematic errors introduced by comparing the results based on different instruments.

The discovery paper by Batalha et al. (2011) reported [Fe/H] = −0.15 ± 0.04 for Kepler-10. We confirm that Kepler-10, with [Fe/H] = −0.141 ± 0.009, is metal-poor relative to the Sun[3]. Kepler-10 is also older than the Sun with an age of 8.4 ± 1.0 Gyr from our derivation, see below. The total space velocity [$V_{\rm tot} = U^2 + V^2 + W^2)^{1/2}$] of Kepler-10 is 97.0 km s^{-1} and the kinematic probability of being from the thick disc is 96% (Dumusque et al. 2014). Therefore direct comparisons of Kepler-10 to the Sun is not adequate. Kepler-10 should be compared against stars of similar metallicity and belonging to the same stellar population. For the 14 Kepler-10 stellar twins without known planets, we show the distribution in [Fe/H] and [X/H] in Figure 3.4. We calculated the Galactic space velocities U, V, W of our sample stars using data from SIMBAD data base with the equations given by e.g., Johnson & Soderblom (1987). We derived the associated probabilities of thin/thick disc membership based on the

[3]Recently, a very similar metallicity of [Fe/H] = −0.14 ± 0.02 was presented by Santos et al. (2015)

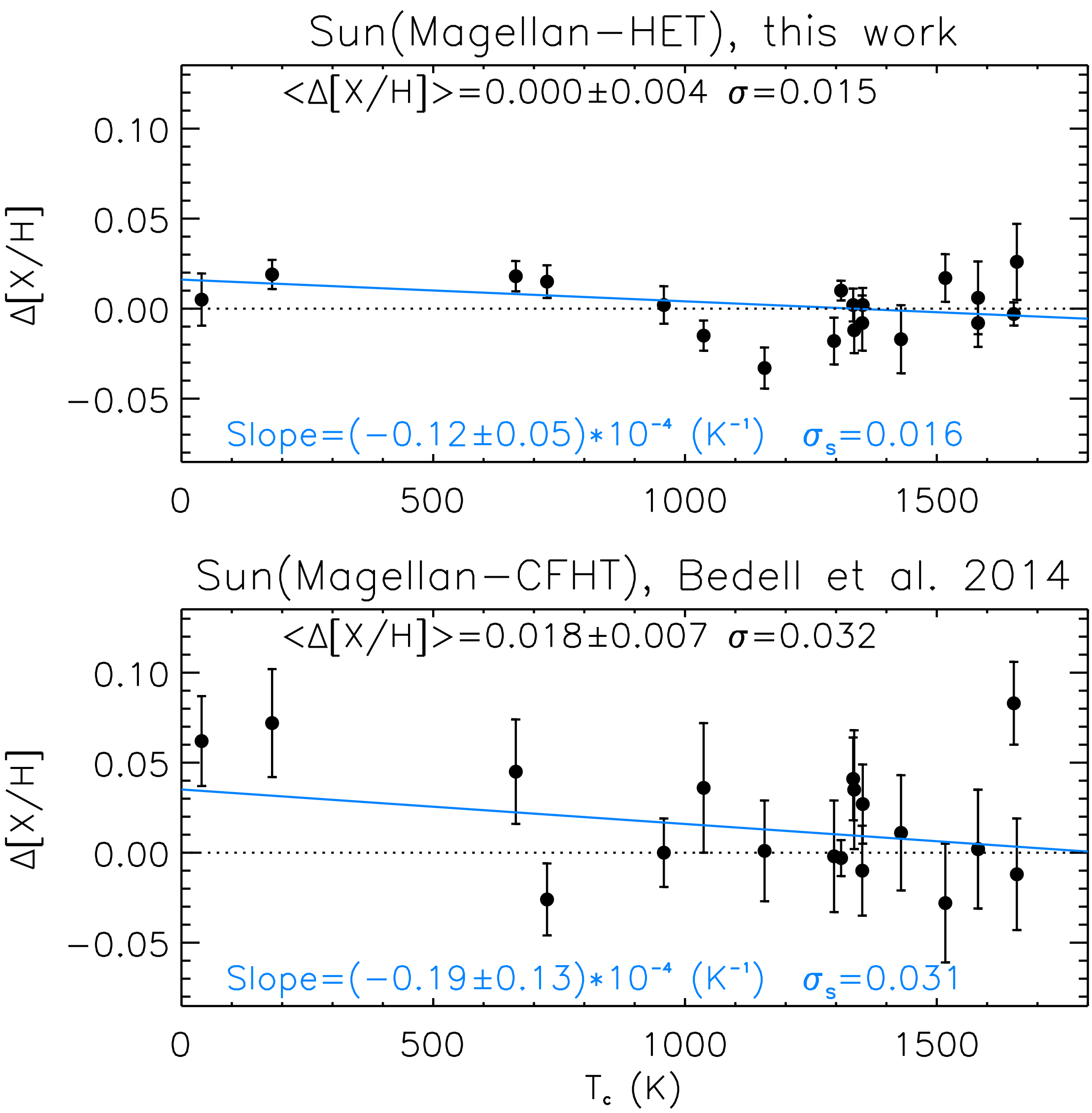

Figure 3.3 Abundance differences Δ[X/H] versus condensation temperature T_c for solar spectra obtained with different instruments (Magellan – HET) for this work (top panel) and for Bedell et al. (2014) (Magellan – CFHT) (bottom panel). The blue solid lines represent the linear fit to our data (top panel) and the Bedell et al. (2014) data (bottom panel), σ_s is the dispersion about the linear fit.

algorithm described by Ramírez et al. (2007, 2013). We computed the stellar ages using the stellar parameters and their errors as given in Table 3.1, placing them on a T_{eff} - log g plane, and comparing these locations with the theoretical isochrones of the Yonsei-Yale group (e.g., Yi et al. 2001; Kim et al. 2002). Details of our age determination technique are provided in Ramírez et al. (2014b).

We have three criteria for thick disc membership: kinematic probability > 60%, age > 7 Gyr and chemical similarity with thick disc stars. All the eight thick disc twins fulfil at least two of these criteria (see Table 3.1). The remaining programme stars are likely thin disc members. Regarding the latter criterion, it is evident from Figure 3.4 (and previous work by Reddy et al. 2006; Bensby et al. 2014) that thin and thick disc stars lie on different and well-defined trends, although there are also some objects that exhibit thick disc kinematics but thin disc abundances (Reddy et al. 2006). In the present work, we are searching for subtle chemical abundance differences among thick disc stars, so it is important that these comparison stars have thick disc chemical abundances.

3.4.2. Δ[X/H] - T_c correlations

The [X/H] ratios confirm that Kepler-10 is a thick disc object and its relatively old age further supports this. Therefore, we will compare Kepler-10 against its thick disc stellar twins in order to compensate for effects of Galactic chemical evolution (GCE). As is seen directly from Figure 3.4, the abundances of Kepler-10 show a systematical pattern relative to the linear fits in the panel that presumably display the GCE as relations between [X/H] and [Fe/H]. E.g., for the five elements with the lowest condensation temperatures, C, O, S, Zn and Na, the blue crosses representing Kepler-10 in the panels of the figure are situated on or above the redline, while for the eight elements with the highest condensation temperature, Mg, Co, Ni, V, Ca, Ti, Al and Sc, Kepler-10 is located on or below the redline. It is easy to demonstrate that if we assume that the real abundances of Kepler-10 would be on the line

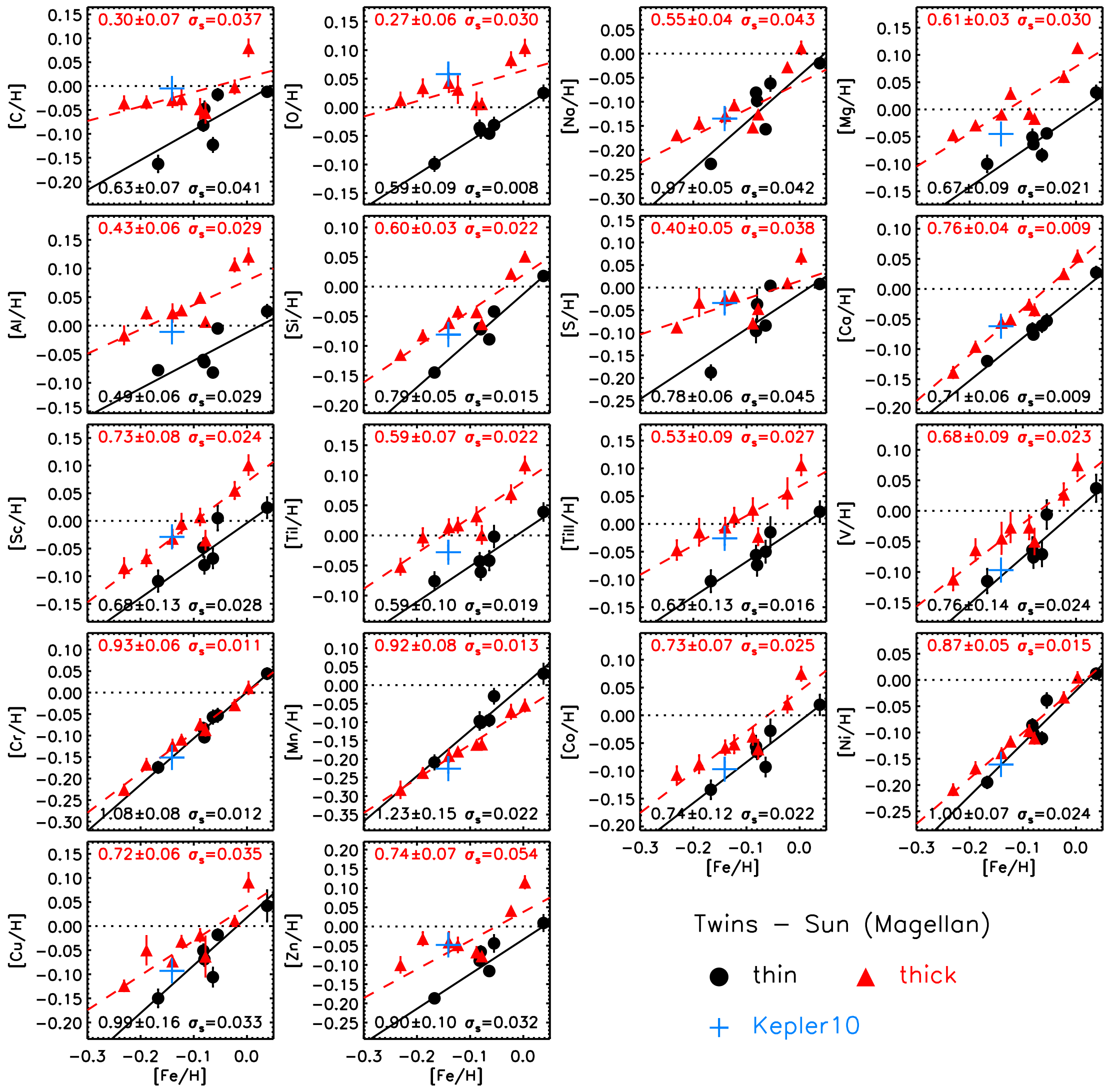

Figure 3.4 [X/H] versus [Fe/H] for various elements for the "Kepler-10 twins" (Twins – Sun (Magellan)). Linear fits for the thin disc counterparts (black circles) and thick disc (red triangles) twins are overplotted, σ_s is the dispersion about the linear fit. The location of Kepler-10 is marked (Kepler-10 – Sun (HET), blue crosses). The size of the crosses are corresponding to the error bars in [X/H] and [Fe/H].

and the observed locations are reflecting independent errors symmetrically distributed (i.e. with equally probable departures in positive or negative directions), the chance of obtaining this systematic effect with T_c by mere chance is less than 1%. In view of the fact that the present study was initiated when the super-Earths of Kepler-10 had been discovered in order to test the planetary signature of the abundance - T_c relation, the systematics of Figure 3.4 is in itself a striking confirmation, indicating that this interpretation must be favoured relative to e.g., chemical evolution effects.

To improve the precision further, we derive strictly differential abundances Δ[X/H] for the eight likely thick disc stellar twins relative to Kepler-10 in Figure 3.5 rather than relative to the Sun as the case for Figure 3.4. We find that a single linear fit provides an appropriate representation of the Δ[X/H] - T_c correlation when comparing the thick disc twins to Kepler-10. Our results demonstrate that the Δ[X/H] - T_c trends could vary from star to star, as reported by Nissen (2015). Five stars (HIP 109821, HIP 99224, HD 106210, HD 115231 and HD 117126) show positive slopes for the single linear fitting but the trends are driven mainly by the abundances of the most volatile elements C and O. HD 87320 shows a positive slope as well but with much larger scatter around the best fit. HIP 9381 and HIP 96124 show large scatters around the zero-slopes with three elements as outliers (Cr, Mn and Fe). These outlier elements could be due to the impact of GCE since these two stars are the most metal-poor and those three elements (Cr, Mn and Fe) exhibit the steepest slopes for the [X/H] versus [Fe/H] in Figure 3.4.

We average the results of the differential abundances Δ[X/H] for these eight thick disc stellar twins [i.e., <thick disc twins (Magellan)> − Kepler-10 (HET)] and show the result in Figure 3.6. As seen already directly from Figure 3.4, Kepler-10 shows a depletion of refractory elements relative to the volatile elements when compared to the average of all the thick disc stellar twins. The average difference is Δ[X/H] = 0.037 ± 0.004 (σ = 0.016). A linear fit to the data has a gradient of (0.29 ± 0.03) × 10^{-4} K^{-1}, corresponding to a > 9σ

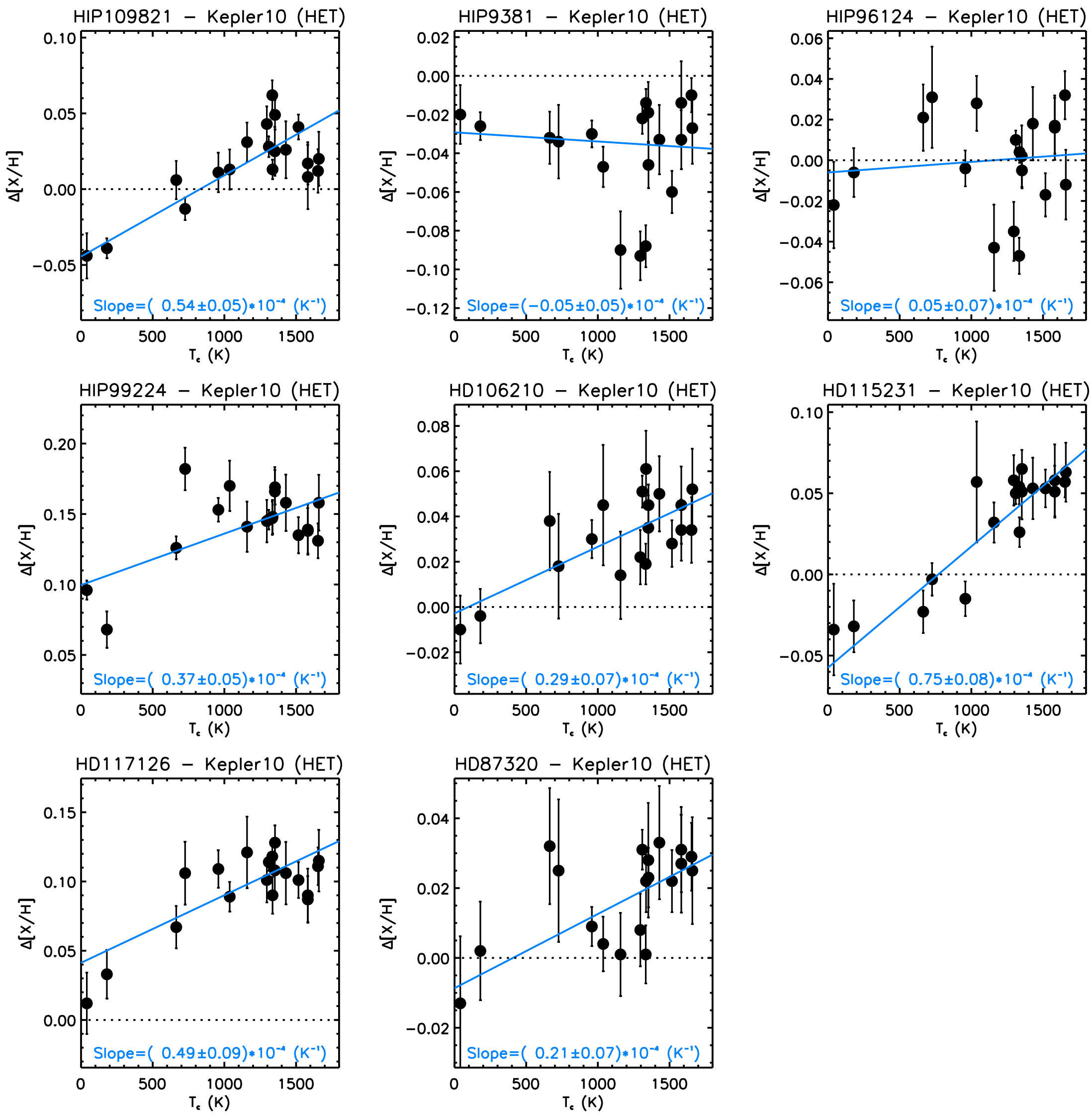

Figure 3.5 Abundance differences Δ[X/H] versus condensation temperature T_c for all the thick disc stellar twins relative to Kepler-10. The blue solid lines show the single linear fit to the results.

significance. Although the trend is mainly driven by C and O, a significant trend [slope = (0.17 ± 0.04) × 10^{-4} K^{-1}] is also present when excluding these two elements. Table 3.2 lists the adopted elemental abundances and associated uncertainties of Kepler-10 and the average of its thick disc stellar twins. In addition, all the derived elemental abundances and associated uncertainties of each programme star with relative to Kepler-10 can be found online (Liu et al. 2016b).

Although the classification of Kepler-10 as a thick disc star, on the basis of its kinematics, age and abundance pattern, one may ask how the abundance pattern relative to T_c would

Table 3.2 [X/H] for Kepler-10 and the average of its thick disc stellar twins.

Element	Kepler-10[a]	Kepler-10[b]	<Thick disc twins>[c]
C	−0.005±0.015	−0.016±0.011	−0.004±0.006
O	0.058±0.010	0.038±0.017	−0.001±0.005
Na	−0.135±0.007	−0.127±0.005	0.033±0.003
Mg	−0.045±0.013	0.002±0.006	0.044±0.004
Al	−0.011±0.005	0.043±0.010	0.050±0.004
Si	−0.081±0.006	−0.086±0.006	0.051±0.002
S	−0.034±0.022	−0.020±0.014	0.029±0.005
Ca	−0.062±0.013	−0.074±0.010	0.038±0.004
Sc	−0.029±0.018	−0.062±0.020	0.049±0.006
Ti I	−0.028±0.012	−0.031±0.014	0.043±0.005
Ti II	−0.026±0.012	−0.004±0.021	0.046±0.006
V	−0.097±0.016	−0.078±0.018	0.051±0.007
Cr	−0.151±0.012	−0.151±0.011	0.031±0.005
Mn	−0.226±0.011	−0.224±0.015	0.026±0.006
Fe	−0.141±0.009	−0.143±0.015	0.033±0.003
Co	−0.097±0.013	−0.104±0.013	0.050±0.006
Ni	−0.161±0.007	−0.159±0.010	0.054±0.004
Cu	−0.093±0.006	−0.094±0.025	0.045±0.007
Zn	−0.048±0.006	−0.038±0.025	0.039±0.006

[a] [X/H] derived with HET data, relative to the Sun.

[b] [X/H] derived with CFHT data, relative to the Sun.

[c] Δ[X/H] derived with respect to Kepler-10 (HET).

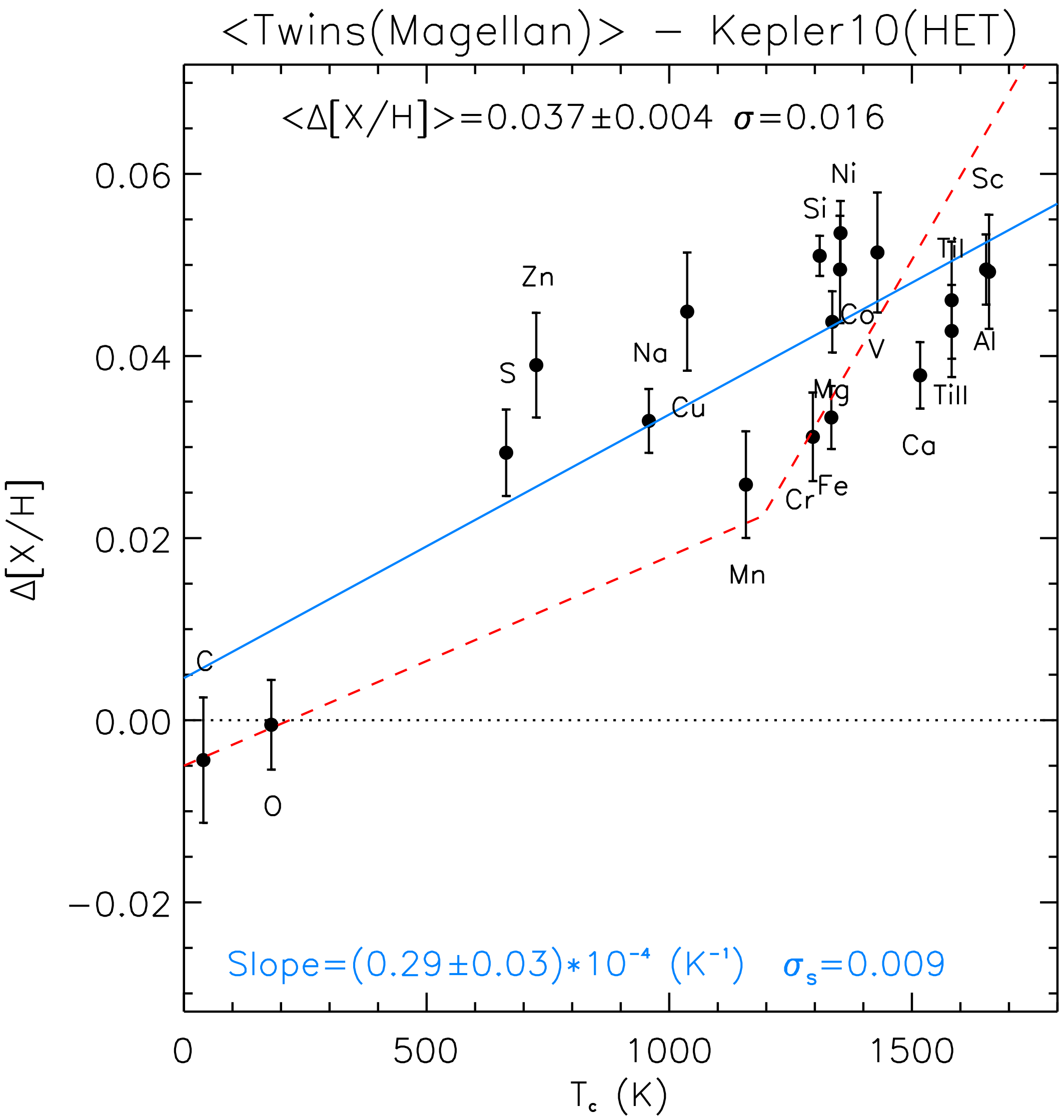

Figure 3.6 Average abundance differences Δ[X/H] versus condensation temperature T_c for the eight thick disc stellar twins relative to Kepler-10. The blue solid line represents the linear fit to the data, σ_s is the dispersion about the linear fit and the red dashed line is the fit from Meléndez et al. (2009) for solar twins – Sun, normalized to Δ[C/H].

look if compared with its thin disc counterpart stars, instead. In Figure 3.7 we display the differences between the mean of [X/H] for the thin disc stars and Kepler-10, again plotted versus T_c. A linear fit to the data has a gradient of $(0.45 \pm 0.03) \times 10^{-4}$ K^{-1}, while the dispersion about the linear fit (σ_s) is 0.044 dex. The trend excluding C and O has a gradient to be $(-0.12 \pm 0.04) \times 10^{-4}$ K^{-1} with 2.6σ significance. We see that the systematic slope of the relation still prevails, but that it is now very much dependent on C and O; the relation for the rest of the elements show a characteristic peak, corresponding to elements with T_c $\sim$ 1200 K. This demonstrates that GCE partly masks the effects of dust-depletion on the abundance pattern.

As a further check of our results, we also repeated the analysis using the CFHT Kepler-10 spectrum and analysed the stellar twins with respect to that spectrum. The results are very similar to those presented in Figures. 3.5 - 3.7.

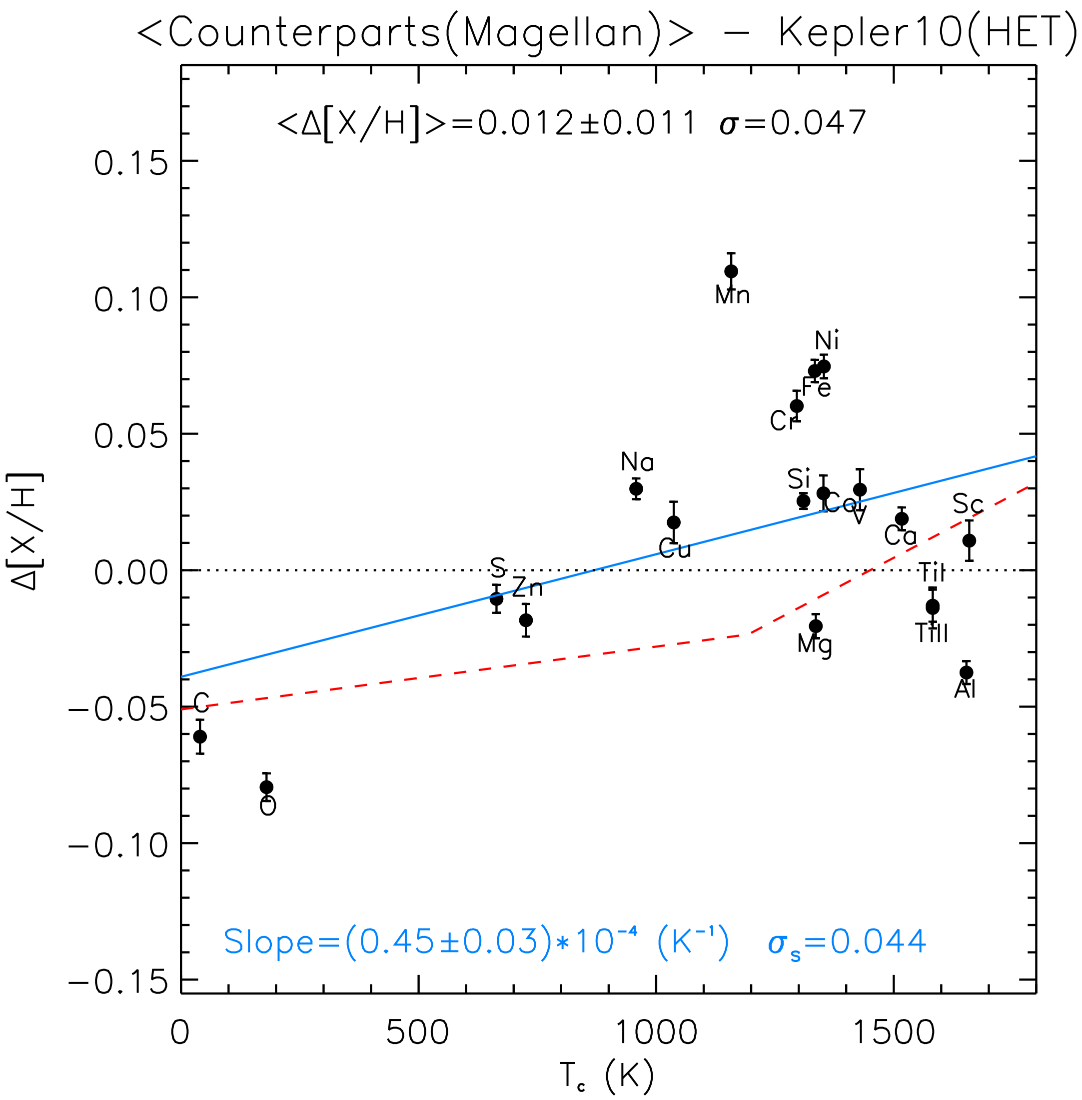

Figure 3.7 Average abundance differences Δ[X/H] versus condensation temperature T_c for the thin disc counterparts relative to Kepler-10. The blue solid line represents the linear fit to the data, σ_s is the dispersion about the linear fit and the red dashed line is the fit from Meléndez et al. (2009) for solar twins – Sun.

3.5. Discussion

As shown in Figure 3.6, there is a deficiency of refractory elements relative to volatile elements in the photosphere of the terrestrial planet host Kepler-10 when compared to the average results of its thick disc stellar twins without known planets. Using the current size of the convective zone of Kepler-10 (0.08 $M_\odot$, Siess et al. 2000), the abundance pattern corresponds to at least 13 Earth masses of rocky material (Chambers 2010) which is comparable to the total mass of planets (20 Earth masses) in the Kepler-10 system. Therefore the differences in chemical composition between Kepler-10 and its thick disc stellar twins could be attributed to the formation of terrestrial planets in the Kepler-10 system, but this requires that the lifetime of the proto-planetary disc was long enough to not deliver its dust-cleansed gas until the convection zone of the star reached its present depth. As we mentioned before, even for the thick disc twins which share similar stellar parameters and ages with Kepler-10, the Δ[X/H] - T_c correlations still vary star to star. In order to investigate this further, we show the histogram of the slopes for the single linear fitting of the T_c trends for the eight thick disc stars in Figure 3.8. The slopes exhibit a broad distribution. We note that two (HIP 9381 and HIP 96124) of the thick disc stars do not show any apparent trends, which complicates the scenario of the chemical signatures of terrestrial planets. If the Δ[X/H] - T_c trends do reflect planet formation, those two stars could be conjectured to also harbour terrestrial planets that have not yet been detected. The first one (HIP 9381) has been observed multiple times with HARPS yet no results have been published. It is also probable that other factors play a role in determining the detailed chemical composition of those stars.

Adibekyan et al. (2014) and Nissen (2015) proposed that the trends between chemical abundance and condensation temperature (T_c) could be due to the differences in the stellar ages. We plot the differential abundances Δ[X/H] - T_c slopes versus stellar ages in Figure

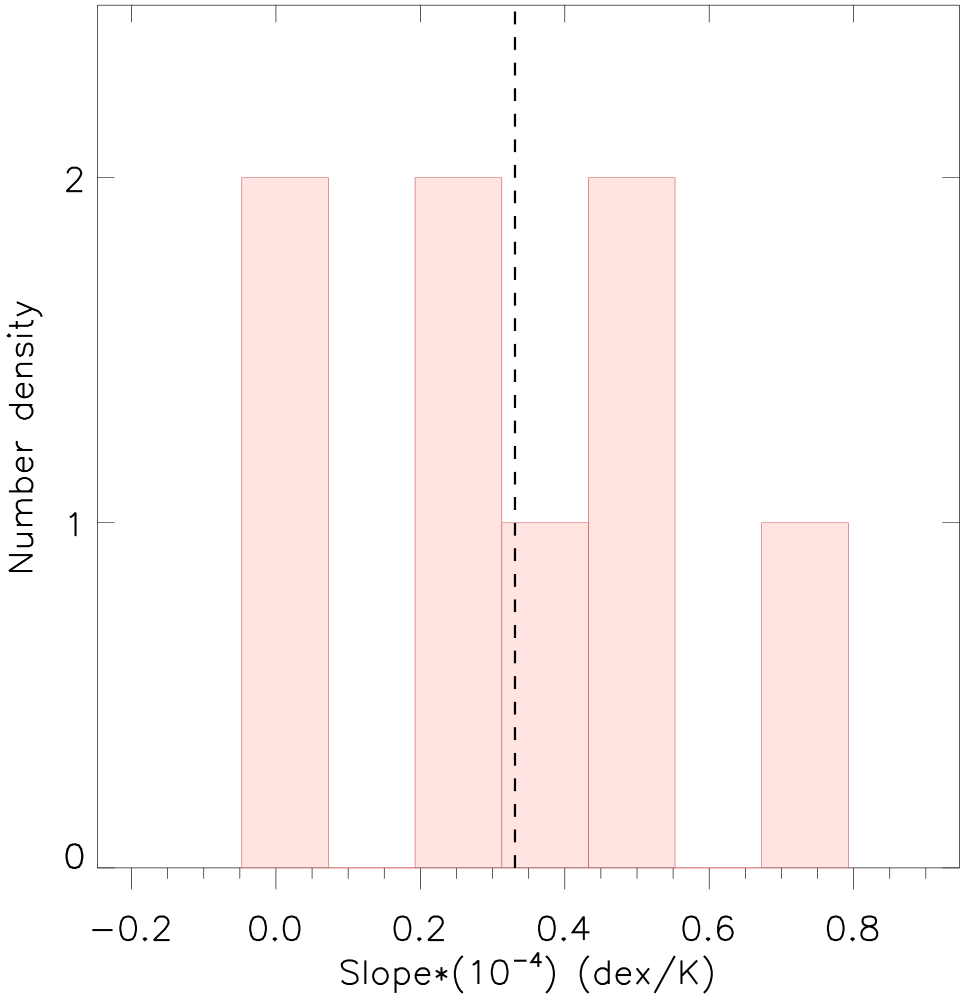

Figure 3.8 Histogram of the slopes when applying a single linear fit to Δ[X/H] - T_c correlations for the eight thick disc stellar twins. The black dashed vertical line represents the location of the mean value of Δ[X/H] versus T_c slopes.

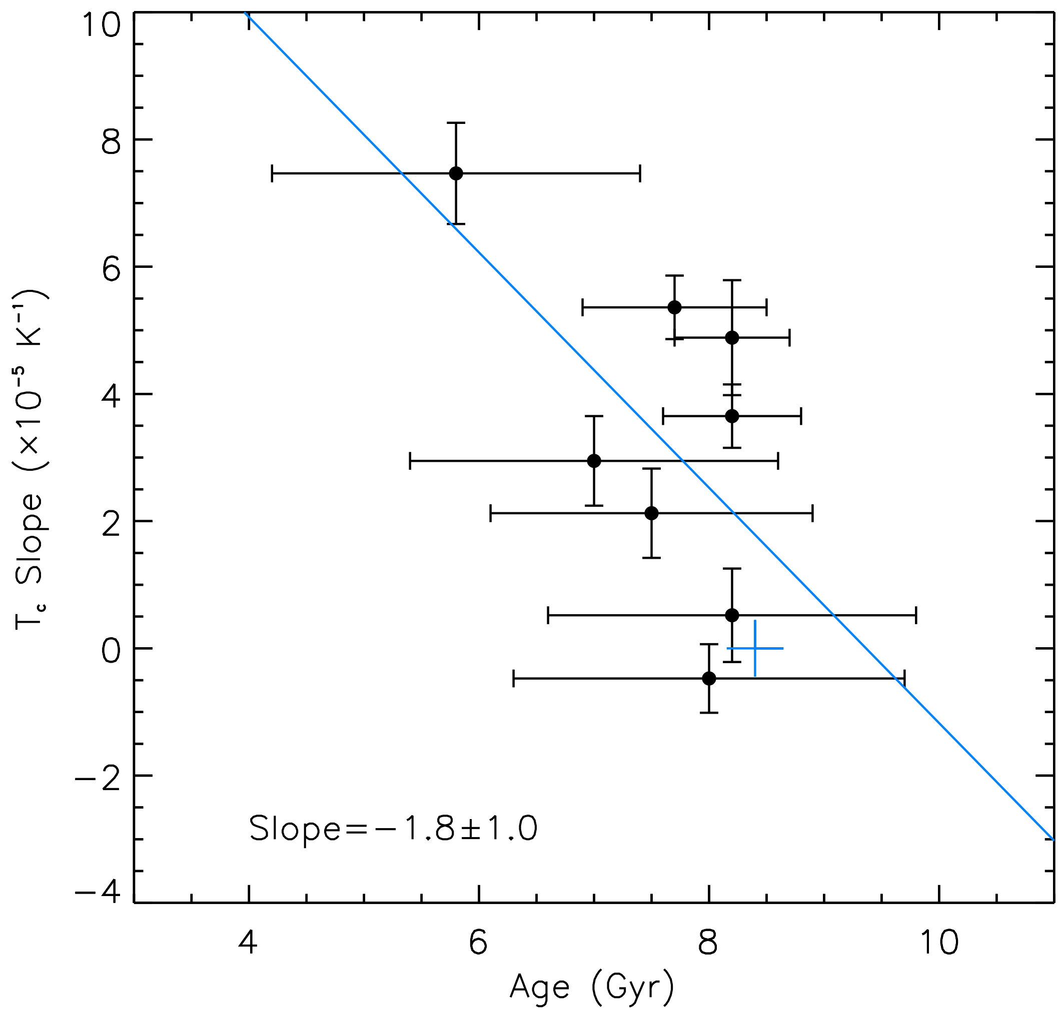

Figure 3.9 Gradient for a single linear fit to Δ[X/H] versus T_c slopes as a function of stellar ages for thick disc stars. Δ[X/H] were measured using Kepler-10 as a reference. The blue solid line represents the linear fit for the thick disc stars. The location of Kepler-10 is marked with blue cross.

3.9. A linear fit to the data is over-plotted (each data point is given equal weight). The gradient is -1.8 ± 1.0 for thick disc twins, using Kepler-10 as a reference. The negative slope is likely driven by the one star younger than 6 Gyr. Without that object, the diagram is a scatter plot such that age alone can not explain the chemical behaviour. We note that for most thick disc twins, although they have similar ages, the Δ[X/H] - T_c slopes can vary by $\sim 6 \times 10^{-5}$ K^{-1}. Therefore, we emphasize again that age alone can not explain the chemical patterns found in Figure 3.5 and Figure 3.6.

It has since long been known that the solar upper atmosphere and wind abundances are affected by anomalies, with respect to the photosphere, in that the elements with a high first ionization potential (FIP; such as Ne and Ar) are depleted relative to those with low potentials (e.g., Fe, Mg, Si, see Feldman & Laming 2000). Effects of this kind could possibly occur differentially in stellar photospheres, and might mimic the abundance correlations with condensation temperature. We have explored this by examining the relation between Δ[X/H] and the FIP in Figure 3.10. Although a correlation is apparent, its significance (4σ) is much less than for the T_c trend. Figure 3.10 might be just as well considered as providing two clumps: C and O, the rest of the elements, respectively. A similar phenomenon was also reported by Ramírez et al. (2010) for the Meléndez et al. (2009) and Ramírez et al. (2009) solar twin data sets. We performed a Spearman correlation test of the abundance differences versus T_c and FIP. The Spearman correlation coefficient is $r_S = +0.68$ when using T_c, but only -0.32 for the FIP. The probability of a correlation arising by chance is 0.2% for T_c, while the probability of the correlation with FIP arise by chance is 20.6%. We emphasize that there is no convincing physical scenario to explain the FIP trend in our results. The FIP effect modifies only the chromospheric and coronal abundances in the Sun, not the photospheric abundances, which is of relevance here.

Already in discussing Figure 3.4 above we could draw the conclusion that clear correlations with condensation temperature exist for the abundances of Kepler-10 relative to its twins. We have studied this further by applying the linear fits of [X/H] versus [Fe/H], but using "Twins - Kepler-10" for self-consistency, to correct the abundances of each twin to the [Fe/H] of Kepler-10 and thus derived GCE corrected results. The corrections are relatively small, reflecting the small range in [Fe/H] of the twins. When plotting the differences between these corrected abundances and those of Kepler-10 versus T_c we obtain a diagram (see Figure 3.11) similar to Figure 3.6, though with a slightly flatter gradient ($(0.24 \pm 0.03) \times 10^{-4}$ K^{-1}) and a marginally larger scatter. Obviously, these GCE corrections can not erase the

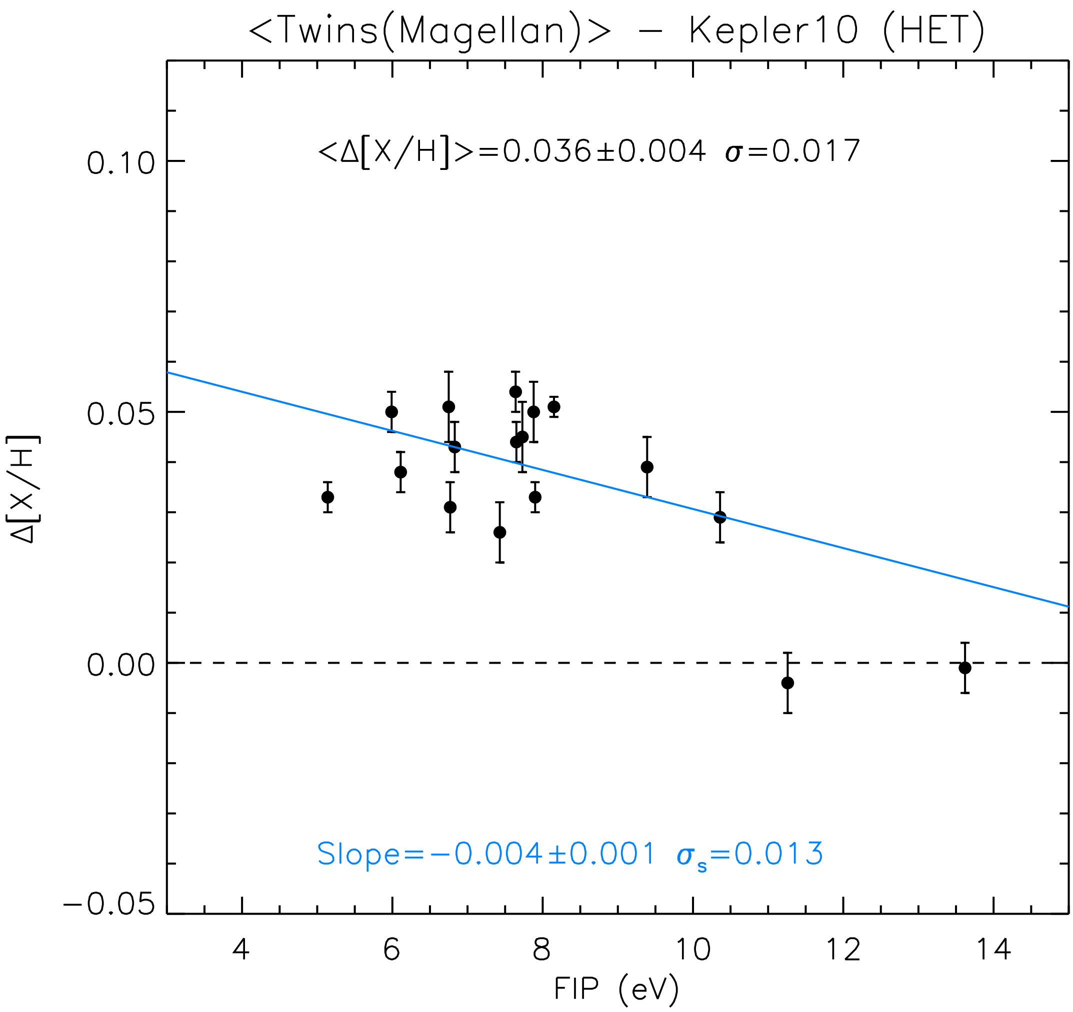

Figure 3.10 Differential chemical abundances Δ[X/H] as a function of FIP. The blue solid line represents the linear fit to the data, σ_s is the dispersion about the linear fit.

Δ[X/H] - T_c trend.[4] One concern regarding the GCE corrections in our analysis is that we are correcting the GCE effects using the abundance ratios - [Fe/H] relations, as was done by Adibekyan et al. (2014). Nissen (2015) demonstrated that age may be a better tracer for the GCE and should be considered when applying the GCE corrections. Indeed a recipe including both age and [Fe/H] could be the best way to estimate the GCE effects. However, the age range of the Kepler-10 thick disc twins is so narrow that we can not, and probably do not need to address an accurate GCE correction using the abundance ratio versus stellar

[4]A similar approach using Si as the reference element does not change our results. We find a slope of (0.214 ± 0.036) × 10^{-4} K^{-1}, i.e., a 5.9σ result.

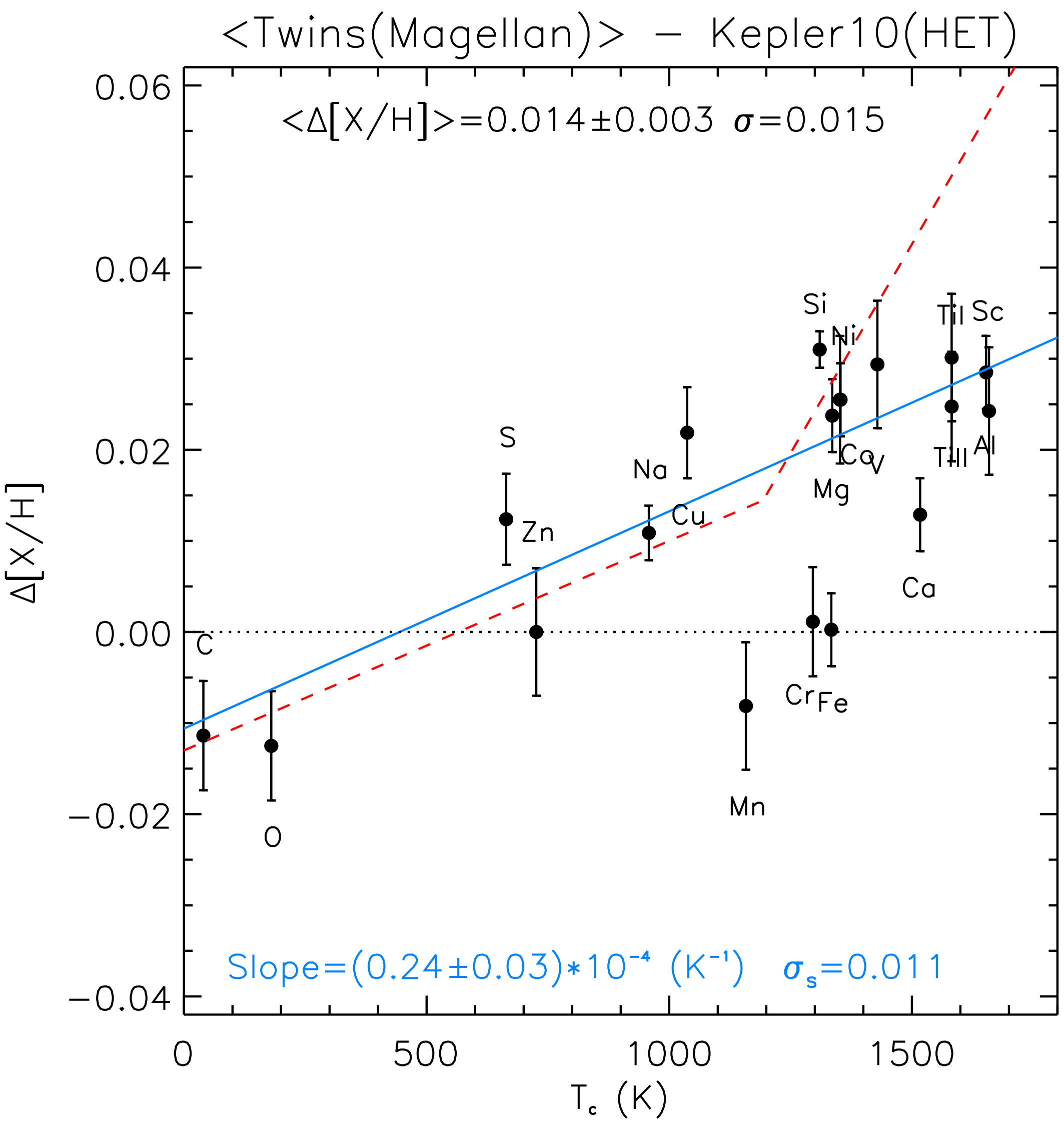

Figure 3.11 Average abundance differences Δ[X/H] versus condensation temperature T_c for the eight thick disc stellar twins relative to Kepler-10 with GCE corrections applied. The Y axis is the same as in Figure 3.6. The blue solid line represents the linear fit to the data, σ_s is the dispersion about the linear fit and the red dashed line is the fit from Meléndez et al. (2009) for solar twins − Sun, normalized to Δ[C/H].

age plots. Additional thick disc stellar twins would clarify this situation further.

When comparing Kepler-10 to its eight thick disc stellar twins, we find that Kepler-10 is depleted in refractory elements. The Δ[X/H] - T_c trends vary star to star which complicates the possible scenario. Chemical signatures of terrestrial planet formation, stellar ages, stellar birth locations, GCE effects, variation in dust-depletion in star-forming regions, etc. may affect our results. We notice that each of the scenarios discussed above may not be fully responsible for the observed abundance while a combination of several factors might affect and produce the current chemical composition of Kepler-10 and its stellar twins.

3.6. Conclusions

We conducted a line-by-line differential abundance study of Kepler-10 and a sample of stellar twins, obtaining extremely high precision based on spectra from three telescopes (CFHT, HET and Magellan). Our analysis reveals subtle chemical differences in the photosphere of Kepler-10 when compared to its stellar twins. We confirm that Kepler-10 is very likely a thick disc star considering its old age (8.4 ± 1.0 Gyr), kinematic probabilities (96% as thick disc member) and abundance ratios (according to Figure 3.4). When comparing Kepler-10 to its thick disc twins, a single linear fit provides an appropriate representation of the Δ[X/H] - T_c trend. We find that Kepler-10 is depleted in refractory elements relative to volatile elements when compared to the majority of thick disc stellar twins. Two of the eight thick disc twins do not show depletion patterns, which is within the small number statistics compatible with Meléndez et al. (2009) and Ramírez et al. (2009, 2010), resulting 15% of solar twins have chemical compositions that match the solar value. The average abundance difference between thick disc twins and Kepler-10 is 0.037 ± 0.004 (σ = 0.016) which corresponds to at least 13 Earth masses of material. One possible explanation could be the formation of terrestrial planets in the Kepler-10 system. However, the results are not as clear as for the solar twins (Meléndez et al. 2009; Ramírez et al. 2010). Other factors (e.g., stellar age, stellar birth location and GCE) might also affect the abundance results.

Naturally the thick disc twins may also harbour similarly large rocky planets as Kepler-10 although they have not yet been detected. Several studies based on current discoveries of exoplanets (Howard et al. 2012; Petigura et al. 2013; Burke et al. 2015) reported estimates of the occurrence rate of rocky planets around different type of stars with different orbits.

Petigura et al. (2013) indicate that at least one in six stars might host a planet with 1 - 2 R_E with period between 5 - 50 d. In this case, the peculiar chemical composition of Kepler-10 could reveal signatures regarding the different planetary masses, orbits, formation efficiency or formation timescale. In order to test the Meléndez et al. (2009) scenario regarding terrestrial planet formation and unravel the possible subtle chemical signatures and better understand the mechanisms of planet formation, more spectra of terrestrial planet host stars and their identical stellar twins with high SNR (> 350) are needed. It is also important to conduct similar analysis with binary stars (e.g., Liu et al. 2014; Mack et al. 2014; Tucci Maia et al. 2014; Biazzo et al. 2015; Ramírez et al. 2015; Saffe et al. 2015; Teske et al. 2015) or open cluster stars (e.g., Brucalassi et al. 2014; Önehag et al. 2011, 2014; Spina et al. 2015) since these systems presumably share the identical initial chemical composition, thus making them ideal targets for tracing small differential abundance differences that could reveal different formation histories of the individual stars and their planets.

Acknowledgments

This work has been supported by the Australian Research Council (grants FL110100012, FT140100554 and DP120100991). JM thanks support by FAPESP (2012/24392-2). DLL thanks the Robert A. Welch Foundation of Houston, Texas for support through grant F-634. TB was supported by the project grant "The New Milky Way" from the Knut and Alice Wallenberg Foundation. Australian access to the Magellan Telescopes was supported through the Collaborative Research Infrastructure Strategy of the Australian Federal Government. The Canada-France-Hawaii Telescope is operated by the National Research Council of Canada, the Institut National des Sciences de l'Univers of the Centre National de la Recherche Scientifique of France, and the University of Hawaii. The Hobby-Eberly Telescope is a joint project of the University of Texas at Austin, the Pennsylvania State University, Ludwig-Maximilians-Universität München, and Georg-August-Universität Göttingen.

CHAPTER 4

THE HYADES OPEN CLUSTER IS CHEMICALLY INHOMOGENEOUS

Context and contributions

The chapter is originally published as *'The Hyades open cluster is chemically inhomogeneous'*, F. Liu, D. Yong, M. Asplund, I. Ramírez, J. Meléndez, 2016, MNRAS, 457, 3934. Modifications of texts have been made in section 4.1 and 4.3. This chapter is included in the thesis as a representation of my contibution to the chemical signatures of planet formation in a benchmark open cluster: the Hyades. The observations were taken by my collaborator, I. Ramírez while I have done all the data reductions and scientific analysis presented in this paper. The whole paper was written by myself with the suggestions provided by the co-authors.

4.1. Introduction

Stars in open clusters share the same age, initial chemical composition and dynamical environment (Randich et al. 2005), and open clusters offer advantages over field stars for studying planet formation. For example, open clusters provide a more controlled sample and reduce systematic uncertainties arising from age, i.e., the only thing that changes from star to star is the mass. The Hyades open cluster is a close-by bench mark open cluster with intermediate age of ∼ 625 - 750 Myr (Perryman et al. 1998; Brandt & Huang 2015). This cluster has been spectroscopically studied before (e.g., Paulson et al. 2003; De Silva et al. 2006; Carrera & Pancino 2011; Maderak et al. 2013; Dutra-Ferreira et al. 2016). In this paper, we present a strictly line-by-line differential abundance analysis, in order to answer the following fundamental questions: (a) What is the level of abundance dispersions in the Hyades? (b) Is the Hyades still chemically homogeneous if we can achieve a much better precision (∼ 0.01 - 0.02 dex)? (c) Can we distinguish minor abundance differences in the Hyades which can be attributed to the planet formation?

4.2. Sample selection and observations

We selected 16 solar-type Hyades stars from Paulson et al. (2003) (hereafter P03) with 5650 K < T_{eff} < 6250 K, see Table 4.1. All of the targets are confirmed Hyades members according to Perryman et al. (1998), except for HD 27835, which was classified as a Hyades member based on its proper motion and radial velocity by Griffin et al. (1988). According to the SIMBAD data base, 8 sample stars might be variables of BY Draconis type where the variability is caused by star spots. Figure 4.1 shows our selected programme stars in the colour-magnitude diagram. Observations of the targets were performed using the Robert G. Tull Coudé Spectrograph (Tull et al. 1995) on the 2.7 m telescope at the McDonald

Observatory during two runs in 2012 October and 2012 December. The spectra have a resolving power of R = 60,000 and signal-to-noise ratio (S/N) ≈ 350 - 400 per pixel near 6500 Å. We reduced the spectra with standard procedures which include bias subtraction, flat-fielding, scattered-light subtraction, 1D spectral extraction, wavelength calibration, and continuum normalization, with IRAF[1]. A portion of the reduced spectra for all the programme stars is shown in Figure 4.2. We note that our S/N ratios are significantly higher than those of P03 who obtained S/N = 100 - 200.

[1]IRAF is distributed by the National Optical Astronomy Observatory, which is operated by Association of Universities for Research in Astronomy, Inc., under cooperative agreement with National Science Foundation.

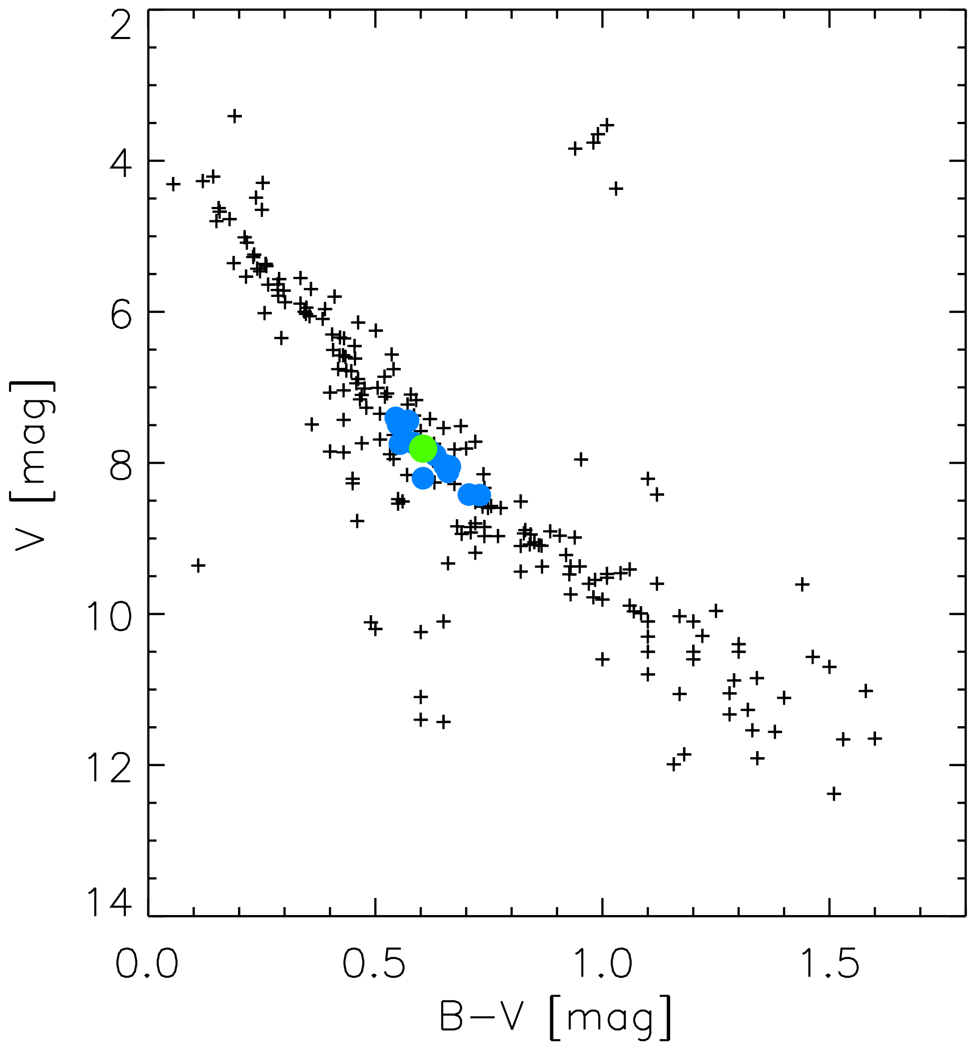

Figure 4.1 Colour-magnitude diagram of the Hyades. The values of B and V magnitude were taken from the Hipparcos Catalog (ESA 1997). The black plus signs represent 218 Hyades members from Perryman et al. (1998) while the blue circles represent our selected programme stars, respectively. The reference star mainly used in this analysis, HD 25825, is the filled green circle.

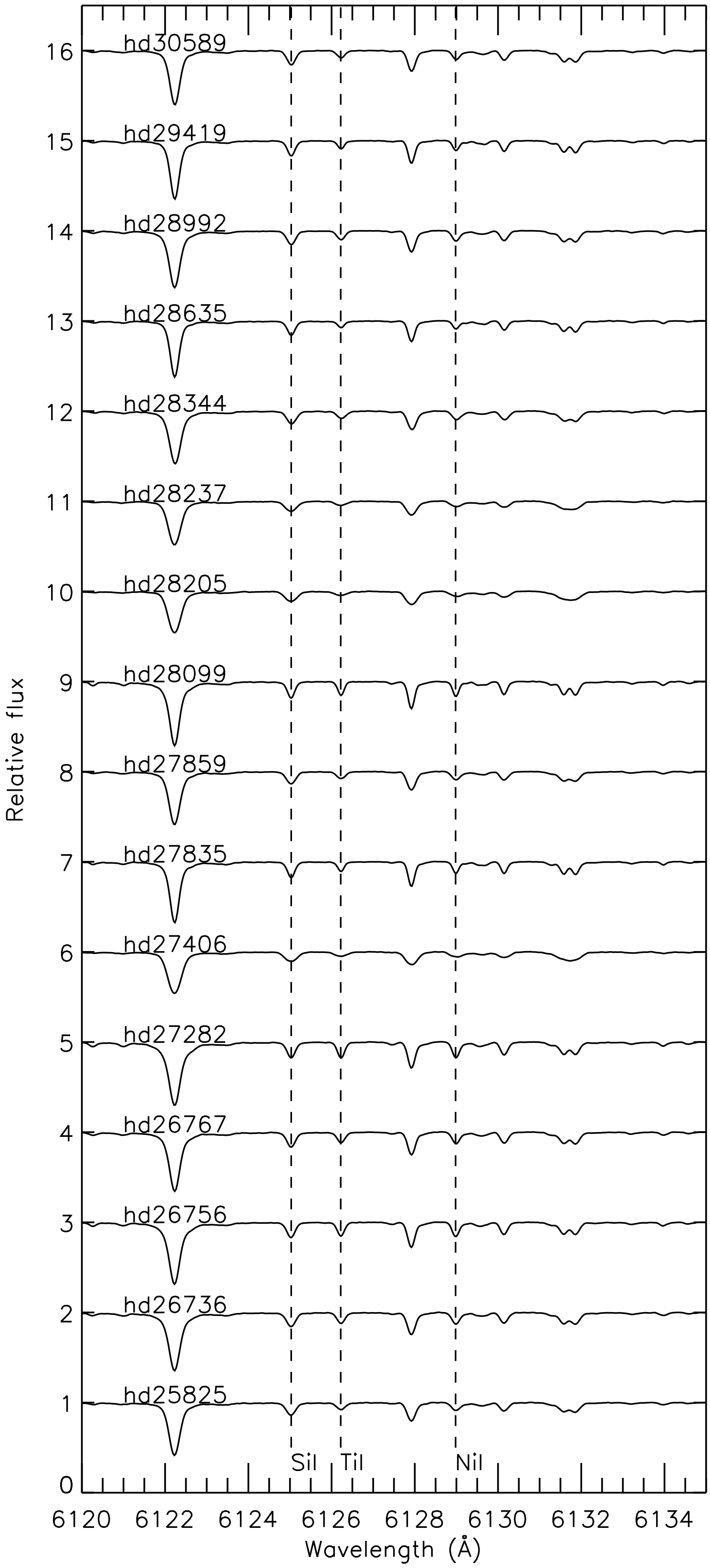

Figure 4.2 A portion of the spectra for all the programme stars. A few atomic lines (Si I, Ti I, Ni I) used in our analysis in this region are marked by the dashed lines.

4.3. Stellar atmospheric parameters and chemical abundances

4.3.1. Line list

The line list employed in our analysis was adopted mainly from Scott et al. (2015b,a) and Grevesse et al. (2015) and complemented with additional unblended lines from Bensby et al. (2005) and Neves et al. (2009). Equivalent widths (EWs) were measured using the ARES code (Sousa et al. 2007). Weak (< 5 mÅ) and most of strong (> 120 mÅ) lines were excluded from the analysis. The atomic line data, as well as the EW measurements, adopted for the abundance analysis can be found online (Liu et al. 2016a). We emphasize that in a strictly line-by-line differential abundance analysis such as ours, the atomic data (e.g., gf values) have essentially no influence on the results since our selected Hyades stars have similar stellar parameters.

4.3.2. Establishing parameters for reference stars

In order to conduct a strictly line-by-line differential analysis, we first need to establish stellar parameters for the reference star(s), and obtained those values in the following manner. We performed a 1D, local thermodynamic equilibrium (LTE) abundance analysis using the 2010 version of MOOG (Sneden 1973) with the ODFNEW grid of Kurucz model atmospheres (Castelli & Kurucz 2003). Detailed description of our analysis technique can be found in chapter 1.5. Lines whose abundances departed from the average by > 2.5σ were clipped and the parameters were re-computed after the sigma clipping. Note that if a given line is excluded in one star, the same line is also excluded in all stars. Note that the procedure was applied to all the sample stars since we wanted to be able to select any star as the reference.

Table 4.1 lists the stellar atmospheric parameters of our sample stars with the Sun as the reference star. The uncertainties in the stellar parameters were derived with the method described by Epstein et al. (2010) and Bensby et al. (2014), which accounts for the co-variances between changes in the stellar parameters. We compared our derived stellar parameters with the previous study by P03 in Figure 4.3. We found that our T_{eff} values follow the one-to-one relation, when compared to P03 results, while this is not the case for $\log g$ and [Fe/H]. The mean differences in T_{eff}, $\log g$ and [Fe/H] between our results and P03 results are 41.4 ± 41.5 K, 0.13 ± 0.07, and 0.04 ± 0.04, respectively. We note that we obtained smaller errors in stellar parameters when compared to the results from P03. The errors in our stellar parameters are $\sigma T_{eff} \approx 28$ K, $\sigma \log g \approx 0.04$, σ[Fe/H] ≈ 0.02 and $\sigma\xi_t \approx 0.04$ km s^{-1}, while the typical errors in stellar parameters from P03 are $\sigma T_{eff} \sim 50$ K, $\sigma \log g \sim 0.2$, σ[Fe/H] ~ 0.05 and $\sigma\xi_t \sim 0.2$ km s^{-1}.

Following Liu et al. (2014, 2016b), we then derived the differential stellar parameters using a strictly line-by-line differential analysis as described above, but compared our programme stars to a selected reference star from our Hyades sample. Choosing a typical Hyades star as the reference can help us to avoid potential systematic errors arising from comparing the higher metallicity Hyades stars with the Sun. HD 25825, with T_{eff} close to the median value, was selected as the reference star. The adopted stellar parameters for this reference star, $T_{eff} = 6094$ K, $\log g = 4.56$, [Fe/H] = 0.14, and $\xi_t = 1.34$ km s^{-1}, were taken from the analysis relative to the Sun (values can be found in Table 4.1). We emphasize that the absolute values are not crucial for our differential abundance analysis. Figure 4.4 shows an example of determining the differential stellar parameters of a programme star (HD 26736) relative to the reference star HD 25825. The line-by-line differential Fe abundance (Δ^{Fe}) is defined as below. We adopt the notation from Meléndez et al. (2012) and Yong et al. (2013), the abundance difference (programme star − reference star) for a line is

$$\delta A_i = A_i^{\text{program star}} - A_i^{\text{reference star}} \tag{4.1}$$

Therefore, $\Delta^{\rm Fe}$ is

$$\Delta^{\rm Fe} = <\delta A_i^{\rm Fe}> = \frac{1}{N}\sum_{i=1}^{N}\delta A_i^{\rm Fe} \tag{4.2}$$

The adopted stellar parameters satisfy the excitation and ionization balance in a differential sense. The best fit $\pm$ 1σ for $\Delta^{\rm Fe}$ versus LEP roughly corresponds to an error in $T_{\rm eff}$ of 30 K, similarly for the reduced EW (log (EW/λ), which corresponds to an error of $\sim$ 0.03 - 0.04 km s^{-1} in $\xi_{\rm t}$. The abundance difference in Fe I and Fe II = 0.000 $\pm$ 0.012, which constrains $\log g$ to a precision of 0.02 - 0.04. The final adopted differential stellar parameters and corresponding errors of our Hyades stars are listed in Table 4.2. Excellent precision in stellar parameters was achieved due to the strictly line-by-line differential analysis technique, which greatly reduces the systematic errors from atomic line data and shortcomings in the 1D LTE modelling of the stellar atmospheres and spectral line formation (e.g., Asplund 2005; Asplund et al. 2009).

4.3.3. Differential chemical abundances

Having established the stellar parameters relative to the selected reference star (HD 25825), we derived differential chemical abundances for 19 elements: C, O, Na, Mg, Al, Si, S, Ca, Sc, Ti, V, Cr, Mn, Fe, Co, Ni, Cu, Zn, and Ba with a strictly line-by-line basis. Hyperfine structure splitting was considered for Sc, V, Cr, Mn, Cu, and Ba using the data from (Kurucz & Bell 1995). NLTE effects in the differential abundance analysis between similar stars such as our sample should be negligible (Meléndez et al. 2012; Monroe et al. 2013). However, we still applied differential NLTE corrections for the O I triplet using the NLTE calculations by Amarsi et al. (2016). We note that photospheric inhomogeneities caused by star spots might induce differential NLTE or 3D effects on the differential abundances. For example, Morel & Micela (2004) showed that the discrepancy between oxygen abundances derived from the forbidden line at 6300 Å and the O I triplet, increase with increasing chromospheric activity. Such finding could imply that NLTE corrections to the oxygen abundances might

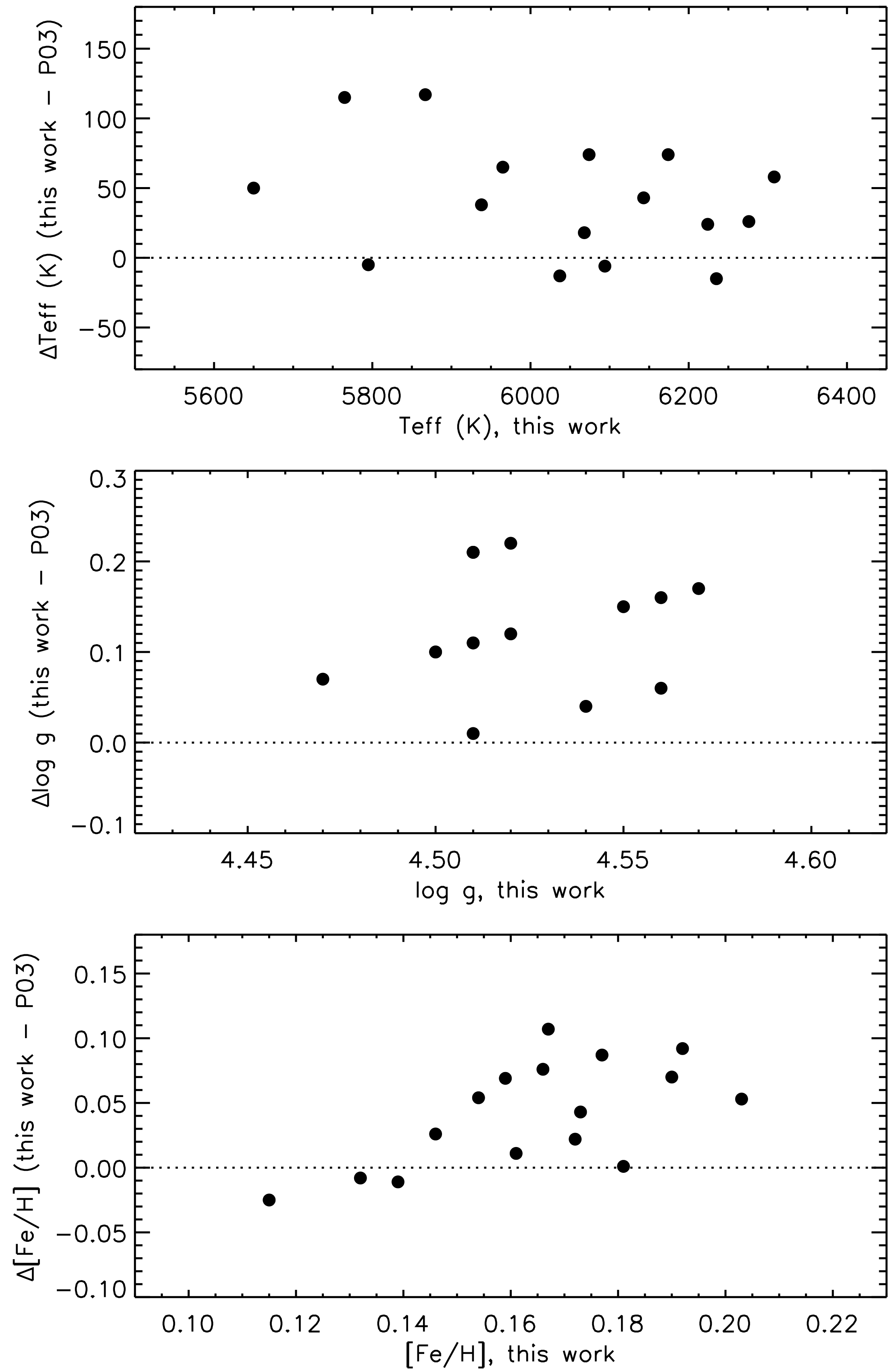

Figure 4.3 Comparison of stellar parameters (top panel: T_{eff}; middle panel: $\log g$; bottom panel: [Fe/H]) determined by this work and the study by P03.

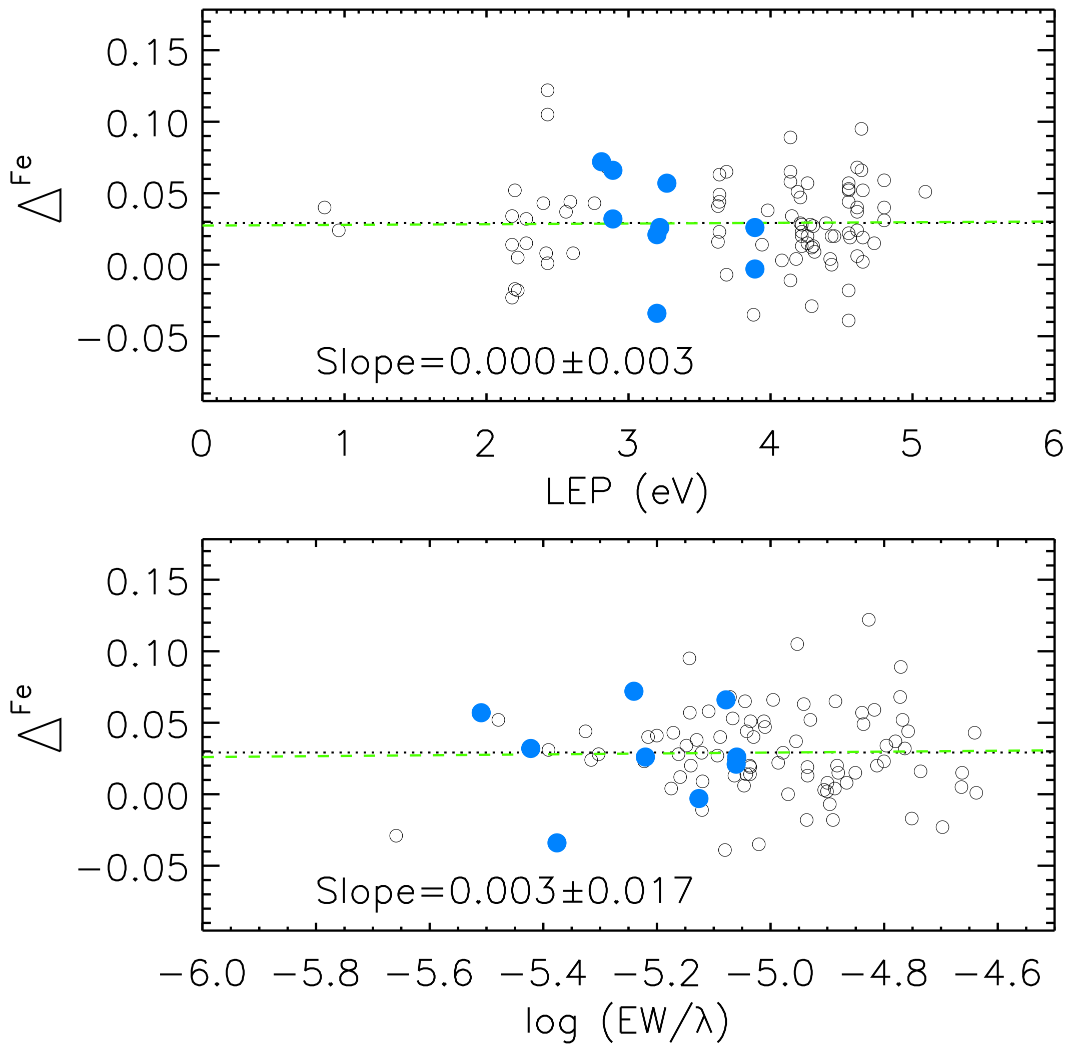

Figure 4.4 Upper panel: differential iron abundances (Δ^{Fe}) of a Hyades star HD 26736 derived on a line-by-line basis with respect to the reference star HD 25825 as a function of LEP; open circles and blue filled circles represent Fe I and Fe II lines, respectively. The black dotted line shows the location of mean Δ^{Fe}, the green dashed line represents the best fit to the data. Lower panel: same as in the top panel but as a function of reduced EW.

Table 4.1 Stellar atmospheric parameters for the programme stars with the Sun as the reference star.

Object	T_{eff} (K)	$\log g$	[Fe/H]	ξ_t (km/s)
HD 25825	6094±32	4.56±0.05	0.139±0.019	1.34±0.04
HD 26736	5867±31	4.50±0.04	0.166±0.017	1.31±0.04
HD 26756	5765±30	4.54±0.04	0.167±0.015	1.17±0.05
HD 26767	5938±25	4.55±0.04	0.190±0.014	1.30±0.04
HD 27282	5650±28	4.51±0.04	0.172±0.015	1.19±0.05
HD 27406	6224±37	4.51±0.05	0.161±0.024	1.42±0.05
HD 27835	6068±24	4.52±0.03	0.177±0.013	1.27±0.03
HD 27859	6037±27	4.51±0.03	0.115±0.016	1.33±0.04
HD 28099	5795±24	4.47±0.04	0.154±0.016	1.22±0.03
HD 28205	6308±36	4.51±0.05	0.192±0.023	1.38±0.04
HD 28237	6235±37	4.51±0.05	0.132±0.023	1.39±0.05
HD 28344	6074±29	4.57±0.04	0.181±0.019	1.29±0.04
HD 28635	6276±25	4.52±0.03	0.159±0.015	1.33±0.03
HD 28992	5965±22	4.51±0.03	0.146±0.012	1.31±0.03
HD 29419	6174±23	4.56±0.04	0.173±0.013	1.32±0.03
HD 30589	6143±22	4.50±0.03	0.203±0.015	1.27±0.03

not be completely adequate for active stars.

The total error in the differential abundance is obtained by adding in quadrature the standard error of the mean and the errors introduced by the uncertainties in stellar atmospheric parameters following the method of Epstein et al. (2010) which includes co-variance terms. For elements that only one spectral line was measured (C and Zn), we estimate the uncertainties by taking into consideration errors due to S/N, continuum setting and the stellar parameters. The quadratic sum of the three uncertainties sources give the errors for these two elements. Tables 4.3 - 4.5 list the differential elemental abundances for our programme stars relative to the reference star HD 25825[2]. The precision of the abundance ratios is ∼ 0.01 - 0.03 dex for most elements. We note that the strictly line-by-line differential analysis

[2]As described before, we define the line-by-line differential abundance for any species, X in this example, as Δ^{X}.

Table 4.2 Stellar atmospheric parameters for the programme stars relative to a reference star (HD 25825).

Object	T_{eff} (K)	$\log g$	[Fe/H]	ξ_t (km/s)
HD 25825[a]	6094	4.56	0.14	1.34
HD 26736	5896±26	4.52±0.04	0.168±0.015	1.37±0.03
HD 26756	5760±24	4.54±0.03	0.163±0.015	1.17±0.04
HD 26767	5944±16	4.56±0.02	0.189±0.008	1.31±0.02
HD 27282	5654±26	4.51±0.04	0.172±0.017	1.20±0.05
HD 27406	6225±32	4.51±0.04	0.159±0.017	1.43±0.04
HD 27835	6070±22	4.53±0.03	0.174±0.013	1.28±0.03
HD 27859	6034±21	4.51±0.03	0.111±0.012	1.34±0.03
HD 28099	5819±28	4.49±0.04	0.161±0.016	1.26±0.04
HD 28205	6306±29	4.51±0.04	0.189±0.015	1.39±0.04
HD 28237	6238±31	4.51±0.04	0.130±0.017	1.40±0.04
HD 28344	6074±16	4.57±0.02	0.180±0.010	1.30±0.02
HD 28635	6278±26	4.53±0.03	0.156±0.012	1.34±0.03
HD 28992	5968±21	4.52±0.03	0.143±0.011	1.32±0.03
HD 29419	6180±25	4.57±0.04	0.171±0.013	1.34±0.03
HD 30589	6142±24	4.50±0.03	0.201±0.011	1.27±0.03

[a] Adopted stellar parameters for the reference star, taken from Table 1.

greatly reduces the abundance errors from atomic data and shortcomings in the 1D LTE modelling of the stellar atmospheres and spectral line formation.

We repeated the procedure by using each programme star as a reference star and determined the corresponding differential stellar parameters and chemical abundances. We note that changing the reference star does not alter our results and conclusions in general.

Table 4.3 Differential abundances Δ^X (C, O, Na, Mg, Al, Si, S, Ca) for our Hyades stars relative to the reference star HD 25825.

Object	Δ^{C}	Δ^{O}	Δ^{Na}	Δ^{Mg}	Δ^{Al}	Δ^{Si}	Δ^{S}	Δ^{Ca}
HD 26736	-0.056±0.027	-0.011±0.030	0.038±0.007	0.039±0.030	0.061±0.033	0.038±0.009	0.087±0.029	0.042±0.016
HD 26756	-0.041±0.027	0.017±0.016	0.035±0.019	0.021±0.042	0.063±0.023	0.029±0.006	0.026±0.064	0.034±0.015
HD 26767	-0.003±0.026	0.050±0.011	0.041±0.004	0.065±0.013	0.073±0.017	0.050±0.005	0.063±0.014	0.054±0.011
HD 27282	-0.055±0.029	0.050±0.030	0.053±0.037	0.061±0.025	0.088±0.016	0.043±0.008	0.093±0.039	0.049±0.011
HD 27406	-0.040±0.026	0.029±0.020	0.028±0.019	-0.052±0.025	0.020±0.015	0.037±0.009	0.039±0.014	0.014±0.015
HD 27835	-0.029±0.026	0.025±0.016	0.019±0.028	0.045±0.029	0.055±0.045	0.031±0.008	0.079±0.037	0.037±0.017
HD 27859	-0.074±0.026	0.010±0.014	-0.010±0.019	-0.007±0.009	-0.026±0.023	-0.023±0.006	0.056±0.051	-0.018±0.013
HD 28099	0.003±0.027	0.019±0.023	0.038±0.019	0.050±0.040	0.081±0.038	0.026±0.011	0.071±0.023	0.033±0.020
HD 28205	-0.032±0.026	0.054±0.012	0.018±0.021	0.022±0.042	0.027±0.027	0.069±0.008	0.087±0.038	0.031±0.011
HD 28237	-0.077±0.026	-0.026±0.018	-0.024±0.012	-0.039±0.017	-0.087±0.061	0.015±0.010	0.021±0.049	-0.018±0.015
HD 28344	-0.027±0.026	0.028±0.022	0.021±0.005	0.033±0.007	0.055±0.013	0.041±0.006	0.058±0.033	0.041±0.010
HD 28635	-0.039±0.026	0.004±0.011	0.018±0.033	0.029±0.029	0.005±0.045	0.026±0.009	0.049±0.050	0.020±0.016
HD 28992	-0.037±0.026	0.028±0.019	0.025±0.010	0.009±0.011	0.033±0.027	0.020±0.007	0.005±0.006	0.005±0.010
HD 29419	-0.032±0.026	0.006±0.020	0.035±0.030	0.044±0.028	0.030±0.035	0.038±0.008	0.077±0.038	0.027±0.014
HD 30589	-0.060±0.026	0.019±0.015	0.055±0.020	0.062±0.019	0.070±0.032	0.075±0.007	0.082±0.053	0.060±0.018

Table 4.4 Differential abundances Δ^{X} (Sc, TiI, TiII, V, CrI, CrII, Mn, Fe) for our Hyades stars relative to the reference star HD 25825.

Object	Δ^{Sc}	Δ^{TiI}	Δ^{TiII}	Δ^{V}	Δ^{CrI}	Δ^{CrII}	Δ^{Mn}	Δ^{Fe}
HD 26736	0.018±0.023	0.048±0.017	-0.025±0.020	0.044±0.0236	0.034±0.017	0.023±0.033	0.051±0.018	0.029±0.010
HD 26756	0.034±0.021	0.048±0.017	-0.008±0.032	0.026±0.0320	0.031±0.015	0.032±0.032	0.045±0.013	0.024±0.009
HD 26767	0.036±0.015	0.065±0.011	0.033±0.018	0.047±0.0239	0.055±0.010	0.060±0.017	0.060±0.009	0.050±0.006
HD 27282	0.049±0.026	0.057±0.018	-0.004±0.030	0.044±0.0366	0.043±0.017	0.037±0.036	0.057±0.019	0.032±0.009
HD 27406	0.018±0.036	0.020±0.023	0.001±0.030	0.013±0.0302	0.004±0.018	0.014±0.024	0.046±0.020	0.020±0.013
HD 27835	0.011±0.031	0.054±0.014	0.038±0.017	0.011±0.0232	0.039±0.012	0.043±0.015	0.028±0.011	0.036±0.009
HD 27859	-0.054±0.020	-0.024±0.014	-0.043±0.012	-0.029±0.0165	-0.030±0.012	-0.020±0.010	-0.031±0.010	-0.028±0.008
HD 28099	-0.012±0.030	0.042±0.021	0.015±0.018	0.021±0.0277	0.029±0.018	0.035±0.035	0.043±0.019	0.022±0.012
HD 28205	0.047±0.039	0.049±0.020	0.031±0.027	0.034±0.0382	0.028±0.018	0.029±0.022	0.050±0.016	0.050±0.011
HD 28237	-0.035±0.028	-0.016±0.020	-0.050±0.032	-0.007±0.0267	-0.023±0.018	-0.045±0.021	0.003±0.023	-0.008±0.013
HD 28344	0.021±0.024	0.062±0.012	0.014±0.018	0.033±0.0186	0.027±0.010	0.042±0.011	0.038±0.010	0.041±0.007
HD 28635	-0.017±0.032	0.032±0.017	0.032±0.016	-0.033±0.0256	0.008±0.014	0.014±0.017	-0.005±0.020	0.018±0.010
HD 28992	-0.022±0.024	0.008±0.013	-0.015±0.016	-0.014±0.0183	0.006±0.012	0.018±0.015	0.018±0.014	0.004±0.008
HD 29419	0.004±0.036	0.054±0.017	0.034±0.017	0.006±0.0236	0.033±0.015	0.010±0.017	0.026±0.017	0.032±0.010
HD 30589	0.047±0.022	0.075±0.015	0.060±0.014	0.021±0.0196	0.061±0.012	0.049±0.013	0.060±0.010	0.062±0.009

Table 4.5 Differential abundances Δ^{X} (Co, Ni, Cu, Zn, Ba) for our Hyades stars relative to the reference star HD 25825.

Object	Δ^{Co}	Δ^{Ni}	Δ^{Cu}	Δ^{Zn}	Δ^{Ba}
HD 26736	0.044±0.026	0.046±0.014	0.058±0.050	0.038±0.028	-0.016±0.015
HD 26756	0.017±0.020	0.035±0.013	0.102±0.072	0.087±0.027	-0.007±0.020
HD 26767	0.046±0.011	0.049±0.009	0.077±0.034	0.077±0.026	0.058±0.012
HD 27282	0.040±0.031	0.044±0.013	0.037±0.029	0.118±0.030	0.029±0.018
HD 27406	0.009±0.038	-0.004±0.019	0.021±0.042	0.001±0.028	0.002±0.027
HD 27835	0.029±0.024	0.042±0.013	0.030±0.034	0.062±0.027	0.022±0.012
HD 27859	-0.040±0.014	-0.028±0.012	-0.025±0.010	0.007±0.026	-0.052±0.010
HD 28099	0.013±0.045	0.033±0.016	0.068±0.068	0.087±0.028	-0.014±0.018
HD 28205	0.021±0.029	0.037±0.016	0.040±0.031	0.018±0.028	0.009±0.018
HD 28237	-0.039±0.030	-0.019±0.018	-0.025±0.019	-0.051±0.028	-0.056±0.020
HD 28344	0.038±0.013	0.038±0.010	0.050±0.023	0.063±0.026	0.045±0.009
HD 28635	0.020±0.031	0.021±0.014	0.009±0.027	-0.011±0.027	-0.011±0.026
HD 28992	-0.020±0.015	0.000±0.012	0.000±0.031	0.029±0.027	-0.008±0.013
HD 29419	0.049±0.031	0.045±0.014	0.041±0.021	0.005±0.027	-0.021±0.015
HD 30589	0.050±0.030	0.073±0.012	0.069±0.027	0.075±0.027	0.010±0.015

4.4. Results and discussions

4.4.1. Chemical signatures of planet formation

Meléndez et al. (2009) performed the first high precision differential abundance analysis of the Sun and solar twins and found that the Sun was chemically unusual when compared to the solar twins. They found a clear correlation between abundance differences (Sun − solar twins) as a function of condensation temperature (T_{cond}) and suggested that this was related to terrestrial planet formation in the early solar environment. Therefore, we investigate whether the chemical signatures of planet formation can be found in our Hyades stars since identifying planets in open clusters is important to test whether the frequency is the same as in field stars and whether there is any dependence of planet frequency on stellar mass (e.g., Cochran et al. 2002). While our programme stars do not host hot Jupiters (Paulson et al. 2004a), we do not yet know whether they host smaller planets.

With our selected reference star (HD 25825), we obtained the differential chemical abundance (Δ^{X}) versus T_{cond} relations for each programme star; T_{cond} were taken from Lodders (2003). In Figure 4.5, we show two sample stars (HD 27859 and HD 30589) with largest, and smallest depletion in refractory elements compared to the reference star (i.e., most negative, and most positive slope, respectively). For HD 27859, the amplitude of depletion is only ≈ 0.03 dex and the significance level of the slope is 2σ. For HD 30589, the amplitude of enrichment is ≈ 0.07 dex and the significance level of the slope is 3.6σ. If the hypothesis suggested by Meléndez et al. (2009) is true, HD 27859 might have higher chance to host a terrestrial planet(s) due to the depletion pattern in refractory elements. However, the low value of Δ^{C}, and the low statistical significance make it hard to draw such a conclusion. We show the histogram of the slopes for the single linear fit to the T_{cond} trends for our Hyades stars in Figure 4.6. The slopes exhibit a broad distribution with a mean of $\sim 0.11 \times 10^{-4}$ K^{-1}. We did not find any programme stars with a clear chemical pattern with high significance. Following Ramírez et al. (2014a), we generated 10,000 Δ^X versus T_{cond} relations, with the Δ^X values drawn from a Gaussian distribution of 0.02 dex of standard deviation (this corresponds to the typical abundance errors in our analysis) centred at zero. We calculated the Δ^X versus T_{cond} slopes for each of these relations and determined their distribution, namely "trial distribution", normalized to have an equal area to the number of programme stars in our real sample. We shift the mean of the "trial distribution" to the mean of T_{cond} slopes of our data and over-plot this "trial distribution" in Figure 4.6. We note that the "trial distribution" has a width very similar to the real distribution of our data. We applied the Kolmogorov-Smirnov (K-S) test to compare the shifted "trial distribution" and the real distribution of our data. We obtained the D-value of ≈ 0.2 and the p-value of ≈ 0.5. This further demonstrates that in fact there are no T_{cond} correlations in our data.

We have repeated the analysis using each programme star in turn as the reference star. We find no clear T_{cond} trends which might indicate the chemical signature of planet formation in our sample stars.

We note that Quinn et al. (2014) detected one hot Jupiter around a Hyades open cluster star and they suggested a hot Jupiter frequency of $1.97^{+0.92}_{-1.07}$% in the Hyades open cluster, which is consistent with the hot Jupiter frequency in the field stars (1.2± 0.38%, Wright et al. 2012), while no hot Jupiters were discovered around our selected Hyades stars (Paulson et al. 2004a). Meibom et al. (2013) detected two planets smaller than Neptunes around two Sun-like stars in the old open cluster NGC 6811 and argued that the small planet frequency in the open cluster stars is the same as the frequency in the field stars. Fressin et al. (2013) predicted that around 15 - 20% of main-sequence FGK field stars host small planets (0.8 - 1.25 $R_\oplus$) with orbital < 85 d. This ratio is consistent with those reported for solar twins (Meléndez et al. 2009; Ramírez et al. 2009, 2010). If we assume a terrestrial planet fraction of 15%, and all terrestrial planets imprint the chemical signatures on to the hosts, then we

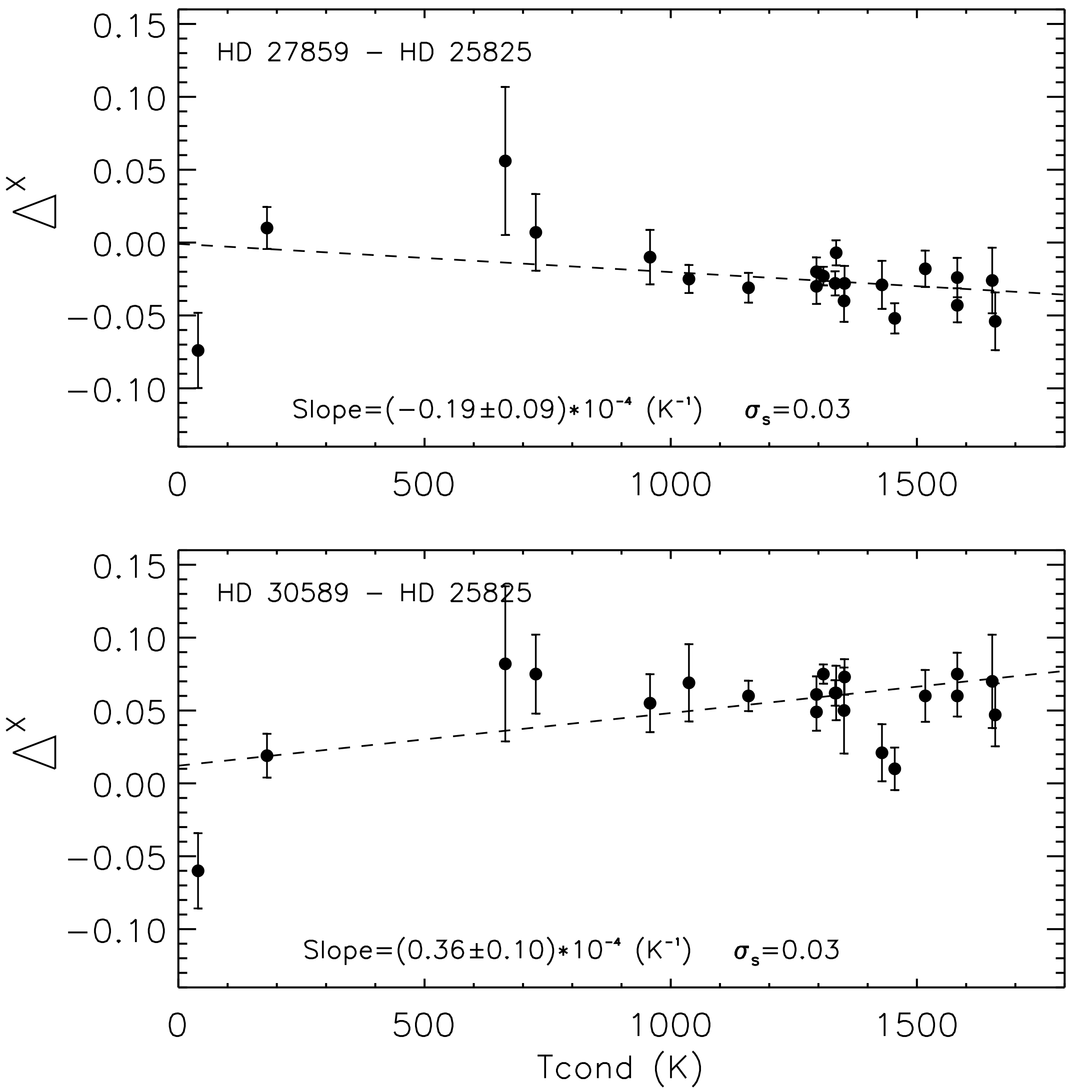

Figure 4.5 Differences in chemical abundances (Δ^X) versus condensation temperature (T_{cond}) for two programme stars relative to the reference star HD 25825 with the most negative slope (HD 27859, upper panel) and most positive slope (HD 30589, lower panel). The dashed lines represent the linear least-squares fits to the data with the respective slopes given in each panel. σ_s is the dispersion about the linear fit.

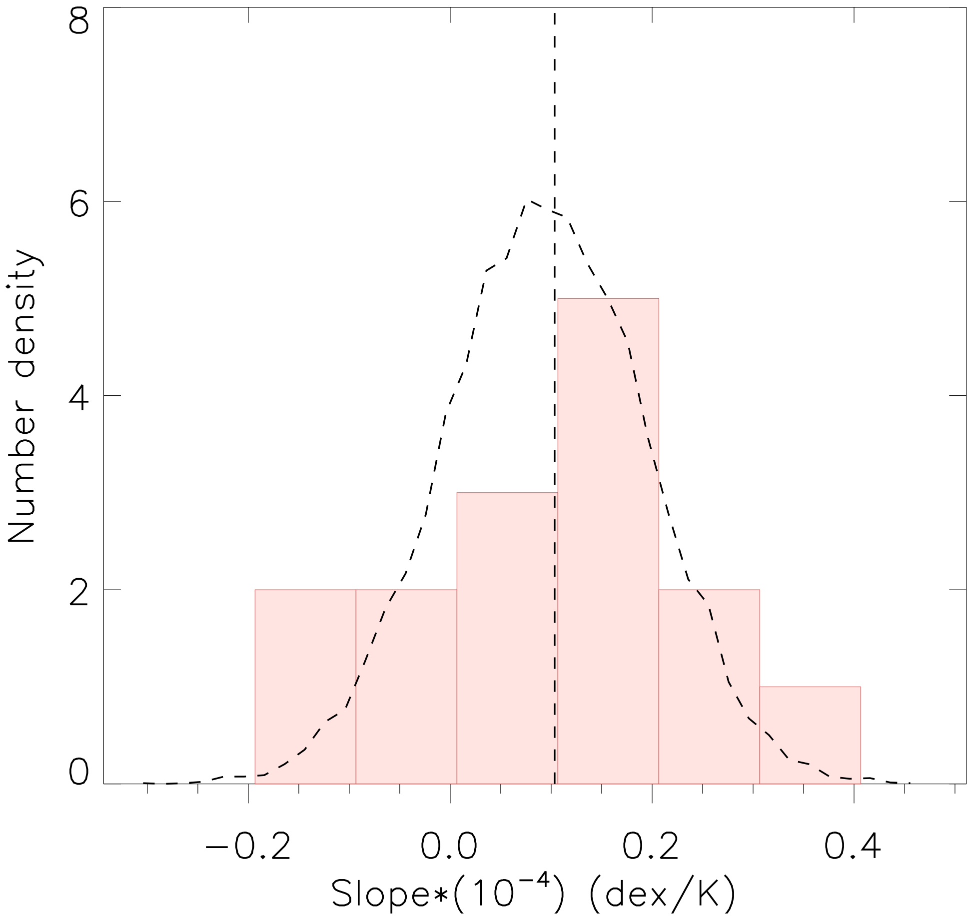

Figure 4.6 Histogram of the slopes when applying a single linear fit to Δ^{X} - T_{cond} for our Hyades stars relative to the reference star HD 25825. The dashed vertical line represents the location of the mean value of Δ^{X} versus T_{cond} slopes. The dashed curve represents the distribution of slopes of data with pure observational noise (see text for details).

would estimate that ≈ 2.4 programme stars should be unusual in their chemical composition in our sample. Given the small number statistics, the null result is consistent with the prediction according to the terrestrial planet frequency in the field stars. Tentatively, we conclude that our analysis thus provides an independent constraint upon the fraction of open cluster stars that might host terrestrial planets.

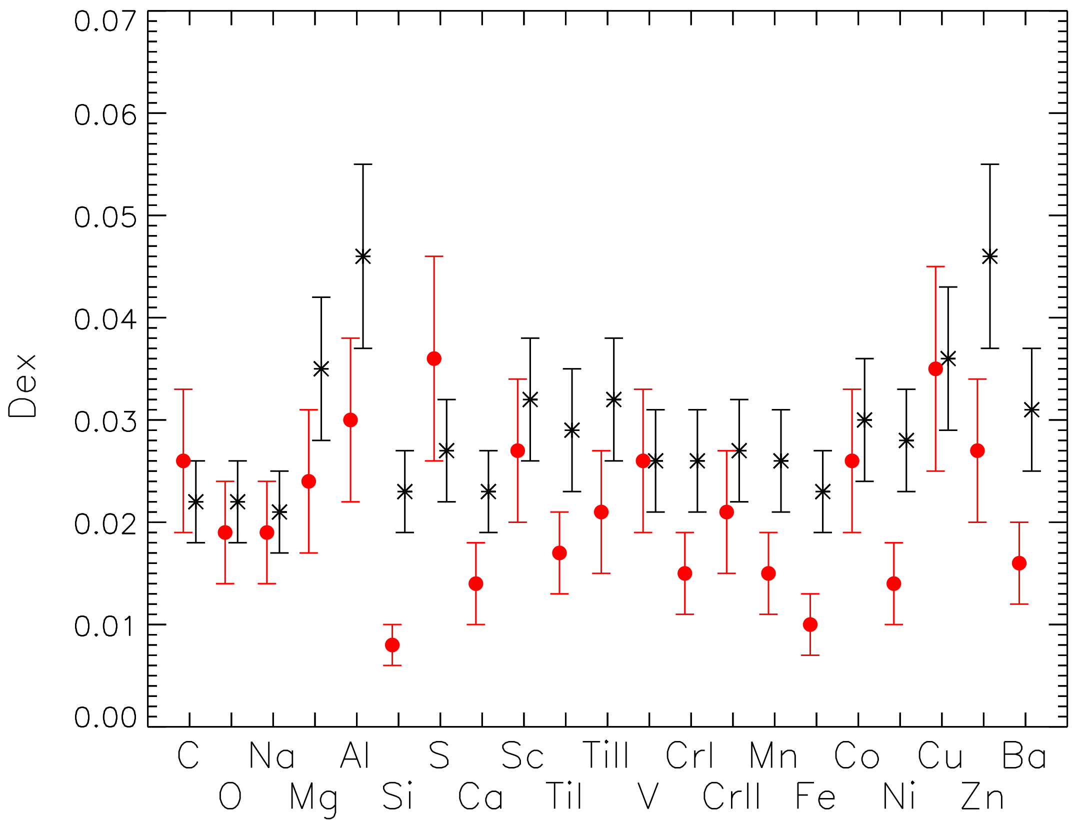

Figure 4.7 Observed abundance dispersions (black asterisk) and average abundance errors (<$\sigma\Delta^{X}$>, red circles) for all species in our sample. These results were obtained when using the reference star HD 25825.

4.4.2. Star-to-star abundance variations among the Hyades stars

In order to detect any chemical signature of planet formation, we have achieved the highest chemical abundance precision ever obtained in an open cluster. With this unique data set, we can study chemical homogeneity among the Hyades open cluster. We plot the average abundance error <$\sigma\Delta^{X}$>, and the measured abundance dispersion (standard deviation), for all elements in Figure 4.7. The main result from this figure is that we have achieved very high precision in the differential chemical abundances of our programme stars by applying the strictly line-by-line analysis technique. The lowest average abundance error is for Si ($< \sigma\Delta^{Si} > = 0.008$ dex) and the highest values is for S ($< \sigma\Delta^{S} > = 0.036$ dex). Previous studies of the Hyades achieved typical abundance errors of ~ 0.05 - 0.06 dex but reaching as

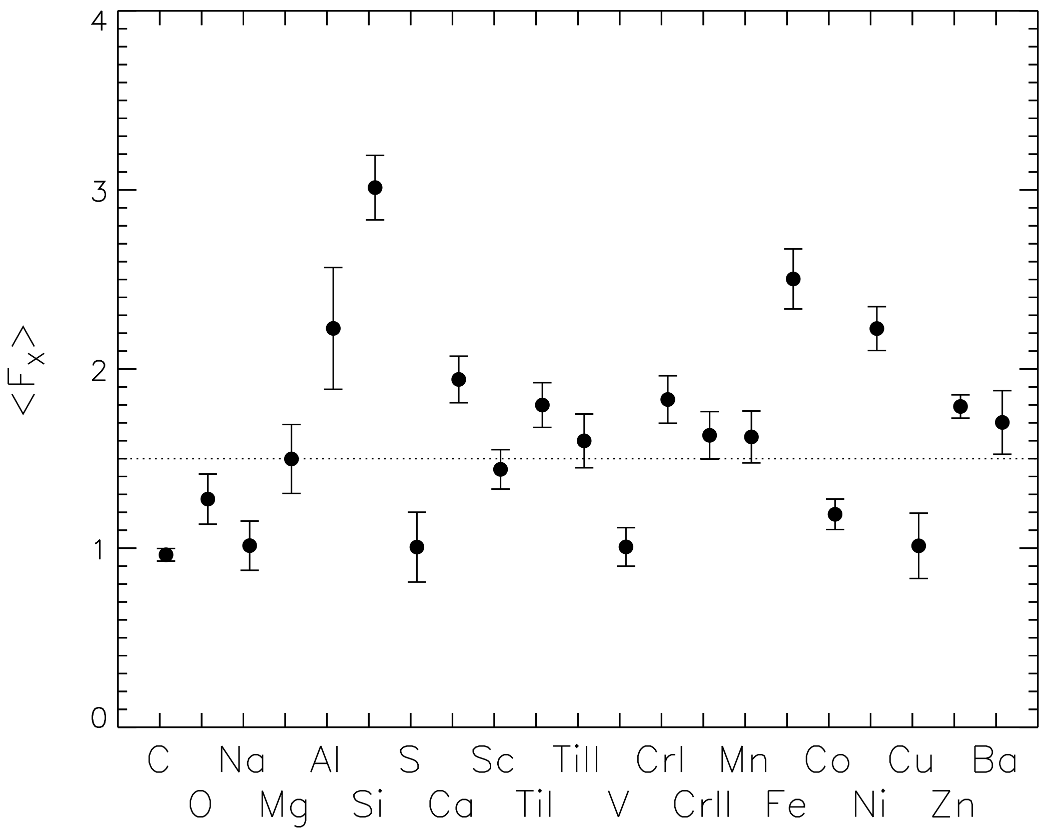

Figure 4.8 The mean F_X for each species using all reference stars in our sample. The dashed line locates at F_X = 1.5, which means that the abundance dispersion is 1.5 times larger than the average measurement error.

low as ~ 0.03 - 0.04 dex for some elements (P03; De Silva et al. 2006). Another important aspect to note in Figure 4.7 is that the measured dispersions for many elements (12 out of 19) are considerably larger than the average abundance errors by a factor of ~ 1.5 - 2. We note that the real abundance errors for C, S and Cu could be overestimated due to the lower S/N around the spectral region of these elements. In Table 4.6, we write the total abundance variation as well as the standard deviation, and the average abundance error for each element, using HD 25825 as the reference star. We find that the average abundance errors are smaller than the observed abundance dispersions for most elements. This is the first evidence that the Hyades is chemically inhomogeneous. An alternative explanation, however, is that we have underestimated the errors.

In order to quantify the level of chemical inhomogeneity, we define the fraction F_X which

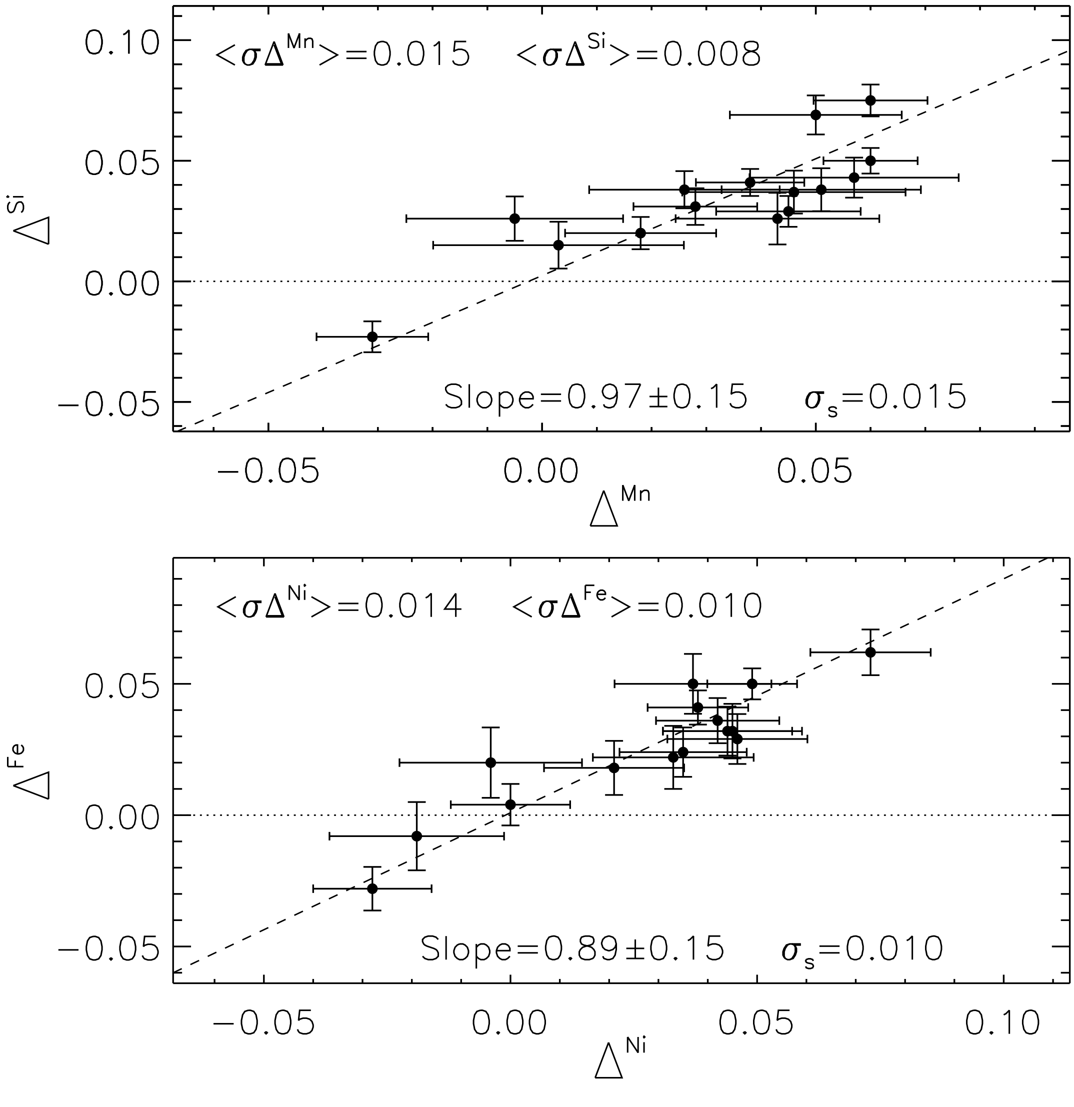

Figure 4.9 Upper panel: Δ^{Si} versus Δ^{Mn}; lower panel: Δ^{Fe} versus Δ^{Ni}, for the programme stars when using the reference star HD 25825. The dashed lines represent linear fits. σ_s is the dispersion about the linear fit. We write the average abundance errors in x-axis and y-axis ($<\sigma\Delta^X>$ and $<\sigma\Delta^Y>$, respectively).

represents the ratio of abundance dispersion to the errors. A value of $F_X = 1$ means that the abundance dispersion is equal to the measurement error while $F_X = 2$ means that the abundance dispersion is twice the measurement error. For a given element using a particular reference star, we performed 10,000 realizations in which we draw random numbers from the observed abundance dispersion distribution and from the distribution of average uncertainties. For a given element, we repeated this exercise using each reference star in turn. From this, we derived the mean F_X for each element using all reference stars and show the results in Figure 4.8. This plot further confirms the results presented in Figure 4.7 using HD 25825 as the reference star.

We searched for correlations between different elements in the differential chemical abundances (Δ^{X} versus Δ^{Y}) to further investigate the abundance variations in our Hyades stars. In Figure 4.9, we plot two examples of Δ^{X} versus Δ^{Y} (Δ^{Si} versus Δ^{Mn} in the upper panel, and Δ^{Fe} versus Δ^{Ni} in the lower panel, respectively). We applied a linear least-squares fit to the data, taking into account errors in both variables and in each panel we show the slope and corresponding uncertainty. Consideration of the slopes and uncertainties of the linear fits reveals that while the amplitude may be small, there are statistically significant, positive correlations between these elements for our programme stars. The significance level of the linear fits are 6σ for both combinations. While underestimating the errors could explain the results presented in Figures 4.7 and 4.8, it is highly unlikely that correlations of such high statistical significance between pairs of elements would arise from underestimating the errors.

We then show Δ^{X} versus Δ^{Y}, for every possible combination of species in Figure 4.10. The dimensions of the x-axis and y-axis are unity, such that a slope of gradient 1.0 would be represented by a straight line from the lower-left corner to the upper-right corner and a slope of gradient 0.0 would be a horizontal line. The different colours in Figure 4.10 indicate corresponding significance levels, which are based on the slopes and the uncertainties. The gradients are always positive and most of them (≈ 90% of the pairs) have significance > 2.5σ. We note that the correlations with Si are of the highest statistical significance, probably because Si has the lowest error. We conclude that there are positive correlations, of high statistical significance, between at least 90% of pairs of elemental abundances. Similar results have been reported for the globular cluster NGC 6752 by Yong et al. (2013). We interpret the ubiquitous positive correlations, often of high statistical significance, between Δ^X and Δ^Y as further indication of a genuine abundance dispersion in the Hyades.

We then calculated the intrinsic abundance scatter for each element in our sample using the selected reference star (HD 25825) in the following manner. For each element, we adopt a Gaussian distribution of width = 0.001 dex (which is the initial guess of the intrinsic abundance scatter) and randomly draw numbers from this distribution (one for each star). Then we add in quadrature another random number drawn from a Gaussian distribution of width corresponding to the error for that element in that programme star. We repeat this process 1000 times for all stars and measure the average produced value. We iterate the whole procedure by increasing the guess of the intrinsic abundance scatter by 0.001 dex until we find the "real intrinsic abundance scatter" which reproduces the observed abundance dispersion. Table 4.6 lists the values of intrinsic abundance scatter for each element in our sample, using HD 25825 as the reference star. We note that the average value of the intrinsic abundance scatter is 0.021 ± 0.003 dex (σ = 0.010).

4.4.3. Detailed examination of systematic errors

We have made several tests to check for possible systematic errors which might affect our results and describe them below.

(a) Systematic errors in EW measurements

Rather than manually measuring the spectral lines with the careful placement of the continuum at the same level in similar stars, an automatic code, ARES (Sousa et al. 2007) was

Table 4.6 The total abundance variation as well as the standard deviation (abundance dispersion), the average abundance error, and the intrinsic abundance scatter for each element in our sample, using HD 25825 as the reference star.

Species	Total variation	Standard deviation	Average error	Intrinsic scatter
C	0.080	0.022	0.026	0.003
O	0.080	0.022	0.019	0.014
Na	0.079	0.021	0.019	0.011
Mg	0.117	0.035	0.024	0.028
Al	0.175	0.046	0.030	0.039
Si	0.098	0.023	0.008	0.024
S	0.088	0.027	0.036	0.001
Ca	0.078	0.023	0.014	0.019
Sc	0.103	0.032	0.027	0.021
TiI	0.099	0.029	0.017	0.026
TiII	0.110	0.032	0.021	0.027
V	0.080	0.026	0.026	0.013
CrI	0.091	0.026	0.015	0.023
CrII	0.105	0.027	0.021	0.019
Mn	0.091	0.026	0.015	0.022
Fe	0.090	0.023	0.010	0.023
Co	0.090	0.030	0.026	0.019
Ni	0.101	0.028	0.014	0.027
Cu	0.127	0.036	0.035	0.017
Zn	0.169	0.046	0.027	0.042
Ba	0.114	0.031	0.016	0.030

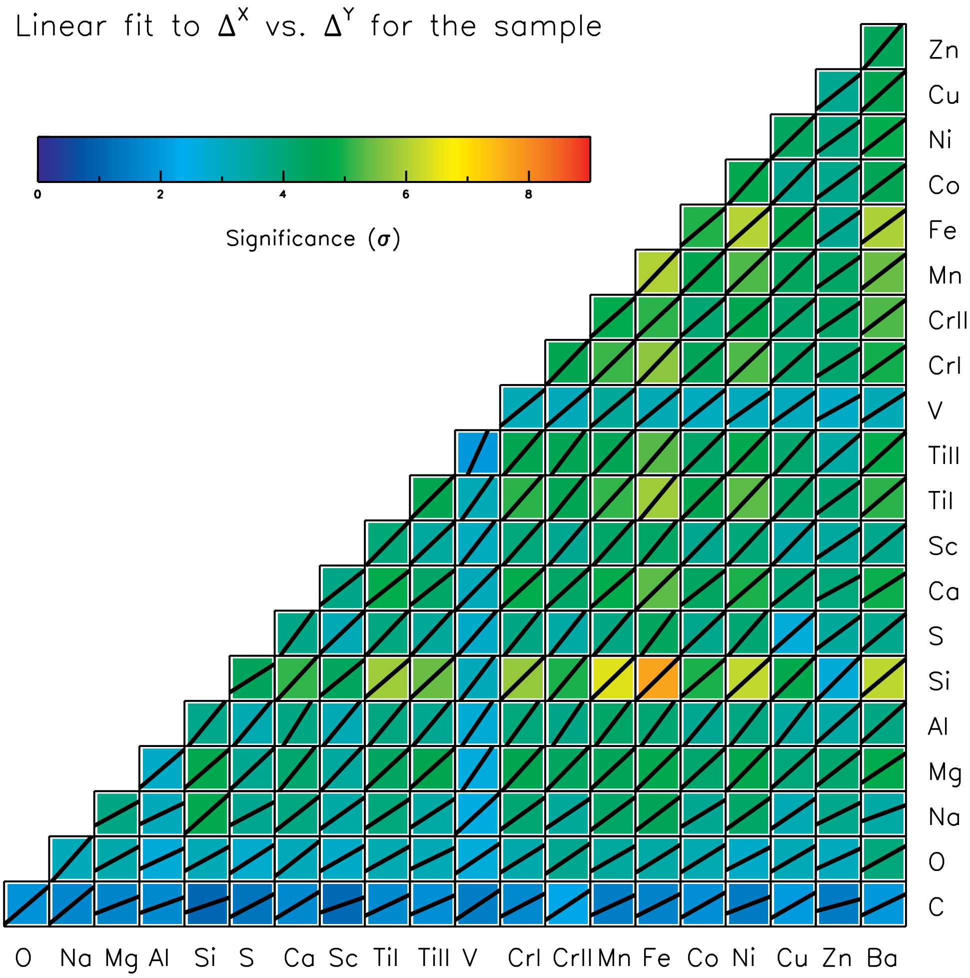

Figure 4.10 Linear least-squares fit to Δ^X versus Δ^Y, for all the combinations of species. The dimensions of the x-axis and y-axis are unity. The colour bar indicates the signifiance of the gradients. These results were obtained when using the reference star HD 25825.

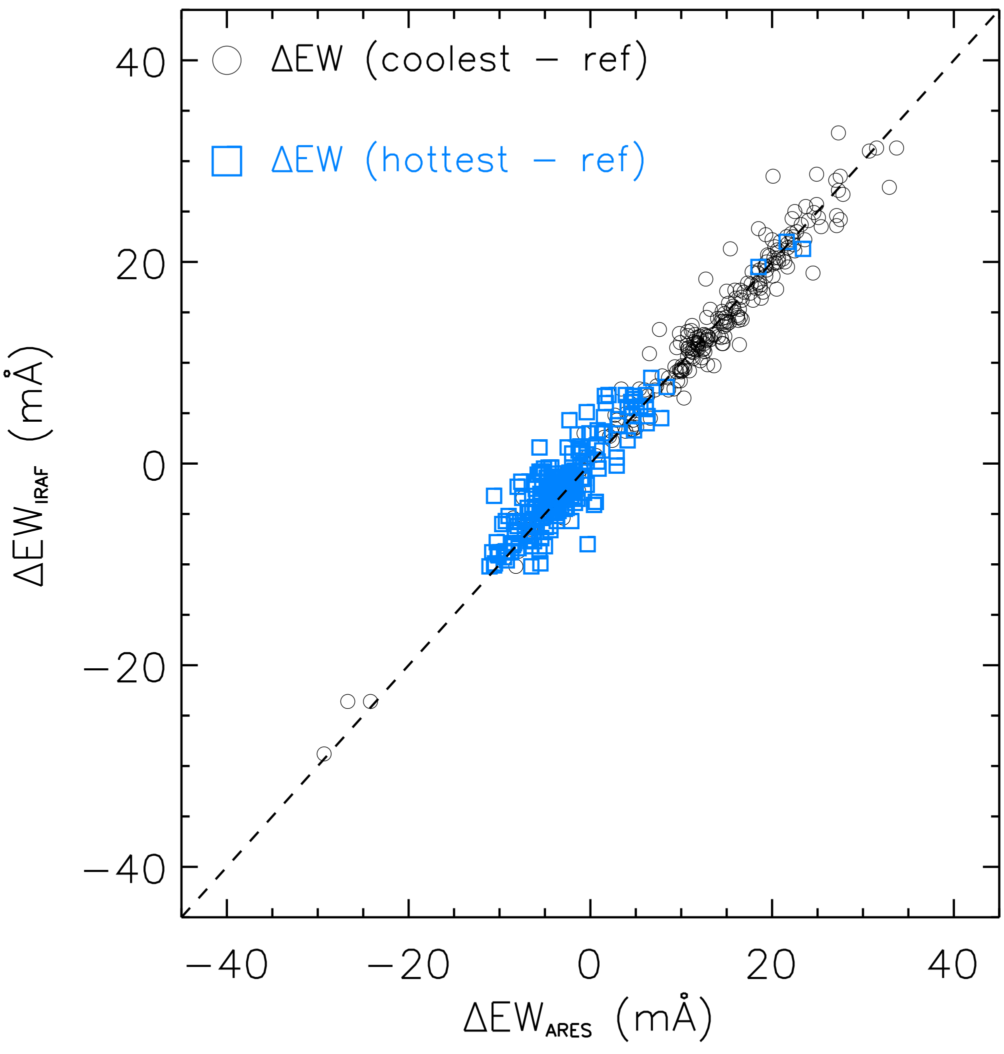

Figure 4.11 Differential EWs of spectral lines of the coolest and the warmest sample stars (HD 27282: black circles and HD 28205: blue rectangles, respectively) with respect to the reference star HD 25825, measured by ARES (x-axis) and IRAF (y-axis). The black dotted line represents the one-to-one relation.

used to measure EWs of the adopted lines in this work. ARES performs a local normalization around each spectral line, which might introduce small systematic differences in the adopted continuum between different lines. Therefore we present a test to compare the differential EWs measured by ARES with that measured manually using IRAF. We measured the differential EWs of spectral lines of the coolest and the warmest sample stars (HD 27282 and HD 28205, respectively) with respect to the reference star HD25825. Figure 4.11 shows the comparison results. The measurements of differential EWs with ARES and IRAF clearly show one-to-one relations, which indicate that no systematic errors are induced due to the use of ARES. We made a further test by restricting only strong lines (> 80 mÅ), while the comparison results are similar as shown in Figure 4.11, which demonstrate the ARES does not necessarily introduce systematic errors in the EWs as a function of effective temperature, as well as microturbulent velocity.

b) Errors in effective temperature

We plot Δ^{X} versus T_{eff} for all the elements in Figures 4.12 and 4.13. These two plots suggest that there may be trends between differential chemical abundances and T_{eff}. Since the total range in T_{eff} is large (~ 660 K), we tentatively attribute these trends to differential NLTE or 3D effects (e.g., Asplund 2005). For example, Zn, that is the worst case, seem to have the right effect for the 472nm line according to Takeda et al. (2005) using the Delta-1 model or Delta-2 model, which could introduce ~ 0.07 dex difference in Δ[Zn/H] for the coolest and the warmest sample stars. Therefore we need to explore whether or not our results (abundance trends between Δ^{X} versus Δ^{Y}) change if we remove the abundance trends with T_{eff}. We removed the abundance trends with T_{eff} in the following way. We defined a new quantity, Δ^{X}_{T}, which is the difference between Δ^{X} and the value of the linear fit to the data at the T_{eff} of the programme star. Then we examine the trends between Δ^{X}_{T} and Δ^{Y}_{T} in Figure 4.14. This figure is similar as Figure 4.10 but we have removed the abundance trends with T_{eff}. The results are essentially unchanged for all pairs of elements: at least 90% of pairs

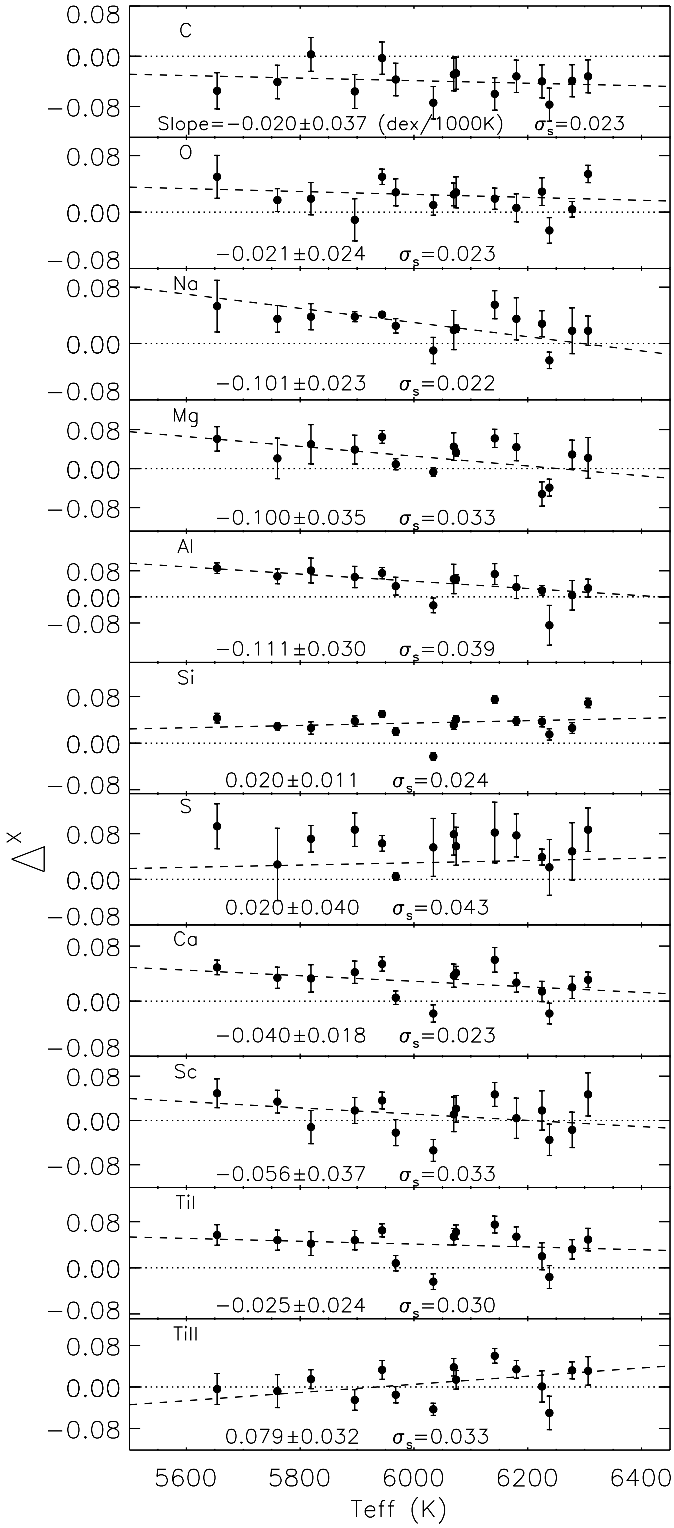

Figure 4.12 Δ^X versus T_{eff} for C, O, Na, Mg, Al, Si, S, Ca, Sc, TiI, and TiII for the programme stars when using the reference star HD 25825. The black dashed lines represent the linear fit to the data. σ_s is the dispersion about the linear fit.

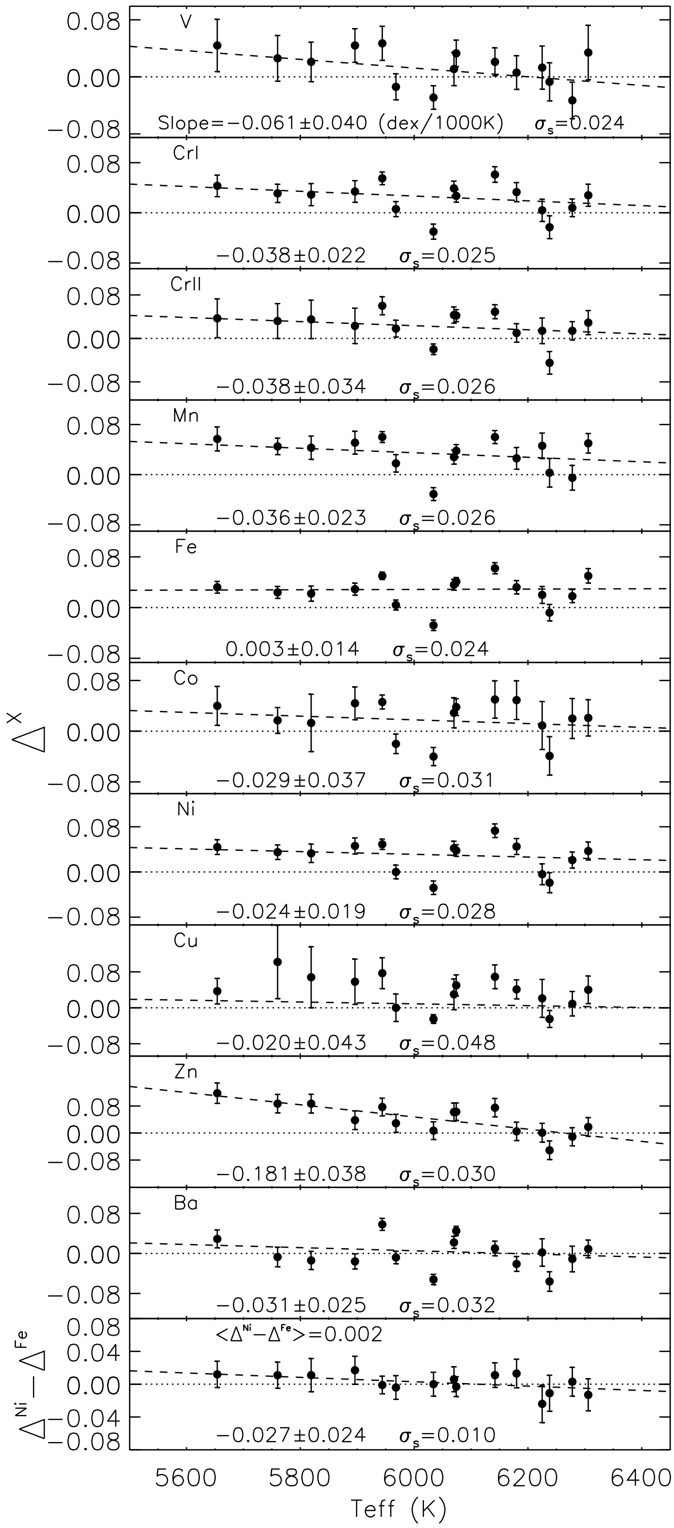

Figure 4.13 Same as Figure 4.12 but for V, CrI, CrII, Mn, Fe, Co, Ni, Cu, Zn, and Ba, as well as ($\Delta^{Ni} - \Delta^{Fe}$) versus T_{eff} for the programme stars when using the reference star HD 25825. The black dashed lines represent the linear fit to the data. σ_s is the dispersion about the linear fit.

of elements show positive correlations of the similar significance as before. We note that none of the elements have slopes that differ by 2σ. In addition, we show the distribution of all the slopes from Figure 4.10 and Figure 4.14 in Figure 4.15. The mean value of the slopes without removing the T_{eff} trends is 0.88 ± 0.02 (σ = 0.27), while the mean value of the slopes with the T_{eff} trends have been removed is 0.95 ± 0.02 (σ = 0.36). This test increases our confidence that our results are not an artefact of systematic errors in terms of T_{eff}.

However, we note that for most elements, the programme stars with T_{eff} > 5900 K show larger abundance variations when compared to the programme stars with T_{eff} ≤ 5900 K. This could be related to the thin convection zones of those stars with T_{eff} > 5900 K since it is easier to imprint abundance anomalies. Another possibility is diffusion. Önehag et al. (2014) detected tentative variations in the open cluster M67 that could be due to atomic diffusion, albeit M67 is much older than the Hyades. Gebran et al. (2010) reported large abundance variations (e.g., ~ 0.2 dex) in A and F stars due to diffusion, although their F stars are hotter than our sample stars by ~ 1000 K. We plot ($\Delta^{\mathrm{Ni}} - \Delta^{\mathrm{Fe}}$) versus T_{eff} in Figure 4.13 (bottom panel). We find that the abundance difference between these two elements is almost zero while the predicted abundance difference from the diffusion model should be ~ +0.2 dex (1.45 $M_{\odot}$ case, Richer et al. 2000). In this scenario, the hotter and more massive stars should have higher Ni to Fe ratios than the cooler and less massive stars. We do not detect such a trend and therefore we do not find evidence in our sample for diffusion effects.

Earlier we noted that systematic errors cancel in a differential analysis. Previous analyses usually spanned a small range in T_{eff} ± 100 K (e.g., Meléndez et al. 2009; Ramírez et al. 2014b). Here, our programme stars span ~ 300 K in T_{eff}. Examination of Figures 4.12 and 4.13 indicate that there are no significant (> 2.5σ) systematic trends between abundance and T_{eff} for most elements except for Na, Al, and Zn, which would suggest that the systematic errors cancel over this range of T_{eff}.

c) Effects of T_{eff}, $\log g$ and ξ_t error vectors

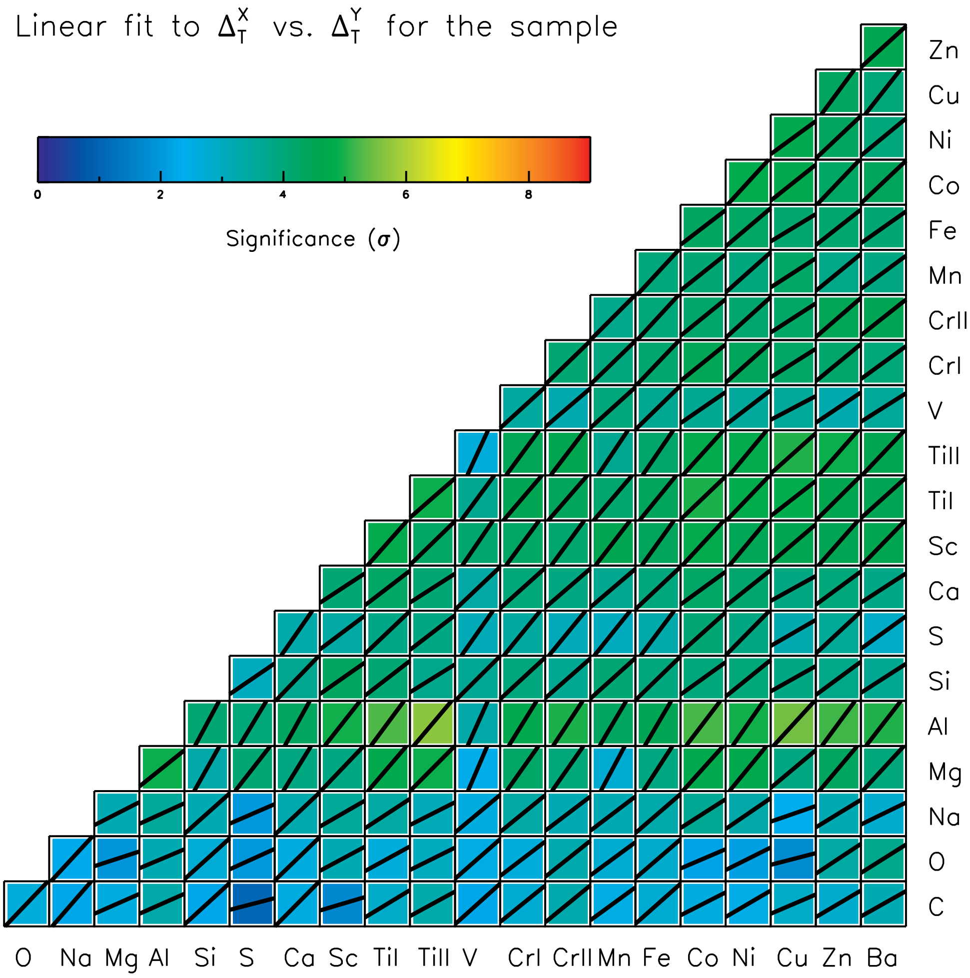

Figure 4.14 Same as Figure 4.10 but the abundance trends with T_{eff} have been removed. These results were obtained when using the reference star HD 25825.

Next we seek to understand whether individual errors in T_{eff}, $\log g$ and ξ_t could induce abundance trends between Δ^X versus Δ^Y that mimic our results. The tests are presented in the following manner. We kept the reference star (HD 25825) fixed. Starting with T_{eff}, we computed new abundances by randomly changing T_{eff} according to the uncertainty (σT_{eff}) for each programme star. Assuming the data all lie at [0.0,0.0] in Δ^X versus Δ^Y, we can then generate a new plot in which the fit to these data effectively represent the "T_{eff} error vector". We can then quantify whether errors in T_{eff} can mimic the measurements. Error vectors can be obtained for $\log g$ and ξ_t, by applying a similar approach using the uncertainties

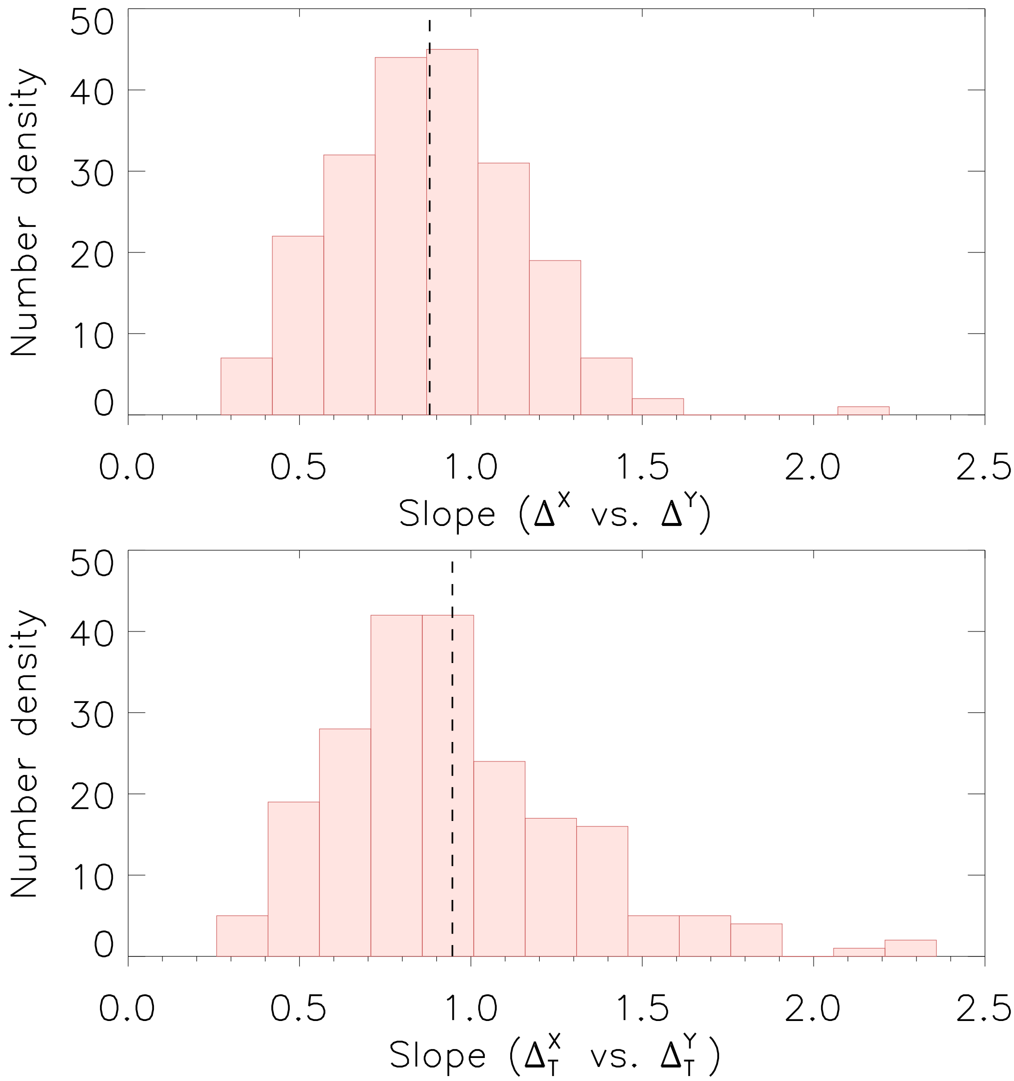

Figure 4.15 The distribution of the slopes for the linear least-squares fits to ΔX versus ΔY, for all the combinations of species without removing the T_{eff} trends (upper panel) and with the T_{eff} trends have been removed (lower panel). The dashed vertical lines represent the location of the mean value of Δ^X versus Δ^Y slopes.

$\sigma\log g$ and $\sigma\xi_t$, respectively. The underlying hypothesis we were testing was whether the distribution in Δ^X versus Δ^Y is a δ function centred at the zero-point and that the observed distribution could be explained entirely by errors in T_{eff} or $\log g$ or ξ_t.

We plot two examples of Δ^X versus Δ^Y (Δ^{Fe} versus Δ^{Al} in the upper panel, and Δ^{Ca} versus Δ^{Si} in the lower panel, respectively) with error vectors of T_{eff}, $\log g$ and ξ_t (blue, magenta and green dashed lines, respectively) in Figure 4.16. It is clear that the errors in T_{eff} or $\log g$ or ξ_t alone can not fully explain the observed trends in Δ^{Fe} versus Δ^{Al} and Δ^{Ca} versus Δ^{Si} since the error vectors are not aligned with the data, and as discussed, the magnitude of the errors is far smaller than the observed dispersions. We applied this test to all the pairs of elements. The fraction of instances in which the error vectors of T_{eff}, $\log g$ and ξ_t are in agreement with the observed trends including uncertainties are 25%, 12% and 20%, respectively. This indicates that the variations of these three stellar parameters can not fully explain the positive correlations for the vast majority (> 75%) of differential elemental abundances shown in Figure 4.10. We also checked our results by multiplying the errors in T_{eff}, $\log g$ and ξ_t by a factor of 2, 3 and 5 and applied the similar manner described above. Naturally this can only increase the amplitude of the error while the direction of the error vector remains unchanged. This test reinforces that our main results are not likely due to systematic errors in stellar parameters.

d) Effects of stellar activity

To investigate the potential effects of stellar activity on our results, we computed the chromospheric activity index $\log R'_{HK}$ as follows. We measured the fluxes in the cores of the Ca II H and K lines using 1 Å triangular passbands. Pseudo-continuum fluxes were measured using 20 Å bandpasses in the continuum at 3901 and 4001 Å. We can thus measure the instrumental S_{inst} index (see, e.g., Wright et al. 2004) from our spectra. We found a linear relationship between our S_{inst} index and S_{Duncan} (values published in Duncan et al. 1991):

$$S_{Duncan} = 0.023(\pm 0.057) + 0.082(\pm 0.180)S_{inst} \tag{4.3}$$

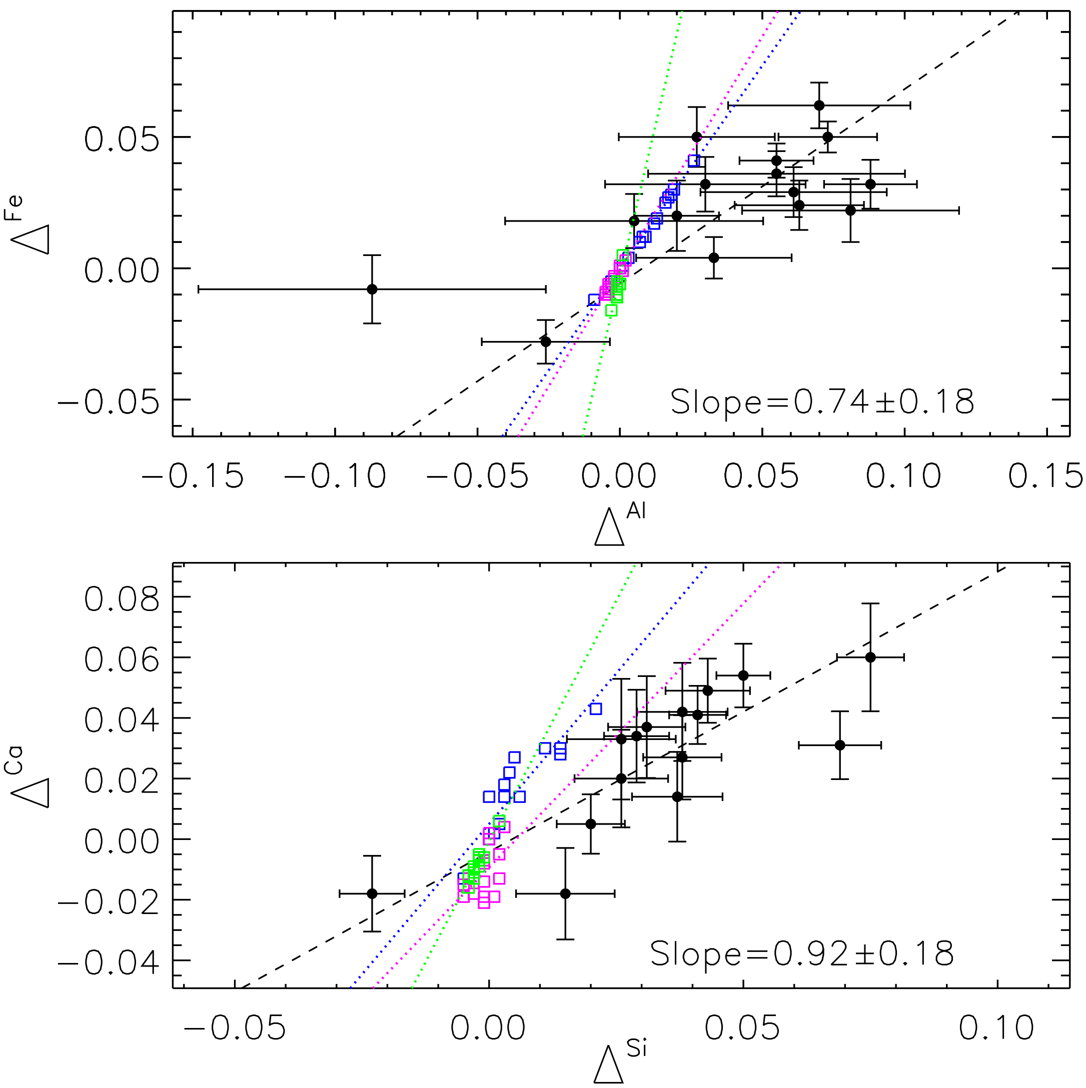

Figure 4.16 Upper panel: Δ^{Fe} versus Δ^{Al}; lower panel: Δ^{Ca} versus Δ^{Si}, for the programme stars when using the reference star HD 25825. The black dashed lines represent the linear least-squares fit to the data. The blue, magenta and green dashed lines represent the error vectors of T_{eff}, $\log g$ and ξ_t, respectively.

Thus we are able to transform our S_{inst} values into a standard Mount Wilson S index scale (S_{MW}). B − V colours listed in the Hipparcos catalog (ESA 1997) were then employed to transform S_{MW} into log $\mathrm{R'_{HK}}$ using equations from Middelkoop (1982) and Noyes et al. (1984). Our measurements of log $\mathrm{R'_{HK}}$ show good agreement with previously published values of common Hyades stars (Duncan et al. 1991; Paulson et al. 2002). When compared to the results from Paulson et al. (2002) (hereafter P02), the mean difference (our values − P02 values) is -0.06 ± 0.06. Thus, our log $\mathrm{R'_{HK}}$ values have errors of the order ~ 0.06 and there is little time variation of this activity index in the programme stars between our observations and those of P02.

We would like to check if the abundance variations and the observed positive correlations of elemental abundances are due to the effects of stellar chromospheric activity. Figure 4.17 shows the stellar activity index log $\mathrm{R'_{HK}}$ versus [Fe/H] for our sample. We did not find any clear relation between the stellar activity index and our derived [Fe/H], no matter our results or P02 results were adopted. Instead, they are distributed more or less randomly. We made this test for all the other elements and found that none of them show correlations with $> 2.5\sigma$ significance. Therefore, the observed abundance variations and correlations of elemental abundances can not be physically attributed to the effects of stellar activity.

4.4.4. Possible explanations for an intrinsic abundance spread

Our results offer the first clear evidence that the Hyades open cluster is chemically inhomogeneous at the ≈ 0.02 dex level. Chemical inhomogeneity at this level can only be detected when the measurement uncertainties are extremely small, as in our study. Here we discuss several potential scenarios, which could explain the observed abundance variations and positive correlations between Δ^{X} versus Δ^{Y} in the Hyades stars. We note that in principle, the possible explanations do not have to be able to create inhomogeneities in all chemical abundances, but only on those that have abundance dispersions above the measurement

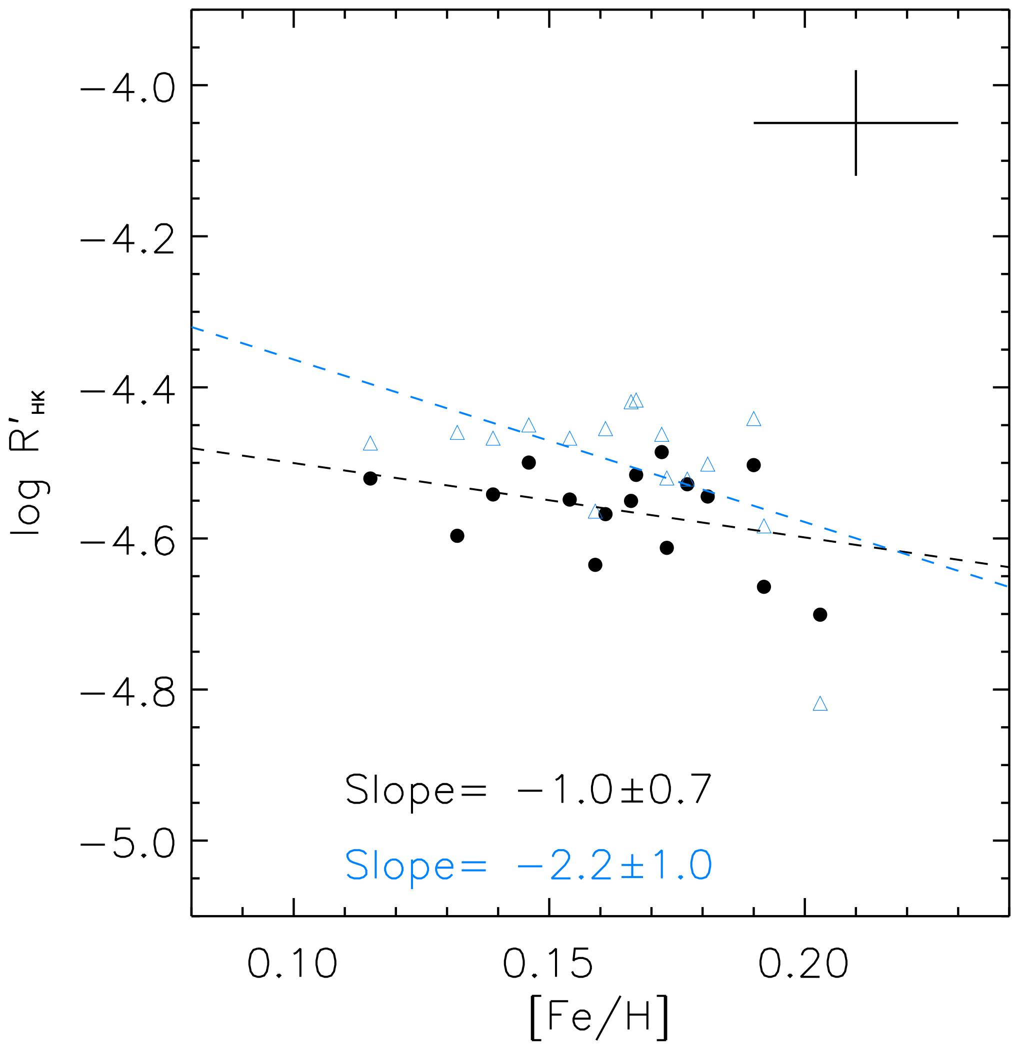

Figure 4.17 The stellar chromospheric activity index log R'_{HK} versus derived [Fe/H] for our Hyades stars. The black circles represent the index measured based on our spectra, while the blue triangles represent the index taken from P02. The black dashed line and the blue dashed line represent the linear least-squares fit to our data and P02 data, respectively.

errors (as in, e.g., Figure 4.8).

a) Inhomogeneous chemical evolution in the proto-cluster environment

In this scenario, we assume that the abundance variations and correlations are due to chemical inhomogeneities in the proto-cluster environment. Our Hyades data indicate that all elements are positively correlated, regardless of their nucleosynthetic origin. For example, the α-element Ca is positively correlated with the Fe-peak element Ni as well as with the *s*-process element Ba. The correlations between light, α-, Fe-peak and neutron-capture elements demand contributions from a variety of nucleosynthetic sources, and it would seem unlikely that this is the explanation. Similarly, GCE would not affect all elements equally such that they evolve in lock-step (e.g., Kobayashi et al. 2011).

b) Supernova ejection in the proto-cluster cloud

Of particular interest is the fact that some of the elements which exhibit star-to-star variations and correlations are synthesized in massive stars that die as core collapse supernovae (SNe II). A typical SNe II from a 15 $M_{\odot}$ produces $\sim 10^{-1}$ $M_{\odot}$ of Fe (Woosley & Weaver 1995). We assume that the mass for the giant molecular cloud from which the Hyades was formed was $\sim$ 800 - 1600 $M_{\odot}$ (Weidemann et al. 1992; Kroupa & Boily 2002). The mass fraction of Fe from that SNe II in such a cloud will be $\sim (1.25 - 0.63) \times 10^{-4}$. The Fe content of the Sun is $\approx 1.5 \times 10^{-3}$ $M_{\odot}$ (Asplund et al. 2009). If we assume [Fe/H] $\approx$ 0.1 dex for our case, the corresponding Fe content will be $\sim 1.9 \times 10^{-3}$ $M_{\odot}$. Thus we can estimate the change in Fe abundance, produced by such a typical SNe II, will be $\approx$ 0.02 - 0.04 dex, which is comparable with the intrinsic abundance scatter in Fe abundance in our sample ($\approx$ 0.023 dex). Therefore, one SNe II can account for the change in Fe abundance in the Hyades.

The supernova timescale (t_{SN}) is $\approx$ 3 Myr and we would expect the open clusters not to be fully homogeneous if they were assembled on timescales longer than the supernova timescale and all gas is expelled once the SNe explodes. Since no clear separation in timescales between chemical homogenization and the star formation, the time required for turbulent mixing to smooth out the proto-cluster gas cloud might be longer than ~ 3 Myr for the Hyades open cluster, if the hypothesis is true. We note that the main constraint derived here is limited not by the constraint on the abundance spread, but instead by whether a core collapse supernovae of a massive star is likely to have occurred and to have polluted the star-forming gas where the Hyades open cluster formed. A further problem of this scenario is that the supernova ejecta can not produce all elements to reveal the abundance variations seen in our results.

c) Dilution with metal-poor gas

One possibility is that metal-poor gas might pollute the molecular star-forming cloud. Theoretical simulations suggested that the gas and dust in star-forming clouds can be very well mixed (Feng & Krumholz 2014), which would lead to an abundance scatter ~ 0.01 - 0.05 dex. However, when we are able to achieve a precision level of ≈ 0.02 dex in our strictly line-by-line differential abundance analysis, we note that the open cluster Hyades shows the inhomogeneities for many elements since the abundance dispersions are ~ 0.025 - 0.045 dex, a factor of 1.5 - 2 larger than the predicted errors, as shown in Figure 4.7, leading to an intrinsic abundance scatter of ~ 0.02 dex. According to Feng & Krumholz (2014), the turbulent mixing during cloud assembly would happen when the star formation efficiency reaches ~ 30 % for the clusters with mass ~ 10^3 $M_\odot$. Therefore, the pollution of metal-poor gas should happen before within ~ 3 Myr. In addition, our results also provide constrains on the intrinsic abundance dispersion in the molecular cloud where the Hyades formed. Using the prediction from Feng & Krumholz (2014), the proto-cluster cloud would have abundance scatter ~ 5 times higher than the abundance scatter in the Hyades, which would lead to ~ 0.1 dex scatter in the gas abundances.

If we assume that the most metal-rich stars represent the "true" abundance of the Hyades, then we can estimate how much dilution is needed to produce the most metal-poor Hyades objects. In the limit that the diluting material is metal-free, then a mixture of eight parts "true" Hyades material to one part diluting material would result in a decrease in [X/H] of 0.04 dex, for all elements. In the more likely event that the diluting material is not metal free, then the mixture shifts in favour of the diluting material. For example, if the diluting material half that of the "true" Hyades composition, then a mixture of 3.5 parts Hyades material to one part diluting material would result in a decrease of 0.05 dex in [X/H]. Theoretical simulations are needed to examine whether such dilution is dynamically plausible. We note that pollution of metal-rich gas is another possibility since the same arguments can apply.

4.5. Conclusion

We have studied the Hyades, a benchmark open cluster, to investigate whether we can detect chemical signatures of planet formation. We analysed 16 solar-type stars in the Hyades based on high resolution, high signal-to-noise ratio (S/N $\approx$ 350 - 400 per pixel) spectra obtained from the McDonald 2.7m telescope, allowing us to achieve very high precision in stellar parameters and differential chemical abundances with uncertainties as small as 0.008 dex for our programme stars.

We did not find any significant correlations in abundance with condensation temperature for our Hyades stars in the Meléndez et al. (2009) scenario. We demonstrated that the observed abundance dispersions in our Hyades stars are a factor for $\approx$ 1.5 - 2 larger than the average measurement errors for most elements, and that there is an intrinsic abundance dispersion of 0.021 ± 0.003 dex (σ = 0.010) in the Hyades open cluster. The differential chemical abundances of at least 90% of pairs of elements have positive correlations with high statistical significance, which strengthens our statement that the Hyades is chemically inhomogeneous. Removing the abundance trends with $T_{\rm eff}$ does not alter our results. We recall that the abundance trends with T_{eff} might be due to modelling errors. We do not find evidence in our data for atomic diffusion effects in the Hyades. Tests on the error vectors of the stellar atmospheric parameters indicate that > 75% of the positive correlations between Δ^X and Δ^Y can not be explained by changing the stellar parameters systematically. Additionally and importantly, these results persist regardless of the choice of reference star, i.e., the results are independent of the reference star. We note that the chemical inhomogeneities are not due to the planet effects, considering the lack of abundance versus T_{cond} trends in our sample. The possible explanations of these abundance variations include: (a) inhomogeneous chemical evolution in the proto-cluster environment, (b) supernova ejection in the proto-cluster cloud, (c) pollution of metal-poor, or metal-rich, gas before complete mixing of the proto-cluster cloud.

Our detailed differential abundance analysis for the Hyades stars provides significant constraints upon the chemical homogeneity of open clusters and a challenge to the current view of Galactic archeology, in terms of "chemical tagging". The Hyades is the first, and thus far only, open cluster to which we have applied high precision chemical abundance techniques. By extension, it may be that other (perhaps all) open clusters are similarly chemically inhomogeneous. Clearly it is important to extend this type of analysis to additional open clusters to identify chemical signatures of planet formation and/or chemical inhomogeneity.

Acknowledgments

This work has been supported by the Australian Research Council (grants FL110100012, FT140100554 and DP120100991). JM thanks support by FAPESP (2012/24392-2). We thank the detailed and helpful suggestions provided by the referee of this paper.

CHAPTER 5

CONCLUSIONS

As noted in the introduction, Meléndez et al. (2009) and follow-up studies (Ramírez et al. 2009, 2010) discovered that the Sun shows a deficiency in refractory elements relative to volatiles when compared to the majority of solar twins. The abundance deficiencies strongly correlate with the condensation temperature (T_{cond}) of the elements. The special abundance pattern of the Sun might be due to dust condensation and terrestrial planet formation in the proto-solar disc that for some reason proceeded more efficiently than for the majority of solar twins. The focus of this thesis is to identify and examine the chemical signatures imprinted by planet formation through the chemical abundances of the host stars. We include field stars (e.g., stellar binaries, terrestrial planet hosts etc.) and open cluster stars in our research to understand whether the formation of planet affects the chemical compositions of their host stars and whether the environment of host stars influences planet formation, especially terrestrial planet formation.

At first, we performed a detailed differential abundance analysis of the HAT-P-1 stellar binary using high-resolution, high signal-to-noise (S/N) spectra from Keck/HIRES. The secondary star in this double system is known to host a close-in Jupiter-like planet while no planet has yet been detected around the primary star. The derived metallicities ([Fe/H]) of the primary and secondary stars are identical within the errors: 0.146 ± 0.014 dex (σ = 0.033 dex) and 0.155 ± 0.007 dex (σ = 0.023 dex), respectively. Extremely precise differential abundance ratios of 23 elements have been measured (mean error of σ[X/Fe] = 0.013 dex) and are found to be indistinguishable between the two stars: Δ[X/Fe] (secondary - primary) = +0.001 ± 0.006 dex (σ = 0.008 dex). Therefore we conclude that the presence of giant planet does not necessarily imprint differences in the chemical compositions of the host stars. The elemental abundances of each star in HAT-P-1 relative to the Sun show an identical, positive correlation with the condensation temperature; their abundance patterns are thus very similar to those observed in the majority of solar twins. In view of the Meléndez et al. (2009) interpretation, we conclude that HAT-P-1 experienced less efficient formation of terrestrial planets than the Sun. This is in line with the expectation that the presence of close-in giant planets prevents the formation or survival of terrestrial planets. Our study of the HAT-P-1 double system underscores how high-precision differential abundance measurements in binary stars with planets can provide important constraints on planet formation. Further efforts are needed to examine the physical characteristics and chemical abundances for additional stellar binaries with giant or terrestrial planets in order to understand the formation and evolution of planetary systems.

Secondly, we conducted a line-by-line differential abundance study of Kepler-10 and a sample of its stellar twins. We achieved extremely high precision abundances using high quality spectra from three telescopes (CFHT, HET and Magellan). Our analysis revealed subtle chemical differences in the photosphere of Kepler-10 when compared to its stellar twins. We confirm that Kepler-10 is very likely a thick disc star considering its old age (8.4 ± 1.0 Gyr), kinematic probabilities (96% as thick disc member) and chemistry. When comparing Kepler-10 to its thick disc twins, a single linear fit provides an appropriate representation of the Δ[X/H] - T_{cond} trend. We find that Kepler-10 is depleted in refractory elements relative to volatile elements when compared to the majority of thick disc stellar twins. Two of the eight thick disc twins do not show depletion patterns, which is within the small number statistics compatible with Meléndez et al. (2009) and Ramírez et al. (2009, 2010) et al.; 15% of solar twins have chemical compositions that match the solar value. The average abundance difference between thick disc twins and Kepler-10 is 0.037 ± 0.004 (σ = 0.016) which corresponds to at least 13 Earth masses of material. One possible explanation for this abundance difference could be the formation of terrestrial planets in the Kepler-10 system. However, the results are not as clear as for the solar twins (Meléndez et al. 2009; Ramírez et al. 2010). Other factors (e.g., stellar age, stellar birth location and GCE) might also affect the abundance results. Naturally the thick disc twins may also harbour similarly large rocky planets as Kepler-10 although they have not yet been detected. Several studies based on current discoveries of exoplanets (Howard et al. 2012; Petigura et al. 2013; Burke et al. 2015) reported estimates of the occurrence rate of rocky planets around different type of stars with different orbits. Petigura et al. (2013) indicate that at least one in six stars might host a planet with 1 - 2 R_E with period between 5 - 50 days. In this case, the peculiar chemical composition of Kepler-10 can reveal signatures regarding the different planetary masses, orbits, formation efficiency or formation timescale. In order to test the Meléndez et al. (2009) scenario regarding terrestrial planet formation and unravel the possible subtle chemical signatures and better understand the mechanisms of planet formation, additional spectra, and differential analysis of terrestrial planet host stars and their identical stellar twins with high S/N are needed.

Finally, we have studied the Hyades, a benchmark open cluster, to investigate whether we can detect chemical signatures of planet formation. We analysed 16 solar-type stars in the Hyades based on high resolution, high S/N ($\approx$ 350 - 400 per pixel) spectra obtained from the McDonald 2.7m telescope, allowing us to achieve very high precision in stellar parameters and differential chemical abundances with uncertainties as small as 0.01 dex for our programme stars. We did not find any significant correlations in abundance with condensation temperature for our Hyades stars in the Meléndez et al. (2009) scenario. We demonstrated that the observed abundance dispersions in our Hyades stars are a factor for ≈ 2 larger than the average measurement errors for most elements, and that there is an intrinsic abundance dispersion of 0.021 ± 0.003 dex ($\sigma = 0.010$) in the Hyades open cluster. At least 90% of pairs of elements have positive correlations with high statistical significance, which strengthens our statement that the Hyades is chemically inhomogeneous. Removing the abundance trends with $T_{\rm eff}$ does not alter our results. We do not find evidence in our data for atomic diffusion effects in the Hyades. Tests on the error vectors of the stellar atmospheric parameters indicate that > 75% of the positive correlations between Δ^X and Δ^Y can not be explained by changing the stellar parameters systematically. Additionally and importantly, these results persist regardless of the choice of reference star, i.e., the results are independent of the reference star. We note that the chemical inhomogeneities are not due to the planet effects, considering the lack of abundance vs. $T_{\rm cond}$ trends in our sample. The possible explanations of these abundance variations include: a) inhomogeneous chemical evolution in the proto-cluster environment, b) supernova ejection in the proto-cluster cloud, (c) pollution of metal-poor, or metal-rich, gas before complete mixing of the proto-cluster cloud. Our detailed differential abundance analysis for the Hyades stars provides significant constraints upon the chemical homogeneity of open clusters and a challenge to the current view of Galactic archeology, in terms of "chemical tagging". The Hyades is the first, and thus far only, open cluster to which we have applied high precision chemical abundance techniques. By extension, it may be that other (perhaps all) open clusters are similarly chemically inhomogeneous. Clearly it is important to extend this type of analysis to additional open clusters to identify chemical signatures of planet formation and/or chemical inhomogeneity.

5.1. Future work

Having gained extensive expertise in high-precision stellar spectroscopy as part of my PhD work, I am now ideally placed to continue investigating the impact of planet formation on the host stars as well as branching out into new fields of research where such extremely carefully stellar abundance analyses are likely to have a profound impact, including the characterization of stellar and planetary systems, detailed study on Galactic chemical evolution (GCE) effects and Galactic archaeology.

5.1.1. Differential abundance analysis on planet hosts, metal-poor stars and open cluster stars

I intend to continue my research on extremely precise measurements of differential chemical abundances for different type of planet hosts (stellar binaries, small planet hosts etc.) using high resolution, high S/N spectra. Recall that binary stars are assumed to share the same origin and chemical composition, which makes them ideal targets for differential abundance analysis (e.g., Liu et al. 2014; Ramírez et al. 2015; Saffe et al. 2015). Any subtle chemical differences in the binary stars could be due to the formation of planets. I also plan to work on small planet hosts to derive accurate stellar parameters and chemical abundances relative to their stellar twins. High quality spectra from Gemini-GRACES have been collected for the future analysis. These results will help us better understand the host stars and also potentially provide significant constraints on the chemical compositions of these small planets.

Whether or not planets, especially small planets, can form around metal-poor stars is of fundamental importance since it can provide significant constraints to the theory of planet formation regarding accretion (e.g., Pollack et al. 1996; Mordasini et al. 2012) or disc instability (e.g., Boss 1997). A few surveys have been conducted with Keck/HIRES and

HARPS but almost no low-mass planets have yet been detected in the sample (Mortier et al. 2012). Assuming that the planet hypothesis proposed by Meléndez et al. (2009) is true, people could identify possible terrestrial planet host solely from their chemical compositions. Therefore I intend to investigate planets around metal-poor stars ([Fe/H] ~ -0.5 to -1.0) by applying such differential abundance analysis, as what has been done for metal-rich stars (Ramírez et al. 2014a), in order to identify potential terrestrial planets in a sample of metal-poor stars. Compared to the more demanding long-term radial velocity monitoring planet search programmes, we only have to obtain high resolution, high S/N spectra for $\sim$ 30 to 50 metal-poor stars around [Fe/H] ~ -0.5 to -1.0. Then we are able to explore the correlations between abundances and condensation temperature (T_{cond}) to determine whether or not terrestrial planets formed around these stars and imprinted chemical signatures in the host stars. From the distribution of the T_{cond} trends, we should be able to estimate the frequency of small planets around stars with sub-solar metallicities as well. This research complements the more traditional RV-based approach to estimate the planet frequency around metal-poor stars (Sozzetti et al. 2006, 2009; Faria et al. 2016). I would be doing an independent analysis which could help us to better understand the fundamental processes involved in planet formation.

In addition, I propose to study several additional benchmark open clusters (e.g., Coma Berenices, Praesepe, Ruprecht 147 and M67 etc.) using strictly line-by-line differential analysis, as I did for the Hyades open cluster, to search for the possible chemical signatures of planet formation and test the chemical inhomogeneity level in different open clusters. Such research can provide important constraints to the timescale of turbulent mixing and star-formation in the open clusters. It is also exciting to analyze the cluster-to-cluster variations. I have collected high quality spectra from Keck/HIRES, HET/HRS and VLT/UVES of these open cluster stars during the past few years.

5.1.2. Galactic chemical evolution (GCE) effects

The local disc population of the Milky Way is subdivided into stars of the thin disc and others belonging to the thick disc, with different distributions for chemical abundances and kinematics (Reddy et al. 2006). According to my previous work, the chemical patterns are different for thin and thick disc stars in terms of abundance ratios versus condensation temperature. Using the data from ongoing large surveys, such as Gaia-ESO (Gilmore et al. 2012), APOGEE (Allende Prieto et al. 2008), GALAH (De Silva et al. 2015) and LAMOST (Zhao et al. 2012), I propose to determine the accurate chemical patterns of the thin/thick stars, which should be distinctive. The results can also provide interesting targets containing information regarding planet formation and GCE effects for high resolution, high S/N spectroscopy follow-up with big telescopes such as Keck, VLT, and Magellan etc. In addition, most of previous studies focus on the relations of abundance ratios [X/Fe] and metallicities [Fe/H], namely, GCE effects. Nissen (2015) indicated that age would be a better tracer for the GCE effects. I propose to conduct further and careful exploration on the GCE effects on thin and thick disc stars with detailed differential chemical abundance analysis using high resolution, high S/N spectra. With the combination of high precision chemical abundances, accurate stellar ages and orbital parameters from Gaia satellite, we could provide robust estimations of GCE effects on thin/thick disc stars. This study can help us better understand the chemical enrichment history and the chemical structure of our Galaxy.

BIBLIOGRAPHY

Adibekyan, V. Z., González Hernández, J. I., Delgado Mena, E., Sousa, S. G., Santos, N. C., Israelian, G., Figueira, P., & Bertran de Lis, S. 2014, A&A, 564, L15

Adibekyan, V. Z., Sousa, S. G., Santos, N. C., Delgado Mena, E., González Hernández, J. I., Israelian, G., Mayor, M., & Khachatryan, G. 2012, A&A, 545, A32

Allende Prieto, C., et al. 2008, Astronomische Nachrichten, 329, 1018

Amarsi, A. M., Asplund, M., Collet, R., & Leenaarts, J. 2016, MNRAS, 455, 3735

Asplund, M. 2005, ARA&A, 43, 481

Asplund, M., Grevesse, N., Sauval, A. J., & Scott, P. 2009, ARA&A, 47, 481

Bakos, G. Á., et al. 2007, ApJ, 656, 552

Baraffe, I., Chabrier, G., Barman, T. S., Selsis, F., Allard, F., & Hauschildt, P. H. 2005, A&A, 436, L47

Batalha, N. M., et al. 2011, ApJ, 729, 27

—. 2013, ApJS, 204, 24

Baumann, P., Ramírez, I., Meléndez, J., Asplund, M., & Lind, K. 2010, A&A, 519, A87

Bedell, M., Meléndez, J., Bean, J. L., Ramírez, I., Leite, P., & Asplund, M. 2014, ApJ, 795, 23

Bensby, T., Feltzing, S., Lundström, I., & Ilyin, I. 2005, A&A, 433, 185

Bensby, T., Feltzing, S., & Oey, M. S. 2014, A&A, 562, A71

Bernstein, R., Shectman, S. A., Gunnels, S. M., Mochnacki, S., & Athey, A. E. 2003, in Society of Photo-Optical Instrumentation Engineers (SPIE) Conference Series, Vol. 4841, Instrument Design and Performance for Optical/Infrared Ground-based Telescopes, ed. M. Iye & A. F. M. Moorwood, 1694–1704

Biazzo, K., et al. 2015, A&A, 583, A135

Blanco-Cuaresma, S., et al. 2015, A&A, 577, A47

Bland-Hawthorn, J., Karlsson, T., Sharma, S., Krumholz, M., & Silk, J. 2010a, ApJ, 721, 582

Bland-Hawthorn, J., Krumholz, M. R., & Freeman, K. 2010b, ApJ, 713, 166

Boesgaard, A. M., & Tripicco, M. J. 1986, ApJ, 302, L49

Boss, A. P. 1997, Science, 276, 1836

Bovy, J. 2016, ApJ, 817, 49

Brandt, T. D., & Huang, C. X. 2015, ApJ, 807, 58

Brucalassi, A., et al. 2014, A&A, 561, L9

Buchhave, L. A., et al. 2012, Nature, 486, 375

Burke, C. J., et al. 2007, ApJ, 671, 2115

—. 2015, ApJ, 809, 8

Carrera, R., & Pancino, E. 2011, A&A, 535, A30

Castelli, F., & Kurucz, R. L. 2003, in IAU Symposium, Vol. 210, Modelling of Stellar Atmospheres, ed. N. Piskunov, W. W. Weiss, & D. F. Gray, A20

Chambers, J. E. 2010, ApJ, 724, 92

Chiang, E., & Laughlin, G. 2013, MNRAS, 431, 3444

Chiappini, C., Matteucci, F., & Romano, D. 2001, ApJ, 554, 1044

Cochran, W. D., Hatzes, A. P., Butler, R. P., & Marcy, G. W. 1997, ApJ, 483, 457

Cochran, W. D., Hatzes, A. P., & Paulson, D. B. 2002, AJ, 124, 565

Coughlin, J. L., et al. 2015, ArXiv e-prints

De Silva, G. M., Freeman, K. C., Asplund, M., Bland-Hawthorn, J., Bessell, M. S., & Collet, R. 2007, AJ, 133, 1161

De Silva, G. M., Sneden, C., Paulson, D. B., Asplund, M., Bland-Hawthorn, J., Bessell, M. S., & Freeman, K. C. 2006, AJ, 131, 455

De Silva, G. M., et al. 2015, MNRAS, 449, 2604

Debes, J. H., & Jackson, B. 2010, ApJ, 723, 1703

Desidera, S., Gratton, R. G., Lucatello, S., & Claudi, R. U. 2006, A&A, 454, 581

Desidera, S., et al. 2004, A&A, 420, 683

—. 2014, A&A, 567, L6

Dumusque, X., et al. 2014, ApJ, 789, 154

Duncan, D. K., et al. 1991, ApJS, 76, 383

Dutra-Ferreira, L., Pasquini, L., Smiljanic, R., Porto de Mello, G. F., & Steffen, M. 2016, A&A, 585, A75

Ecuvillon, A., Israelian, G., Santos, N. C., Mayor, M., & Gilli, G. 2006, A&A, 449, 809

Edvardsson, B., Andersen, J., Gustafsson, B., Lambert, D. L., Nissen, P. E., & Tomkin, J. 1993, A&A, 275, 101

Eisner, J. A., Plambeck, R. L., Carpenter, J. M., Corder, S. A., Qi, C., & Wilner, D. 2008, ApJ, 683, 304

Epstein, C. R., Johnson, J. A., Dong, S., Udalski, A., Gould, A., & Becker, G. 2010, ApJ, 709, 447

ESA. 1997, The Hipparcos and Tycho Catalogues, ESA SP-1200

Fabbian, D., Asplund, M., Barklem, P. S., Carlsson, M., & Kiselman, D. 2009, A&A, 500, 1221

Faria, J. P., et al. 2016, ArXiv e-prints

Feldman, U., & Laming, J. M. 2000, Phys. Scr, 61, 222

Feng, Y., & Krumholz, M. R. 2014, Nature, 513, 523

Fischer, D. A., & Valenti, J. 2005, ApJ, 622, 1102

Freeman, K., & Bland-Hawthorn, J. 2002, ARA&A, 40, 487

Fressin, F., et al. 2013, ApJ, 766, 81

Friel, E. D., & Boesgaard, A. M. 1992, ApJ, 387, 170

Friel, E. D., et al. 2014, A&A, 563, A117

Gaidos, E. 2015, ApJ, 804, 40

Gebran, M., Vick, M., Monier, R., & Fossati, L. 2010, A&A, 523, A71

Gilmore, G., et al. 2012, The Messenger, 147, 25

Gonzalez, G. 1997, MNRAS, 285, 403

González Hernández, J. I., Delgado-Mena, E., Sousa, S. G., Israelian, G., Santos, N. C., Adibekyan, V. Z., & Udry, S. 2013, A&A, 552, A6

González Hernández, J. I., Israelian, G., Santos, N. C., Sousa, S., Delgado-Mena, E., Neves, V., & Udry, S. 2010, ApJ, 720, 1592

Gratton, R. G., Bonanno, G., Claudi, R. U., Cosentino, R., Desidera, S., Lucatello, S., & Scuderi, S. 2001, A&A, 377, 123

Grevesse, N., Scott, P., Asplund, M., & Sauval, A. J. 2015, A&A, 573, A27

Griffin, R. F., Griffin, R. E. M., Gunn, J. E., & Zimmerman, B. A. 1988, AJ, 96, 172

Haghighipour, N. 2011, Contemporary Physics, 52, 403

Hartman, J. D., et al. 2009, ApJ, 695, 336

Howard, A. W., et al. 2012, ApJS, 201, 15

Ida, S., & Lin, D. N. C. 2004, ApJ, 616, 567

Israelian, G., et al. 2009, Nature, 462, 189

Johnson, D. R. H., & Soderblom, D. R. 1987, AJ, 93, 864

Kim, Y.-C., Demarque, P., Yi, S. K., & Alexander, D. R. 2002, ApJS, 143, 499

Kobayashi, C., Karakas, A. I., & Umeda, H. 2011, MNRAS, 414, 3231

Kraft, R. P. 1994, PASP, 106, 553

Kroupa, P., & Boily, C. M. 2002, MNRAS, 336, 1188

Kubryk, M., Prantzos, N., & Athanassoula, E. 2015, A&A, 580, A126

Kurucz, R. L., & Bell, B. 1995, Atomic line list, Kurucz CD-ROM, No. 23, Cambridge, MA: Smithsonian Astrophysical Observatory

Lada, C. J., & Lada, E. A. 2003, ARA&A, 41, 57

Latham, D. W., et al. 2011, ApJ, 732, L24

Laws, C., & Gonzalez, G. 2001, ApJ, 553, 405

Lin, D. N. C., Bodenheimer, P., & Richardson, D. C. 1996, Nature, 380, 606

Liu, F., Asplund, M., Ramírez, I., Yong, D., & Meléndez, J. 2014, MNRAS, 442, L51

Liu, F., Yong, D., Asplund, M., Ramírez, I., & Meléndez, J. 2016a, MNRAS, 457, 3934

Liu, F., et al. 2016b, MNRAS, 456, 2636

Lodders, K. 2003, ApJ, 591, 1220

Lovis, C., & Mayor, M. 2007, A&A, 472, 657

Mack, III, C. E., Schuler, S. C., Stassun, K. G., & Norris, J. 2014, ApJ, 787, 98

Maderak, R. M., Deliyannis, C. P., King, J. R., & Cummings, J. D. 2013, AJ, 146, 143

Mann, A. W., et al. 2015, arXiv:1512.00483

Manset, N., & Donati, J.-F. 2003, in Society of Photo-Optical Instrumentation Engineers (SPIE) Conference Series, Vol. 4843, Polarimetry in Astronomy, ed. S. Fineschi, 425–436

Masseron, T., & Gilmore, G. 2015, MNRAS, 453, 1855

Mayor, M., & Queloz, D. 1995, Nature, 378, 355

Mayor, M., et al. 2011, ArXiv e-prints

Meibom, S., et al. 2013, Nature, 499, 55

Meléndez, J., Asplund, M., Gustafsson, B., & Yong, D. 2009, ApJ, 704, L66

Meléndez, J., et al. 2012, A&A, 543, A29

Middelkoop, F. 1982, A&A, 107, 31

Mochejska, B. J., et al. 2006, AJ, 131, 1090

Monroe, T. R., et al. 2013, ApJ, 774, L32

Mordasini, C., Alibert, Y., Klahr, H., & Henning, T. 2012, A&A, 547, A111

Morel, T., & Micela, G. 2004, A&A, 423, 677

Mortier, A., Santos, N. C., Sozzetti, A., Mayor, M., Latham, D., Bonfils, X., & Udry, S. 2012, A&A, 543, A45

Neves, V., Santos, N. C., Sousa, S. G., Correia, A. C. M., & Israelian, G. 2009, A&A, 497, 563

Nissen, P. E. 2015, A&A, 579, A52

Noyes, R. W., Hartmann, L. W., Baliunas, S. L., Duncan, D. K., & Vaughan, A. H. 1984, ApJ, 279, 763

Önehag, A., Gustafsson, B., & Korn, A. 2014, A&A, 562, A102

Önehag, A., Korn, A., Gustafsson, B., Stempels, E., & Vandenberg, D. A. 2011, A&A, 528, A85

Pasquini, L., et al. 2012, A&A, 545, A139

Paulson, D. B., Cochran, W. D., & Hatzes, A. P. 2004a, AJ, 127, 3579

Paulson, D. B., Saar, S. H., Cochran, W. D., & Hatzes, A. P. 2002, AJ, 124, 572

Paulson, D. B., Saar, S. H., Cochran, W. D., & Henry, G. W. 2004b, AJ, 127, 1644

Paulson, D. B., Sneden, C., & Cochran, W. D. 2003, AJ, 125, 3185

Pepper, J., Stanek, K. Z., Pogge, R. W., Latham, D. W., DePoy, D. L., Siverd, R., Poindexter, S., & Sivakoff, G. R. 2008, AJ, 135, 907

Perryman, M. A. C., et al. 1998, A&A, 331, 81

Petigura, E. A., Marcy, G. W., & Howard, A. W. 2013, ApJ, 770, 69

Pichardo, B., Moreno, E., Allen, C., Bedin, L. R., Bellini, A., & Pasquini, L. 2012, AJ, 143, 73

Plávalová, E., & Solovaya, N. A. 2013, AJ, 146, 108

Pollack, J. B., Hubickyj, O., Bodenheimer, P., Lissauer, J. J., Podolak, M., & Greenzweig, Y. 1996, Icarus, 124, 62

Quinn, S. N., et al. 2012, ApJ, 756, L33

—. 2014, ApJ, 787, 27

Ramírez, I., Allende Prieto, C., & Lambert, D. L. 2007, A&A, 465, 271

—. 2013, ApJ, 764, 78

Ramírez, I., Asplund, M., Baumann, P., Meléndez, J., & Bensby, T. 2010, A&A, 521, A33

Ramírez, I., & Meléndez, J. 2005, ApJ, 626, 446

Ramírez, I., Meléndez, J., & Asplund, M. 2009, A&A, 508, L17

—. 2014a, A&A, 561, A7

Ramírez, I., Meléndez, J., Cornejo, D., Roederer, I. U., & Fish, J. R. 2011, ApJ, 740, 76

Ramírez, I., et al. 2014b, A&A, 572, A48

—. 2015, ApJ, 808, 13

Randich, S., et al. 2005, The Messenger, 121, 18

Reddy, B. E., Lambert, D. L., & Allende Prieto, C. 2006, MNRAS, 367, 1329

Reddy, B. E., Tomkin, J., Lambert, D. L., & Allende Prieto, C. 2003, MNRAS, 340, 304

Richer, J., Michaud, G., & Turcotte, S. 2000, ApJ, 529, 338

Rogers, L. A. 2015, ApJ, 801, 41

Saffe, C., Flores, M., & Buccino, A. 2015, A&A, 582, A17

Santos, N. C., Israelian, G., & Mayor, M. 2004, A&A, 415, 1153

Santos, N. C., et al. 2015, A&A, 580, L13

Sato, B., et al. 2007, ApJ, 661, 527

Schuler, S. C., Cunha, K., Smith, V. V., Ghezzi, L., King, J. R., Deliyannis, C. P., & Boesgaard, A. M. 2011a, ApJ, 737, L32

Schuler, S. C., Flateau, D., Cunha, K., King, J. R., Ghezzi, L., & Smith, V. V. 2011b, ApJ, 732, 55

Scott, P., Asplund, M., Grevesse, N., Bergemann, M., & Sauval, A. J. 2015a, A&A, 573, A26

Scott, P., et al. 2015b, A&A, 573, A25

Siess, L., Dufour, E., & Forestini, M. 2000, A&A, 358, 593

Smiljanic, R., Pasquini, L., Charbonnel, C., & Lagarde, N. 2010, A&A, 510, A50

Sneden, C. 1973, ApJ, 184, 839

Sobeck, J. S., et al. 2011, AJ, 141, 175

Sousa, S. G., Santos, N. C., Israelian, G., Mayor, M., & Monteiro, M. J. P. F. G. 2007, A&A, 469, 783

Sozzetti, A., Torres, G., Latham, D. W., Carney, B. W., Stefanik, R. P., Boss, A. P., Laird, J. B., & Korzennik, S. G. 2006, ApJ, 649, 428

Sozzetti, A., Torres, G., Latham, D. W., Stefanik, R. P., Korzennik, S. G., Boss, A. P., Carney, B. W., & Laird, J. B. 2009, ApJ, 697, 544

Spina, L., Meléndez, J., & Ramírez, I. 2016, A&A, 585, A152

Spina, L., et al. 2015, A&A, 582, L6

Takeda, Y., Hashimoto, O., Taguchi, H., Yoshioka, K., Takada-Hidai, M., Saito, Y., & Honda, S. 2005, PASJ, 57, 751

Teske, J. K., Ghezzi, L., Cunha, K., Smith, V. V., Schuler, S. C., & Bergemann, M. 2015, ApJ, 801, L10

Ting, Y.-S., De Silva, G. M., Freeman, K. C., & Parker, S. J. 2012, MNRAS, 427, 882

Tucci Maia, M., Meléndez, J., & Ramírez, I. 2014, ApJ, 790, L25

Tull, R. G. 1998, in Society of Photo-Optical Instrumentation Engineers (SPIE) Conference Series, Vol. 3355, Optical Astronomical Instrumentation, ed. S. D'Odorico, 387–398

Tull, R. G., MacQueen, P. J., Sneden, C., & Lambert, D. L. 1995, PASP, 107, 251

Udry, S., & Santos, N. C. 2007, ARA&A, 45, 397

Udry, S., et al. 2007, A&A, 469, L43

van Saders, J. L., & Gaudi, B. S. 2011, ApJ, 729, 63

Vogt, S. S., et al. 1994, in Society of Photo-Optical Instrumentation Engineers (SPIE) Conference Series, Vol. 2198, Instrumentation in Astronomy VIII, ed. D. L. Crawford & E. R. Craine, 362

Weidemann, V., Jordan, S., Iben, Jr., I., & Casertano, S. 1992, AJ, 104, 1876

Williams, J. P., & Cieza, L. A. 2011, ARA&A, 49, 67

Woosley, S. E., & Weaver, T. A. 1995, ApJS, 101, 181

Wright, J. T., Marcy, G. W., Butler, R. P., & Vogt, S. S. 2004, ApJS, 152, 261

Wright, J. T., Marcy, G. W., Howard, A. W., Johnson, J. A., Morton, T. D., & Fischer, D. A. 2012, ApJ, 753, 160

Yi, S., Demarque, P., Kim, Y.-C., Lee, Y.-W., Ree, C. H., Lejeune, T., & Barnes, S. 2001, ApJS, 136, 417

Yong, D., et al. 2013, MNRAS, 434, 3542

Zhao, G., Zhao, Y.-H., Chu, Y.-Q., Jing, Y.-P., & Deng, L.-C. 2012, Research in Astronomy and Astrophysics, 12, 723